Online Appendix to "Combining Proxies and Narrative Sign Restrictions: Revisiting the Effects of Technology Shocks"

Yang Yang*

School of Finance

Zhongnan University of Economics and Law

Ren Zhang†

Department of Finance & Economics

McCoy College of Business

Texas State University

This version: March 11, 2025

*Nanhu Avenue, Wuchang District, Wuhan, Hubei 430073, China. yangyanghnwg@zuel.edu.cn.

†601 University Dr, San Marcos, TX 78666, United States. r_z79@txstate.edu.

Contents

A Bayesian Posterior Inferences

In this Online Appendix, we detail our posterior inferences using various priors on the orthonormal matrix. Section A.1 derives the posterior density and outlines the procedure for drawing structural parameters with a uniform prior over orthonormal matrix. Section A.2 discusses applying our identification approach with a robust prior as in Giacomini and Kitagawa (2021). Section A.3 extends the method of Arias et al. (2024) to conduct joint inference with a uniform prior over impulse responses.

A.1 Benchmark Inference with a Uniform Prior on the Orthonormal Matrix

Following Arias et al. (2021), we assume that the proxy SVAR structural parameters $(\tilde{A}_0, \tilde{A}_+)$ have a prior distribution $\pi(\tilde{A}_0, \tilde{A}_+)$ proportional to a normal-generalized-normal density $NGN_{(\nu,\Phi,\Psi,\Omega)}(\tilde{A}_0, \tilde{A}_+)$

$$\begin{aligned}
&\pi(\tilde{A}_0, \tilde{A}_+) \propto NGN_{(\nu,\Phi,\Psi,\Omega)}(\tilde{A}_0, \tilde{A}_+) \\
&\propto \underbrace{\left|\det(\tilde{A}_0)\right|^{\nu-\tilde{n}} e^{-0.5 vec(\tilde{A}_0)'\Phi vec(\tilde{A}_0)}}_{\text{generalized-normal}} \underbrace{e^{-0.5(vec(\tilde{A}_+)-\Psi vec(\tilde{A}_0))'\Omega^{-1}(vec(\tilde{A}_+)-\Psi vec(\tilde{A}_0))}}_{\text{conditional normal}}, \qquad \text{(A.1)}
\end{aligned}$$

where ν is a scalar, Φ is an $\tilde{n}^2 \times \tilde{n}^2$ block diagonal matrix, Ψ is an $\tilde{m}\tilde{n} \times \tilde{n}^2$ block diagonal matrix, and Ω is an $\tilde{m}\tilde{n} \times \tilde{m}\tilde{n}$ block diagonal matrix with $\tilde{n} = n + k$ and $\tilde{m} = p\tilde{n} + 1$.

The posterior distribution of $(\tilde{A}_0, \tilde{A}_+)$ conditional on narrative sign restrictions and zero restrictions induced by exogeneity condition and block restrictions is associated with the prior distribution, $\pi(\tilde{A}_0, \tilde{A}_+)$, and likelihood function, $\pi(y^T|\tilde{A}_0, \tilde{A}_+)$, in the form of:

$$\begin{aligned}
&\pi(\tilde{A}_0, \tilde{A}_+|y^T, N(\tilde{A}_0, \tilde{A}_+, y^T) > 0_{s\times 1}, \beta(\tilde{A}_0, \tilde{A}_+) = 0_{k(n-k)\times 1}, \alpha(\tilde{A}_0, \tilde{A}_+) = 0_{kn(p+1)\times 1}) \\
\propto &\pi(y^T|\tilde{A}_0, \tilde{A}_+, N(\tilde{A}_0, \tilde{A}_+, y^T) > 0_{s\times 1}, \beta(\tilde{A}_0, \tilde{A}_+) = 0_{k(n-k)\times 1}, \alpha(\tilde{A}_0, \tilde{A}_+) = 0_{kn(p+1)\times 1})\pi(\tilde{A}_0, \tilde{A}_+) \\
\propto &\pi(y^T|\tilde{A}_0, \tilde{A}_+, N(\tilde{A}_0, \tilde{A}_+, y^T) > 0_{s\times 1}) \\
&\pi(\tilde{A}_0, \tilde{A}_+|\beta(\tilde{A}_0, \tilde{A}_+) = 0_{k(n-k)\times 1}, \alpha(\tilde{A}_0, \tilde{A}_+) = 0_{kn(p+1)\times 1}) \qquad \text{(A.2)} \\
\propto &\mathbb{I}\left\{N(\tilde{A}_0, \tilde{A}_+, y^T) > 0_{s\times 1}\right\}\left[\varpi(\tilde{A}_0, \tilde{A}_+)\right]^{-1} \\
&\pi(y^T|\tilde{A}_0, \tilde{A}_+)\pi(\tilde{A}_0, \tilde{A}_+|\beta(\tilde{A}_0, \tilde{A}_+) = 0_{k(n-k)\times 1}, \alpha(\tilde{A}_0, \tilde{A}_+) = 0_{kn(p+1)\times 1}), \qquad \text{(A.3)}
\end{aligned}$$

where $\mathbb{I}\{.\}$ is an indicator function, which takes the value of one if narrative sign restrictions are satisfied and zero otherwise. The term $\varpi(\tilde{A}_0, \tilde{A}_+)$ signifies the ex-ante probability that narrative sign restrictions are satisfied. Equation (A.2) holds because zero restrictions do not truncate the likelihood function. However, narrative sign restrictions hinge on data observations and thus may truncate likelihood. In particular, the truncated likelihood can be written as a reweighting of the likelihood function as in equation (A.3), with weights inversely proportional to $\varpi(\tilde{A}_0, \tilde{A}_+)$. Following Arias et al. (2021), we assume that the likelihood function, $\pi(y^T|\tilde{A}_0, \tilde{A}_+)$, is Gaussian so that

$$\begin{aligned}
&\pi(y^T|\tilde{A}_0, \tilde{A}_+)\pi(\tilde{A}_0, \tilde{A}_+|\beta(\tilde{A}_0, \tilde{A}_+) = 0_{k(n-k)\times 1}, \alpha(\tilde{A}_0, \tilde{A}_+) = 0_{kn(p+1)\times 1}) \\
&\begin{cases} \propto NGN_{(\tilde{v},\tilde{\Phi},\tilde{\Psi},\tilde{\Omega})}(\tilde{A}_0, \tilde{A}_+), & \text{if} \quad \beta(\tilde{A}_0, \tilde{A}_+) = 0_{k(n-k)\times 1}, \alpha(\tilde{A}_0, \tilde{A}_+) = 0_{kn(p+1)\times 1}; \\ = 0, & \text{otherwise;} \end{cases}
\end{aligned} \tag{A.4}$$

where $\tilde{v} = T + \nu$, $\tilde{\Omega} = (I_{\tilde{n}} \otimes \tilde{X}'\tilde{X} + \Omega^{-1})^{-1}$, $\tilde{\Psi} = \tilde{\Omega}(I_{\tilde{n}} \otimes \tilde{X}'\tilde{Y} + \Omega^{-1}\Psi)$, $\tilde{\Phi} = I_{\tilde{n}} \otimes \tilde{Y}'\tilde{Y} + \Phi + \Psi'\Omega^{-1}\Psi - \tilde{\Psi}'\tilde{\Omega}^{-1}\tilde{\Psi}$, $\tilde{Y} = [\ \tilde{y}_1 \ \cdots \ \tilde{y}_T\ ]'$, and $\tilde{X} = [\ \tilde{x}_1 \ \cdots \ \tilde{x}_T\ ]'$.

In practice, we do not make draws directly from the target density specified by equation (11) as the number of zero restrictions is large. Instead, we draw posteriors from a proposal distribution conditional on zero and narrative sign restrictions and then embed it in an importance sampling algorithm. Following Arias et al. (2021), we first draw the orthogonal triangular-block parameters defined by $(\tilde{\Lambda}_0, \tilde{\Lambda}_+, \text{diag}(Q_1, Q_2))$ and then map the parameters into proxy SVAR structural parameters, $(\tilde{A}_0, \tilde{A}_+)$, by

$$(\tilde{\Lambda}_0, \tilde{\Lambda}_+, \text{diag}(Q_1, Q_2)) \xrightarrow{f} (\underbrace{\tilde{\Lambda}_0 \text{diag}(Q_1, Q_2)}_{\tilde{A}_0}, \underbrace{\tilde{\Lambda}_+ \text{diag}(Q_1, Q_2)}_{\tilde{A}_+}), \tag{A.5}$$

where $\tilde{\Lambda}_0$ is an $\tilde{n} \times \tilde{n}$ matrix, $\tilde{\Lambda}_+$ is an $\tilde{m} \times \tilde{n}$ matrix, Q_1 is an $n \times n$ orthonormal matrix, and Q_2 is a $k \times k$ orthonormal matrix. To guarantee that block restrictions are satisfied, we implement the procedure of Waggoner and Zha (2003) to generate independent draws of the parameters $(\tilde{\Lambda}_0, \tilde{\Lambda}_+)$ from a restricted NGN posterior distribution characterized by $NGN_{(\hat{v},\hat{\Phi},\hat{\Psi},\hat{\Omega})}(\tilde{\Lambda}_0, \tilde{\Lambda}_+)$, where $(\hat{v}, \hat{\Phi}, \hat{\Psi}, \hat{\Omega})$ is designated to $(\tilde{v}, \tilde{\Phi}, \tilde{\Psi}, \tilde{\Omega})$, and the matrix $\tilde{\Lambda}_0$ is restricted to be upper-triangular with positive diagonal elements. The matrix $\tilde{\Lambda}'_+ = [\ \tilde{\Lambda}'_1 \ \cdots \ \tilde{\Lambda}'_p \ \ d'\ ]$ embraces a vector d and matrices $\tilde{\Lambda}'_i$ with the lower

left-hand $k \times n$ block being zero. For the orthogonal matrix $\text{diag}(Q_1, Q_2)$, we execute the Arias et al. (2018) approach to produce independent draws conditional on the zero restrictions induced by "exogeneity condition" specified by equation (7). In line with Arias et al. (2021), we make independent draws of $(\tilde{A}_0, \tilde{A}_+)$ from a proposal density conditional on zero restrictions induced by exogeneity condition and block restrictions by combining the routes of Waggoner and Zha (2003) and Arias et al. (2018) as detailed in Algorithm A.1.

Algorithm A.1 *1. Produce independent draws of the parameters $(\tilde{\Lambda}_0, \tilde{\Lambda}_+)$ from the restricted $NGN_{(\hat{v},\hat{\Phi},\hat{\Psi},\hat{\Omega})}(\tilde{\Lambda}_0, \tilde{\Lambda}_+)$ using the method of Waggoner and Zha (2003). In particular, denote $\tilde{\lambda}_{0,j}$ and $\tilde{\lambda}_{+,j}$ as the j-th columns of $\tilde{\Lambda}_0$ and $\tilde{\Lambda}_+$, respectively. $\tilde{\lambda}_{0,j}$ and $\tilde{\lambda}_{+,j}$ are of the form*

$$\tilde{\lambda}_{0,j} = U_j \gamma_{0,j} \quad \text{and} \quad \tilde{\lambda}_{+,j} = V_j \gamma_{+,j}. \tag{A.6}$$

U_j is the first j column of $I_{\tilde{n}}$. V_j is block diagonal with the first p blocks as the first n columns of $I_{\tilde{n}}$ and the last block commensurate with scalar one for $1 \leq j \leq n$ and $I_{\tilde{m}}$ for $n+1 \leq j \leq \tilde{n}$. $\gamma_{0,j}$ is random and drawn from a generalized-normal distribution with parameters $\hat{v}$ and S_j^{-1}. $\gamma_{+,j}$ is drawn conditional on $\gamma_{0,j}$ from a normal distribution with mean $P_j \gamma_{0,j}$ and variance H_j, where $H_j = (V_j' \hat{\Omega}_j^{-1} V_j)^{-1}$, $P_j = H_j V_j' \hat{\Omega}_j^{-1} \hat{\Psi}_j U_j$, and $S_j = (U_j' \hat{\Phi}_j U_j + U_j' \hat{\Psi}_j' \hat{\Omega}_j^{-1} \hat{\Psi}_j U_j - P_j' H_j^{-1} P_j)^{-1}$.

2. *For $i = 1, 2$ and $1 \leq j \leq d_i$, draw $\alpha_{i,j} \in R^{d_i - n_{i,j}}$ independently from a standard normal distribution and set $w_{i,j} = \alpha_{i,j} / \parallel \alpha_{i,j} \parallel$, where $d_1 = n$, $d_2 = k$, $n_{1,j} = k + j - 1$ for $1 \leq j \leq n - k$, $n_{1,j} = j - 1$ for $n - k + 1 \leq j \leq n$, and $n_{2,j} = j - 1$.*

3. *For $i = 1, 2$ recursively define $Q_i = [\ q_{i,1} \ \cdots \ q_{i,d_i}\ ]$ by $q_{i,j} = K_{i,j} w_{i,j}$ for any $d_i \times (d_i - n_{i,j})$ matrix $K_{i,j}$ whose columns form an orthonormal basis for the null space of the $n_{i,j} \times d_i$ matrix*

$$M_{i,j} = [\ \tilde{G}_{i,j}(\tilde{\Lambda}_0, \tilde{\Lambda}_+)' \ \ q_{i,1} \ \cdots \ q_{i,j-1}\ ]',$$

where $\tilde{G}_{i,j}(\tilde{\Lambda}_0, \tilde{\Lambda}_+)$ is $\tilde{G}_j(\tilde{\Lambda}_0, \tilde{\Lambda}_+)$ if $i = 1$ and is an empty matrix if $i = 2$, and $\tilde{G}_j(\tilde{\Lambda}_0, \tilde{\Lambda}_+)$ is $J(\tilde{\Lambda}_0^{-1})' L'$ if $1 \leq j \leq n - k$ and is an empty matrix if $n - k + 1 \leq j \leq n$.

4. *Map the resulting draws of $(\tilde{\Lambda}_0, \tilde{\Lambda}_+, diag(Q_1, Q_2))$ to the proxy SVAR structural parameters $(\tilde{A}_0, \tilde{A}_+)$ using f in (A.5).*

Arias et al. (2021) demonstrate that the proposal density of $(\tilde{A}_0, \tilde{A}_+)$ is

$$p(\tilde{A}_0, \tilde{A}_+) \propto NGN_{(\hat{v},\hat{\Phi},\hat{\Psi},\hat{\Omega})}(\tilde{\Lambda}_0, \tilde{\Lambda}_+)|\det(N'_{(\tilde{A}_0,\tilde{A}_+)}D\xi(\tilde{A}_0, \tilde{A}_+)'D\xi(\tilde{A}_0, \tilde{A}_+)N_{(\tilde{A}_0,\tilde{A}_+)})|^{1/2}, \tag{A.7}$$

where $D\xi(\tilde{A}_0, \tilde{A}_+)$ denotes the derivative of ξ evaluated at $(\tilde{A}_0, \tilde{A}_+)$, $N_{(\tilde{A}_0,\tilde{A}_+)}$ is a matrix whose columns form an orthonormal basis for the null space of $D\beta(\tilde{A}_0, \tilde{A}_+)$, $\xi = (f \circ g)^{-1}$ is a composite function of f and g with function g defined as $(\tilde{\Lambda}_0, \tilde{\Lambda}_+, w) \xrightarrow{g} (\tilde{\Lambda}_0, \tilde{\Lambda}_+, \text{diag}(Q_1, Q_2))$, and $w = (w_{1,1}, \cdots, w_{1,n}, w_{2,1}, \cdots, w_{2,k})$. To draw structural parameters from the target density, we need an additional importance sampling step with importance weights defined as the ratio between the target density and proposal density:

$$\tau_i = \frac{\left[\varpi(\tilde{A}_0, \tilde{A}_+)\right]^{-1} NGN_{(\tilde{v},\tilde{\Phi},\tilde{\Psi},\tilde{\Omega})}(\tilde{A}_0, \tilde{A}_+)}{p(\tilde{A}_0, \tilde{A}_+)}. \tag{A.8}$$

A.2 Inference under Robust Prior

Our benchmark analysis uses a uniform prior over the orthonormal matrix, reflecting a belief in equal density across observationally equivalent models when parameterized in their orthogonal reduced form. However, as pointed out by Baumeister and Hamilton (2015) and Giacomini and Kitagawa (2021), this uniform prior can inadvertently be informative about the marginal distribution of impulse responses. To address this, Giacomini and Kitagawa (2021) propose a robust prior framework that avoids specifying a particular distribution for the orthonormal matrix. This approach has been applied to proxy SVAR and narrative sign methods by Giacomini et al. (2022b) and Giacomini et al. (2023), respectively. In this section, we propose an algorithm that integrates the proxy SVAR approach from Giacomini et al. (2022b) with the narrative sign method of Giacomini et al. (2023) within a unified robust prior framework.

Unlike our benchmark framework, our posterior inference here is based on a conditional prior for the orthonormal matrix and unconditional likelihood following Giacomini et al. (2023), rather than an unconditional prior for the orthonormal matrix and conditional likelihood. This is because the robust prior approach requires an optimization step to solve for the upper and lower bounds concerning the orthonormal matrix. When historical decomposition restrictions are imposed, the unconditional prior can be revised by data, which is undesirable for the optimization step. To avoid this issue, we base our inference on a conditional prior, which, as shown below, is not revisable by

data.

We begin with the prior for $(\tilde{\Lambda}_0, \tilde{\Lambda}_+, \text{diag}(Q_1, Q_2))$:

$$\pi(\tilde{\Lambda}_0, \tilde{\Lambda}_+, \text{diag}(Q_1, Q_2)) = \pi(\tilde{\Lambda}_0, \tilde{\Lambda}_+)\pi(\text{diag}(Q_1, Q_2)|\tilde{\Lambda}_0, \tilde{\Lambda}_+). \tag{A.9}$$

Following Giacomini et al. (2023), the posterior of $(\tilde{\Lambda}_0, \tilde{\Lambda}_+, \text{diag}(Q_1, Q_2))$ under narrative sign restrictions and the zero restrictions induced by block restrictions and exogeneity conditions, is given by

$$\begin{aligned}
&\pi(\tilde{\Lambda}_0, \tilde{\Lambda}_+, \text{diag}(Q_1, Q_2)|y^T, N(\tilde{A}_0, \tilde{A}_+, y^T) > 0_{s\times 1}, \beta(\tilde{A}_0, \tilde{A}_+) = 0_{k(n-k)\times 1}, \alpha(\tilde{A}_0, \tilde{A}_+) = 0_{kn(p+1)\times 1}) \\
&\begin{cases}
\propto \pi(\tilde{\Lambda}_0, \tilde{\Lambda}_+, \text{diag}(Q_1, Q_2)|y^T, N(\tilde{A}_0, \tilde{A}_+, y^T) > 0_{s\times 1}), \quad \text{if} \quad \beta(\tilde{A}_0, \tilde{A}_+) = 0_{k(n-k)\times 1}, \\
\qquad\qquad\qquad\qquad\qquad\qquad\qquad\qquad\qquad\qquad \alpha(\tilde{A}_0, \tilde{A}_+) = 0_{kn(p+1)\times 1}; \\
= 0, \quad \text{otherwise},
\end{cases} \\
&\begin{cases}
\propto \pi(y^T, N(\tilde{A}_0, \tilde{A}_+, y^T) > 0_{s\times 1}|\tilde{\Lambda}_0, \tilde{\Lambda}_+, \text{diag}(Q_1, Q_2))\pi(\tilde{\Lambda}_0, \tilde{\Lambda}_+, \text{diag}(Q_1, Q_2)), \\
\qquad\qquad\qquad\qquad\qquad\qquad \text{if} \quad \beta(\tilde{A}_0, \tilde{A}_+) = 0_{k(n-k)\times 1}, \alpha(\tilde{A}_0, \tilde{A}_+) = 0_{kn(p+1)\times 1}; \\
= 0, \quad \text{otherwise},
\end{cases} \\
&\begin{cases}
\propto \pi(y^T|\tilde{\Lambda}_0, \tilde{\Lambda}_+)\pi(\tilde{\Lambda}_0, \tilde{\Lambda}_+)\pi(\text{diag}(Q_1, Q_2)|\tilde{\Lambda}_0, \tilde{\Lambda}_+), \quad \text{if} \quad N(\tilde{A}_0, \tilde{A}_+, y^T) > 0_{s\times 1}, \\
\qquad\qquad\qquad\qquad\qquad\qquad \beta(\tilde{A}_0, \tilde{A}_+) = 0_{k(n-k)\times 1}, \alpha(\tilde{A}_0, \tilde{A}_+) = 0_{kn(p+1)\times 1}; \\
= 0, \quad \text{otherwise},
\end{cases} \\
&\begin{cases}
\propto \pi(\tilde{\Lambda}_0, \tilde{\Lambda}_+|y^T)\pi(\text{diag}(Q_1, Q_2)|\tilde{\Lambda}_0, \tilde{\Lambda}_+), \quad \text{if} \quad N(\tilde{A}_0, \tilde{A}_+, y^T) > 0_{s\times 1}, \\
\qquad\qquad\qquad\qquad\qquad\qquad \beta(\tilde{A}_0, \tilde{A}_+) = 0_{k(n-k)\times 1}, \alpha(\tilde{A}_0, \tilde{A}_+) = 0_{kn(p+1)\times 1}; \\
= 0, \quad \text{otherwise},
\end{cases}
\end{aligned} \tag{A.10}$$

where $(\tilde{A}_0, \tilde{A}_+) = f(\tilde{\Lambda}_0, \tilde{\Lambda}_+, \text{diag}(Q_1, Q_2))$, with f as the mapping from the reduced-form parameters to the structural parameters. This formula shows that the prior of the reduced-form parameters $(\tilde{\Lambda}_0, \tilde{\Lambda}_+)$ can be revised by sample data, while the prior of the rotation matrix $\text{diag}(Q_1, Q_2)$ cannot. Rather than specifying a single prior for $(\text{diag}(Q_1, Q_2)|\tilde{\Lambda}_0, \tilde{\Lambda}_+)$, the robust Bayesian approach considers a set of all such priors, denoted as $\Pi(\text{diag}(Q_1, Q_2)|\tilde{\Lambda}_0, \tilde{\Lambda}_+)$. Using $\Pi(\text{diag}(Q_1, Q_2)|\tilde{\Lambda}_0, \tilde{\Lambda}_+)$, we obtain a class of priors for $(\tilde{\Lambda}_0, \tilde{\Lambda}_+, \text{diag}(Q_1, Q_2))$:

$\Pi(\tilde{\Lambda}_0, \tilde{\Lambda}_+, \text{diag}(Q_1, Q_2)) = \{\pi(\tilde{\Lambda}_0, \tilde{\Lambda}_+, \text{diag}(Q_1, Q_2)) = \pi(\tilde{\Lambda}_0, \tilde{\Lambda}_+)\pi(\text{diag}(Q_1, Q_2)|\tilde{\Lambda}_0, \tilde{\Lambda}_+) :$
$\pi(\text{diag}(Q_1, Q_2)|\tilde{\Lambda}_0, \tilde{\Lambda}_+) \in \Pi(\text{diag}(Q_1, Q_2)|\tilde{\Lambda}_0, \tilde{\Lambda}_+)\}$.

Combining $\Pi(\tilde{\Lambda}_0, \tilde{\Lambda}_+, \text{diag}(Q_1, Q_2))$ with the unconditional likelihood and all identification restrictions, we generate a class of posteriors for $(\tilde{\Lambda}_0, \tilde{\Lambda}_+, \text{diag}(Q_1, Q_2))$ as follows:

$$\Pi(\tilde{\Lambda}_0, \tilde{\Lambda}_+, \text{diag}(Q_1, Q_2)|y^T, N(\tilde{A}_0, \tilde{A}_+, y^T) > 0_{s\times 1}, \beta(\tilde{A}_0, \tilde{A}_+) = 0_{k(n-k)\times 1}, \alpha(\tilde{A}_0, \tilde{A}_+) = 0_{kn(p+1)\times 1})$$
$$= \Big\{\pi(\tilde{\Lambda}_0, \tilde{\Lambda}_+, \text{diag}(Q_1, Q_2)|y^T, N(\tilde{A}_0, \tilde{A}_+, y^T) > 0_{s\times 1}, \beta(\tilde{A}_0, \tilde{A}_+) = 0_{k(n-k)\times 1}, \alpha(\tilde{A}_0, \tilde{A}_+) = 0_{kn(p+1)\times 1})$$
$$\begin{cases} \propto \pi(\tilde{\Lambda}_0, \tilde{\Lambda}_+|y^T)\pi(\text{diag}(Q_1, Q_2)|\tilde{\Lambda}_0, \tilde{\Lambda}_+), \quad \text{if} \quad N(\tilde{A}_0, \tilde{A}_+, y^T) > 0_{s\times 1}, \\ \qquad\qquad\qquad\qquad\qquad\qquad \beta(\tilde{A}_0, \tilde{A}_+) = 0_{k(n-k)\times 1}, \alpha(\tilde{A}_0, \tilde{A}_+) = 0_{kn(p+1)\times 1}; \\ = 0, \quad \text{otherwise}, \end{cases}$$
$$: \pi(\text{diag}(Q_1, Q_2)|\tilde{\Lambda}_0, \tilde{\Lambda}_+) \in \Pi(\text{diag}(Q_1, Q_2)|\tilde{\Lambda}_0, \tilde{\Lambda}_+)\Big\}$$

Without loss of generality, we assume the object of interest is the impulse response of the i-th variable to the j-th shock at horizon h, denoted as $\eta_{ij,h}$. Since $\eta_{ij,h}$ can be calculated from $(\tilde{\Lambda}_0, \tilde{\Lambda}_+, \text{diag}(Q_1, Q_2))$, this impulse response can be expressed as $\eta_{ij,h}(\tilde{\Lambda}_0, \tilde{\Lambda}_+, \text{diag}(Q_1, Q_2))$.

The class of posteriors for $(\tilde{\Lambda}_0, \tilde{\Lambda}_+, \text{diag}(Q_1, Q_2))$ induces a class of posteriors for $\eta_{ij,h}(\tilde{\Lambda}_0, \tilde{\Lambda}_+, \text{diag}(Q_1, Q_2))$. Giacomini and Kitagawa (2021) suggest summarizing this class of posteriors by reporting the "set of posterior means":

$$\left[\int l(\tilde{\Lambda}_0, \tilde{\Lambda}_+)\pi(\tilde{\Lambda}_0, \tilde{\Lambda}_+ \mid y^T)d(\tilde{\Lambda}_0, \tilde{\Lambda}_+), \int u(\tilde{\Lambda}_0, \tilde{\Lambda}_+)\pi(\tilde{\Lambda}_0, \tilde{\Lambda}_+ \mid y^T)d(\tilde{\Lambda}_0, \tilde{\Lambda}_+)\right], \quad \text{(A.11)}$$

where $l(\tilde{\Lambda}_0, \tilde{\Lambda}_+) =$
$\inf_{\text{diag}(Q_1,Q_2)} \{\eta_{ij,h}(\tilde{\Lambda}_0, \tilde{\Lambda}_+, \text{diag}(Q_1, Q_2)) : \pi(\text{diag}(Q_1, Q_2)|\tilde{\Lambda}_0, \tilde{\Lambda}_+) \in \Pi(\text{diag}(Q_1, Q_2)|\tilde{\Lambda}_0, \tilde{\Lambda}_+)\}$
and $u(\tilde{\Lambda}_0, \tilde{\Lambda}_+) =$
$\sup_{\text{diag}(Q_1,Q_2)} \{\eta_{ij,h}(\tilde{\Lambda}_0, \tilde{\Lambda}_+, \text{diag}(Q_1, Q_2)) : \pi(\text{diag}(Q_1, Q_2)|\tilde{\Lambda}_0, \tilde{\Lambda}_+) \in \Pi(\text{diag}(Q_1, Q_2)|\tilde{\Lambda}_0, \tilde{\Lambda}_+)\}$.

Giacomini and Kitagawa (2021) also suggest reporting a robust credible region with credibility level α (see Proposition 1 of Giacomini and Kitagawa (2021)). This robust

credible region represents the shortest interval estimate for $\eta_{ij,h}(\tilde{\Lambda}_0, \tilde{\Lambda}_+, \text{diag}(Q_1, Q_2))$ such that the posterior probability assigned to the interval is at least α. In the following, we provide numerical algorithms to conduct robust Bayesian inference for proxy SVARs under narrative restrictions, approximating the set of posterior means and the associated robust credible interval.

Algorithm A.2 *1. Draw independent parameters $(\tilde{\Lambda}_0, \tilde{\Lambda}_+)$ using Step 1 in Algorithm A.1.*

2. *Draw parameters (Q_1, Q_2) with Steps 2-3 in Algorithm A.1. Map $(\tilde{\Lambda}_0, \tilde{\Lambda}_+, diag(Q_1, Q_2))$ to the proxy SVAR structural parameters $(\tilde{A}_0, \tilde{A}_+)$ using $(\tilde{A}_0, \tilde{A}_+) = f(\tilde{\Lambda}_0, \tilde{\Lambda}_+, diag(Q_1, Q_2))$. If $N(\tilde{A}_0, \tilde{A}_+, y^T) > 0_{s\times 1}$ is satisfied, retain (Q_1, Q_2) and proceed; Otherwise, generate new draws of (Q_1, Q_2) (up to a maximum of L times) until the narrative sign restrictions are satisfied. If no draws of (Q_1, Q_2) satisfy the restrictions after L attempts, return to Step 1 and draw new sets of reduced-form parameters.*

3. *Repeat Step 2 until K draws of (Q_1, Q_2) are obtained. Let $\{(Q_1^{(k)}, Q_2^{(k)}), k = 1, \cdots, K\}$ be the K draws of (Q_1, Q_2) that satisfy $N(\tilde{A}_0, \tilde{A}_+, y^T) > 0_{s\times 1}$. Calculate $l(\tilde{\Lambda}_0, \tilde{\Lambda}_+) = \min_k \eta_{ij,h}(\tilde{\Lambda}_0, \tilde{\Lambda}_+, diag(Q_1^{(k)}, Q_2^{(k)}))$ and $u(\tilde{\Lambda}_0, \tilde{\Lambda}_+) = \max_k \eta_{ij,h}(\tilde{\Lambda}_0, \tilde{\Lambda}_+, diag(Q_1^{(k)}, Q_2^{(k)}))$.*

4. *Repeat Steps 1-3 M times to obtain the lower and upper bounds of impulse responses conditional on reduced-form parameters, $[l(\tilde{\Lambda}_0^{(m)}, \tilde{\Lambda}_+^{(m)}), u(\tilde{\Lambda}_0^{(m)}, \tilde{\Lambda}_+^{(m)})]$ for $m = 1, \cdots, M$. Approximate the set of posterior means using the sample averages of $l(\tilde{\Lambda}_0^{(m)}, \tilde{\Lambda}_+^{(m)})$ and $u(\tilde{\Lambda}_0^{(m)}, \tilde{\Lambda}_+^{(m)})$.*

5. *To approximate the smallest robust credible region with credibility $\alpha \in (0, 1)$, we define $d(\eta, \tilde{\Lambda}_0, \tilde{\Lambda}_+) = \max\{|\eta - l(\tilde{\Lambda}_0, \tilde{\Lambda}_+)|, |\eta - u(\tilde{\Lambda}_0, \tilde{\Lambda}_+)|\}$ and let $\hat{z}_\alpha(\eta)$ be the sample α quantile of $\{d\left(\eta, \tilde{\Lambda}_0^{(m)}, \tilde{\Lambda}_+^{(m)}\right), m = 1, \ldots, M\}$. The approximated smallest robust credible interval is then centered at $\arg\min_\eta \hat{z}_\alpha(\eta)$ with a radius of $\min_\eta \hat{z}_\alpha(\eta)$.*

Algorithm A.2 approximates the intervals $[l(\tilde{\Lambda}_0, \tilde{\Lambda}_+), u(\tilde{\Lambda}_0, \tilde{\Lambda}_+)]$ at each draw of $(\tilde{\Lambda}_0, \tilde{\Lambda}_+)$ using Monte Carlo simulation. The constructed lower and upper bounds can be inaccurate when the draws of $(\text{diag}(Q_1, Q_2))$ do not span the random space. An alternative way to obtain the interval is through solving an optimization problem as in Giacomini and Kitagawa (2021) as follows:

Algorithm A.3 *In Algorithm A.2, replace step 3 with the following:*

3′. At each draw of $(\tilde{\Lambda}_0, \tilde{\Lambda}_+)$ *, compute* $[l(\tilde{\Lambda}_0, \tilde{\Lambda}_+), u(\tilde{\Lambda}_0, \tilde{\Lambda}_+)]$ *by solving the following constrained nonlinear optimization problem:*

$$l(\tilde{\Lambda}_0, \tilde{\Lambda}_+) = \arg \min_{\text{diag}(Q_1, Q_2)} \eta_{ij,h} \left(\tilde{\Lambda}_0, \tilde{\Lambda}_+, \text{diag}(Q_1, Q_2)\right),$$

$$s.t. \quad Q_1'Q_1 = I_n, \quad Q_2'Q_2 = I_k, \quad N\left(f\left(\tilde{\Lambda}_0, \tilde{\Lambda}_+, \text{diag}(Q_1, Q_2)\right)\right) > 0_{s\times 1},$$
$$\beta\left(f\left(\tilde{\Lambda}_0, \tilde{\Lambda}_+, \text{diag}(Q_1, Q_2)\right)\right) = 0_{k(n-k)\times 1}, \quad \alpha\left(f\left(\tilde{\Lambda}_0, \tilde{\Lambda}_+, \text{diag}(Q_1, Q_2)\right)\right) = 0_{kn(p+1)\times 1},$$

and

$$u(\tilde{\Lambda}_0, \tilde{\Lambda}_+) = \arg \max_{\text{diag}(Q_1, Q_2)} \eta_{ij,h} \left(\tilde{\Lambda}_0, \tilde{\Lambda}_+, \text{diag}(Q_1, Q_2)\right)$$

under the same set of constraints.

A.3 Joint Inference with a Uniform Prior for Impulse Responses

Arias et al. (2024) introduce a complementary alternative to the robust prior framework for researchers aiming to perform posterior inference without favoring any specific vector of impulse responses a priori. The authors demonstrate that a uniform prior over orthogonal matrices is both sufficient and necessary for inference based on a uniform joint prior distribution over the identified set of impulse responses. Additionally, they propose a method for conducting inference under traditional sign restrictions.

However, the Arias et al. (2024) framework cannot be directly applied to our approach due to the zero restrictions imposed by proxy exogeneity assumptions and narrative sign restrictions. In this section, we outline a method to perform joint inference under these identification restrictions using uniform priors over impulse responses, necessitating an additional importance sampling step. This method is applicable to any identification strategy that involves zero, traditional sign, and narrative sign restrictions.

We use the same notations as in our benchmark analysis. Focusing on the posterior distribution of impulse responses, we consider the impulse response parameterization of the SVAR model. It is defined as $\left(\tilde{L}_0, \cdots, \tilde{L}_p, \tilde{c}\right)$, where the element in row i and column j of the $\tilde{n} \times \tilde{n}$ matrix $\tilde{L}_k$ represents the impulse response of the i-th variable to the j-th structural shock at horizon h_k. The matrices $\tilde{L}_k$ are functions of the structural parameters and are defined recursively as follows:

$$\tilde{L}_0 = \left(\tilde{A}_0^{-1}\right)', \tag{A.12}$$

and

$$\tilde{L}_k = \sum_{\ell=1}^{k} \left(\tilde{A}_\ell \tilde{A}_0^{-1} \right)' \tilde{L}_{k-\ell}, \tag{A.13}$$

for $1 \leq k \leq p$. The matrices $\tilde{A}_k$ are in turn the inverse functions of the impulse response parameterization and are recursively defined as

$$\tilde{A}_0 = \left(\tilde{L}_0^{-1} \right)', \tag{A.14}$$

and

$$\tilde{A}_k = \left(\tilde{L}_k \tilde{L}_0^{-1} \right)' \tilde{A}_0 - \sum_{\ell=1}^{k-1} \left(\tilde{L}_{k-\ell} \tilde{L}_0^{-1} \right)' \tilde{A}_\ell, \tag{A.15}$$

for $1 \leq k \leq p$.

Let $\tilde{L}_+' = \begin{bmatrix} \tilde{L}_1' & \cdots & \tilde{L}_p' & \tilde{c}' \end{bmatrix}$. The impulse response parameterization can be represented as $\left(\tilde{L}_0, \tilde{L}_+\right)$. The mapping from the structural parameterization to the impulse response parameterization is denoted by function h, defined as:

$$(\tilde{A}_0, \tilde{A}_+) \xrightarrow{h} (\tilde{L}_0, \tilde{L}_+). \tag{A.16}$$

The inverse mapping is given by:

$$(\tilde{L}_0, \tilde{L}_+) \xrightarrow{h^{-1}} (\tilde{A}_0, \tilde{A}_+). \tag{A.17}$$

Accordingly, the narrative sign restrictions, zero restrictions induced by block restrictions, and zero restrictions from the IV exogeneity conditions can be represented as functions of impulse responses and data observations: $N\left(h^{-1}\left(\tilde{L}_0, \tilde{L}_+\right), y^T\right) > 0_{s\times 1}$, $\beta\left(h^{-1}\left(\tilde{L}_0, \tilde{L}_+\right)\right) = 0_{k(n-k)\times 1}$, and $\alpha\left(h^{-1}\left(\tilde{L}_0, \tilde{L}_+\right)\right) = 0_{kn(p+1)\times 1}$.

We impose a uniform prior distribution for $(\tilde{L}_0, \tilde{L}_+)$:

$$\pi(\tilde{L}_0, \tilde{L}_+) \propto 1. \tag{A.18}$$

The posterior distribution of $(\tilde{L}_0, \tilde{L}_+)$, conditional on narrative sign restrictions and zero restrictions induced by exogeneity condition and block restrictions is associated with the

prior distribution, $\pi(\tilde{L}_0, \tilde{L}_+)$, and likelihood function, $\pi\left(y^T|h^{-1}\left(\tilde{L}_0, \tilde{L}_+\right)\right)$, expressed as:

$$\begin{aligned}
&\pi\left(\tilde{L}_0, \tilde{L}_+|y^T, N\left(h^{-1}\left(\tilde{L}_0, \tilde{L}_+\right), y^T\right) > 0_{s\times 1}, \beta\left(h^{-1}\left(\tilde{L}_0, \tilde{L}_+\right)\right) = 0_{k(n-k)\times 1}, \alpha\left(h^{-1}\left(\tilde{L}_0, \tilde{L}_+\right)\right) = 0_{kn(p+1)\times 1}\right) \\
\propto &\pi\left(y^T|h^{-1}\left(\tilde{L}_0, \tilde{L}_+\right), N\left(h^{-1}\left(\tilde{L}_0, \tilde{L}_+\right), y^T\right) > 0_{s\times 1}, \beta\left(h^{-1}\left(\tilde{L}_0, \tilde{L}_+\right)\right) = 0_{k(n-k)\times 1}, \alpha\left(h^{-1}\left(\tilde{L}_0, \tilde{L}_+\right)\right) = 0_{kn(p+1)\times 1}\right) \pi(\tilde{L}_0, \tilde{L}_+) \\
\propto &\pi\left(y^T|h^{-1}\left(\tilde{L}_0, \tilde{L}_+\right), N\left(h^{-1}\left(\tilde{L}_0, \tilde{L}_+\right), y^T\right) > 0_{s\times 1}, \beta\left(h^{-1}\left(\tilde{L}_0, \tilde{L}_+\right)\right) = 0_{k(n-k)\times 1}, \alpha\left(h^{-1}\left(\tilde{L}_0, \tilde{L}_+\right)\right) = 0_{kn(p+1)\times 1}\right).
\end{aligned} \tag{A.19}$$

Thus, the posterior distribution of $(\tilde{L}_0, \tilde{L}_+)$ is proportional to the conditional likelihood function. The target density of the posterior of $(\tilde{L}_0, \tilde{L}_+)$ can be formulated by:

$$\begin{aligned}
&\pi\left(\tilde{L}_0, \tilde{L}_+|y^T, N\left(h^{-1}\left(\tilde{L}_0, \tilde{L}_+\right), y^T\right) > 0_{s\times 1}, \beta\left(h^{-1}\left(\tilde{L}_0, \tilde{L}_+\right)\right) = 0_{k(n-k)\times 1}, \alpha\left(h^{-1}\left(\tilde{L}_0, \tilde{L}_+\right)\right) = 0_{kn(p+1)\times 1}\right) \\
&\begin{cases}
\propto \left[\varpi\left(h^{-1}\left(\tilde{L}_0, \tilde{L}_+\right)\right)\right]^{-1} NGN_{(\tilde{v}^*, \tilde{\Phi}^*, \tilde{\Psi}^*, \tilde{\Omega}^*)}\left(h^{-1}\left(\tilde{L}_0, \tilde{L}_+\right)\right), & \text{if} \quad N\left(h^{-1}\left(\tilde{L}_0, \tilde{L}_+\right), y^T\right) > 0_{s\times 1}, \\
\qquad\qquad\qquad\qquad\qquad\qquad\qquad\qquad\qquad\qquad \beta\left(h^{-1}\left(\tilde{L}_0, \tilde{L}_+\right)\right) = 0_{k(n-k)\times 1}, \alpha\left(h^{-1}\left(\tilde{L}_0, \tilde{L}_+\right)\right) = 0_{kn(p+1)\times 1}; \\
= 0, \quad \text{otherwise},
\end{cases}
\end{aligned} \tag{A.20}$$

where $\tilde{v}^* = T + \tilde{n}$, $\tilde{\Omega}^* = (I_{\tilde{n}} \otimes \tilde{X}'\tilde{X})^{-1}$, $\tilde{\Psi}^* = \tilde{\Omega}^*(I_{\tilde{n}} \otimes \tilde{X}'\tilde{Y})$, and $\tilde{\Phi}^* = I_{\tilde{n}} \otimes \tilde{Y}'\tilde{Y} - \tilde{\Psi}^{*\prime}\tilde{\Omega}^{*^{-1}}\tilde{\Psi}^*$.

As in our benchmark case, we cannot draw directly from the target density as the domain of the target density has been truncated by the imposed restrictions. Instead, we generate posterior samples from a proposal distribution that is conditioned on the zero and narrative sign restrictions, which we then incorporate into an importance sampling algorithm. We use Algorithm 1 in the main text to draw reduced-form parameters $(\tilde{\Lambda}_0, \tilde{\Lambda}_+, w)$, and subsequently map these draws to $(\tilde{L}_0, \tilde{L}_+)$ as follows:

$$(\tilde{\Lambda}_0, \tilde{\Lambda}_+, w) \xrightarrow{g\circ f\circ h} (\tilde{L}_0, \tilde{L}_+). \tag{A.21}$$

The proposal density for $(\tilde{L}_0, \tilde{L}_+)$ is given by:

$$p(\tilde{L}_0, \tilde{L}_+) \propto NGN_{(\hat{v}^*, \hat{\Phi}^*, \hat{\Psi}^*, \hat{\Omega}^*)}(\tilde{\Lambda}_0, \tilde{\Lambda}_+)|\det(N^{*\prime}_{(\tilde{L}_0, \tilde{L}_+)} D\xi^*(\tilde{L}_0, \tilde{L}_+)' D\xi^*(\tilde{L}_0, \tilde{L}_+) N^*_{(\tilde{L}_0, \tilde{L}_+)})|^{1/2}, \tag{A.22}$$

where $D\xi^*(\tilde{L}_0, \tilde{L}_+)$ represents the derivative of ξ^* evaluated at $(\tilde{L}_0, \tilde{L}_+)$, $N^*_{(\tilde{L}_0, \tilde{L}_+)}$ is a matrix whose columns form an orthonormal basis for the null space of $D\beta\left(h^{-1}\left(\tilde{L}_0, \tilde{L}_+\right)\right)$, $\xi^* = (g \circ f \circ h)^{-1}$ is a composite function. The selection of $(\hat{v}^*, \hat{\Phi}^*, \hat{\Psi}^*, \hat{\Omega}^*)$ is critical. In practice, these parameters can be chosen to maximize the effective sample size of the importance sampler.

To draw $(\tilde{L}_0, \tilde{L}_+)$ from the target density, we perform an importance sampling step,

with importance weights defined as the ratio between the target density and the proposal density:

$$\tau_i^* = \frac{\left[\varpi\left(h^{-1}\left(\tilde{L}_0, \tilde{L}_+\right)\right)\right]^{-1} NGN_{(\tilde{\nu}^*, \tilde{\Phi}^*, \tilde{\Psi}^*, \tilde{\Omega}^*)}\left(h^{-1}\left(\tilde{L}_0, \tilde{L}_+\right)\right)}{p(\tilde{L}_0, \tilde{L}_+)}. \tag{A.23}$$

The following algorithm can draw posterior samples of the impulse responses. The key difference from Algorithm 1 in the main text is the variation in the importance sampling weight.

1. **Algorithm A.4** *1. Use Algorithm A.1 to independently draw $(\tilde{\Lambda}_0, \tilde{\Lambda}_+, w)$. Map the resulting draws of $(\tilde{\Lambda}_0, \tilde{\Lambda}_+, w)$ to $(\tilde{L}_0, \tilde{L}_+)$.*

   2. *Check whether $N\left(h^{-1}\left(\tilde{L}_0, \tilde{L}_+\right), y^T\right) > 0_{s\times 1}$ is satisfied.*

   3. *If not, discard the draw. Otherwise, calculate $\varpi\left(h^{-1}\left(\tilde{L}_0, \tilde{L}_+\right)\right)$ as follows:*

      (a) Simulate M independent draws of $\tilde{\varepsilon}_t$ from the standard normal distribution.

      (b) Approximate $\varpi\left(h^{-1}\left(\tilde{L}_0, \tilde{L}_+\right)\right)$ by the proportion of the M draws that satisfy $N\left(h^{-1}\left(\tilde{L}_0, \tilde{L}_+\right), y^T\right) > 0_{s\times 1}$.

   4. *Return to Step 1 until the required number of draws has been obtained.*

   5. *Re-sample $(\tilde{L}_0, \tilde{L}_+)$ with replacement using the importance weights in equation (A.23).*

After generating the samples, we can present the marginal distribution of the impulse responses using pointwise credible sets or conduct joint inference following the approach of Inoue and Kilian (2022) and Arias et al. (2024). We reiterate the steps as follows. Let ϑ represent the n^{irf}-dimensional vector of unknown impulse responses, obtained by appropriately stacking the impulse responses of interest. Let $L(\vartheta, \bar{\vartheta})$ denote a loss function, where $\bar{\vartheta}$ is an $n^{irf} \times 1$ vector. Following Inoue and Kilian (2022), we use an absolute loss function, defined as:

$$L(\vartheta, \bar{\vartheta}) = \sum_{j=1}^{n^{irf}} \left|\vartheta_j - \bar{\vartheta}_j\right|,$$

where ϑ_j and $\bar{\vartheta}_j$ are the j-th elements of ϑ and $\bar{\vartheta}$, respectively. The estimator of the impulse responses ϑ is given by:

$$\widehat{\bar{\vartheta}}_M = \underset{\bar{\vartheta} \in \widehat{\vartheta}_M}{\operatorname{argmin}} \frac{1}{M} \sum_{i=1}^{M} L\left(\vartheta^{(i)}, \bar{\vartheta}\right), \tag{A.24}$$

where M is the number of posterior draws, $\widehat{\vartheta}_M$ consists of M posterior draws of the impulse responses ϑ, and $\vartheta^{(i)}$ is the i-th posterior draw.

Following Inoue and Kilian (2022), we define the $(1-\alpha)100\%$ joint credible set based on the loss function $L(\vartheta, \bar{\vartheta})$ as:

$$\widehat{\Theta}_{1-\alpha,L} = \left\{\bar{\vartheta} \in \vartheta : E_\vartheta(L(\vartheta, \bar{\vartheta})) \leq c_{1-\alpha,L}\right\}, \tag{A.25}$$

where $c_{1-\alpha,L}$ is the smallest number such that the posterior probability of $\widehat{\Theta}_{1-\alpha,L}$ is $1-\alpha$. In practice, the joint credible set in (A.25) is constructed by sorting $\frac{1}{M}\sum_{i=1}^{M} L\left(\vartheta^{(i)}, \vartheta^{(1)}\right)$, $\frac{1}{M}\sum_{i=1}^{M} L\left(\vartheta^{(i)}, \vartheta^{(2)}\right)$, …, $\frac{1}{M}\sum_{i=1}^{M} L\left(\vartheta^{(i)}, \vartheta^{(M)}\right)$ in ascending order and retaining the first $(1-\alpha)100\%$ draws, starting with the draw with the lowest value.

B Mathematical Illustration of How Narrative Information Aids Identification

This section demonstrates how combining proxy exogeneity with narrative sign restrictions can enhance shock identification, utilizing the data-generating processes outlined in Section 3 of the main text. We focus mainly on shock-sign restrictions for analytical tractability, though some insights discussed in this section also apply to other types of narrative sign restrictions. It is important to note that this section focuses exclusively on shock identification, and all discussions are conditional on the given reduced-form parameters.

In Section B.1, we derive the admissible set of rotation angles that satisfy both shock-sign and IV exogeneity restrictions. Section B.2 investigates the role of proxy exogeneity restrictions in recovering the true shocks, both when the IVs are valid and when they are not, and examines how identification performance may be compromised when IV exogeneity restrictions are violated. Finally, in Section B.3, we evaluate the role of shock-sign restrictions in sharpening the inferences. We also demonstrate that the sharpness of shock-sign restrictions differs across periods with varying true shock sizes. The restrictions are sharper when being imposed on periods with smaller true shocks.

B.1 General Analysis of the Admissible Set of Rotation Angles

We start by augmenting the SVAR model (Equation 15 in the main text) model with the IV generating process (Equation 16) as:

$$\underbrace{\begin{bmatrix} y_{1t} \\ y_{2t} \\ y_{3t} \\ m_{1t} \\ m_{2t} \end{bmatrix}}_{\tilde{y}_t} = \underbrace{\begin{bmatrix} b_{11} & b_{12} & b_{13} & 0 & 0 \\ b_{21} & b_{22} & b_{23} & 0 & 0 \\ b_{31} & b_{32} & b_{33} & 0 & 0 \\ 0 & 1 & \theta_1 & \xi_1 & 0 \\ 0 & \theta_2 & 1 & 0 & \xi_2 \end{bmatrix}}_{\tilde{B}} \underbrace{\begin{bmatrix} \varepsilon_{1t} \\ \varepsilon_{2t} \\ \varepsilon_{3t} \\ v_{1t} \\ v_{2t} \end{bmatrix}}_{\tilde{\varepsilon}_t}. \tag{B.1}$$

The SVAR shock identification is formulated as:

$$\underbrace{\begin{bmatrix} y_{1t} \\ y_{2t} \\ y_{3t} \\ m_{1t} \\ m_{2t} \end{bmatrix}}_{\tilde{y}_t} = \underbrace{\begin{bmatrix} \sigma_{11} & 0 & 0 & 0 & 0 \\ \sigma_{21} & \sigma_{22} & 0 & 0 & 0 \\ \sigma_{31} & \sigma_{32} & \sigma_{33} & 0 & 0 \\ \sigma_{41} & \sigma_{42} & \sigma_{43} & \sigma_{44} & 0 \\ \sigma_{51} & \sigma_{52} & \sigma_{53} & \sigma_{54} & \sigma_{55} \end{bmatrix}}_{\Sigma_{tr}} \underbrace{\begin{bmatrix} q_{11} & q_{12} & q_{13} & 0 & 0 \\ q_{21} & q_{22} & q_{23} & 0 & 0 \\ q_{31} & q_{32} & q_{33} & 0 & 0 \\ 0 & 0 & 0 & q_{44} & q_{45} \\ 0 & 0 & 0 & q_{54} & q_{55} \end{bmatrix}}_{Q} \underbrace{\begin{bmatrix} \varepsilon^*_{1t} \\ \varepsilon^*_{2t} \\ \varepsilon^*_{3t} \\ v^*_{1t} \\ v^*_{2t} \end{bmatrix}}_{\tilde{\varepsilon}^*_t}, \tag{B.2}$$

where Σ_{tr} is the lower-triangular Cholesky factor (with positive diagonal elements) of $\Sigma = \tilde{B}\tilde{B}'$, Q is an orthonormal matrix, and $\tilde{\varepsilon}^*_t$ is the SVAR-identified structural shocks.

The "exogeneity condition" requires both IVs to be uncorrelated with ε^*_{1t} as expressed by:

$$\sigma_{41}q_{11} + \sigma_{42}q_{21} + \sigma_{43}q_{31} = 0, \tag{B.3}$$

and

$$\sigma_{51}q_{11} + \sigma_{52}q_{21} + \sigma_{53}q_{31} = 0. \tag{B.4}$$

In addition, the rotation matrix Q is orthonormal so that:

$$q^2_{11} + q^2_{21} + q^2_{31} = 1. \tag{B.5}$$

Without loss of generality, we apply the "sign normalization" condition $q_{11} > 0$, which ensures that the impact response of y_{1t} to ε_{1t} is positive. We can determine the values of q_{11}, q_{21} and q_{31} conditional on the (estimated) variance-covariance matrix using Equations (B.3), (B.4), (B.5), and the sign normalization condition. Thus, the IV exogeneity restriction allows us to point-identify the untargeted shock, ε^*_{1t}, in a model with three endogenous variables and two proxies. In a general SVAR model with more endogenous variables, proxy exogeneity restrictions may not exactly identify the untargeted shocks. However, they would effectively distinguish between targeted and untargeted shocks. The role of narrative sign restrictions is to differentiate between the targeted shocks.

Given the above discussion, we express the shock identification by rewriting Equation (B.2) as follows:

$$\underbrace{\begin{bmatrix} y_{1t} \\ y_{2t} \\ y_{3t} \\ m_{1t} \\ m_{2t} \end{bmatrix}}_{\tilde{y}_t} = \underbrace{\begin{bmatrix} \sigma_{11} & 0 & 0 & 0 & 0 \\ \sigma_{21} & \sigma_{22} & 0 & 0 & 0 \\ \sigma_{31} & \sigma_{32} & \sigma_{33} & 0 & 0 \\ \sigma_{41} & \sigma_{42} & \sigma_{43} & \sigma_{44} & 0 \\ \sigma_{51} & \sigma_{52} & \sigma_{53} & \sigma_{54} & \sigma_{55} \end{bmatrix}}_{\Sigma_{tr}} \underbrace{\begin{bmatrix} q_{11} & \tilde{q}_{11} & \tilde{q}_{12} & 0 & 0 \\ q_{21} & \tilde{q}_{21} & \tilde{q}_{22} & 0 & 0 \\ q_{31} & \tilde{q}_{31} & \tilde{q}_{32} & 0 & 0 \\ 0 & 0 & 0 & 1 & 0 \\ 0 & 0 & 0 & 0 & 1 \end{bmatrix}}_{M} \underbrace{\begin{bmatrix} 1 & 0 & 0 & 0 & 0 \\ 0 & q^*_{11} & q^*_{12} & 0 & 0 \\ 0 & q^*_{21} & q^*_{22} & 0 & 0 \\ 0 & 0 & 0 & q_{44} & q_{45} \\ 0 & 0 & 0 & q_{54} & q_{55} \end{bmatrix}}_{\tilde{Q}} \underbrace{\begin{bmatrix} \varepsilon^*_{1t} \\ \varepsilon^*_{2t} \\ \varepsilon^*_{3t} \\ v^*_{1t} \\ v^*_{2t} \end{bmatrix}}_{\tilde{\varepsilon}^*_t}$$

$$= \underbrace{\begin{bmatrix} \tilde{\sigma}_{11} & \tilde{\sigma}_{12} & \tilde{\sigma}_{13} & 0 & 0 \\ \tilde{\sigma}_{21} & \tilde{\sigma}_{22} & \tilde{\sigma}_{23} & 0 & 0 \\ \tilde{\sigma}_{31} & \tilde{\sigma}_{32} & \tilde{\sigma}_{33} & 0 & 0 \\ 0 & \tilde{\sigma}_{42} & \tilde{\sigma}_{43} & \tilde{\sigma}_{44} & \tilde{\sigma}_{45} \\ 0 & \tilde{\sigma}_{52} & \tilde{\sigma}_{53} & \tilde{\sigma}_{54} & \tilde{\sigma}_{55} \end{bmatrix}}_{\Sigma^M_{tr}} \underbrace{\begin{bmatrix} 1 & 0 & 0 & 0 & 0 \\ 0 & q^*_{11} & q^*_{12} & 0 & 0 \\ 0 & q^*_{21} & q^*_{22} & 0 & 0 \\ 0 & 0 & 0 & q_{44} & q_{45} \\ 0 & 0 & 0 & q_{54} & q_{55} \end{bmatrix}}_{\tilde{Q}} \underbrace{\begin{bmatrix} \varepsilon^*_{1t} \\ \varepsilon^*_{2t} \\ \varepsilon^*_{3t} \\ v^*_{1t} \\ v^*_{2t} \end{bmatrix}}_{\tilde{\varepsilon}^*_t}, \tag{B.6}$$

where the first equation rotates the Cholesky factor, Σ_{tr}, with a rotation matrix M, to impose the proxy exogeneity restrictions. The first column of M is solved by Equations (B.3), (B.4), and (B.5). The second equation further identifies the targeted shocks, ε^*_{2t} and ε^*_{3t}, by rotating the second and third columns of the candidate impact matrix, Σ^M_{tr}, with an orthonormal matrix, $\tilde{Q}$. The structure of matrix $\tilde{Q}$ enables us to identify the targeted shocks using additional restriction without affecting the identification of ε^*_{1t}. This clearly illustrates how exogeneity restrictions aid in identification. Without these restrictions, we would need to determine the 3×3 upper-left submatrix of Q in Equation (B.2). With the exogeneity restrictions, we only need to pin down the 2×2 submatrix of $\tilde{Q}$, defined as:

$$Q^* = \begin{bmatrix} q^*_{11} & q^*_{12} \\ q^*_{21} & q^*_{22} \end{bmatrix}. \tag{B.7}$$

We apply the "sign normalization" that the diagonal elements of the orthonormal matrix Q^* are non-negative. Then, we can specify Q^* as

$$Q^* = \left\{ \begin{bmatrix} \cos\theta & -\sin\theta \\ \sin\theta & \cos\theta \end{bmatrix} : \theta \in [-\pi/2, \pi/2] \right\}, \tag{B.8}$$

where θ is known as the rotation angle in the literature.

To evaluate the implementation of shock-sign restrictions, we express the identified SVAR shocks as functions of data observations and parameters by rewriting Equation (B.6) as follows:

$$\tilde{\varepsilon}_t^* = \tilde{Q}'(\Sigma_{tr}^M)^{-1}\tilde{y}_t. \tag{B.9}$$

Applying the rotation angle in Equation (B.8), we express the "shock-sign restriction" that ε_{2i}^* is positive for selected periods $i \in \{1, 2, ..., T\}$ as:

$$\varepsilon_{2i}^* = e_2'\tilde{Q}'(\Sigma_{tr}^M)^{-1}\tilde{y}_i = \cos\theta\,(a_{21}y_{1i} + a_{22}y_{2i} + a_{23}y_{3i}) + \sin\theta\,(a_{31}y_{1i} + a_{32}y_{2i} + a_{33}y_{3i}) > 0,$$

where e_2 is the selection vector, and a_{ij} is the element in the i-th row and j-th column of the matrix $(\Sigma_{tr}^M)^{-1}$. Similarly, we express the "shock-sign restriction" that ε_{3j}^* is positive for selected periods $j \in \{1, 2, ..., T\}$ as:

$$\varepsilon_{3j}^* = e_3'\tilde{Q}'(\Sigma_{tr}^M)^{-1}\tilde{y}_j = -\sin\theta\,(a_{21}y_{1j} + a_{22}y_{2j} + a_{23}y_{3j}) + \cos\theta\,(a_{31}y_{1j} + a_{32}y_{2j} + a_{33}y_{3j}) > 0.$$

Thus, the admission set of the rotation angles with both shock-sign and proxy exogeneity restrictions is expressed as:

$$\theta \in \left\{\theta : h_{1i}\cos\theta + h_{2i}\sin\theta > 0, -h_{1j}\sin\theta + h_{2j}\cos\theta > 0, \theta \in [-\pi/2, \pi/2]\right\}, \tag{B.10}$$

for selected periods i and j, where $h_{1i} = a_{21}y_{1i} + a_{22}y_{2i} + a_{23}y_{3i}$ and $h_{2i} = a_{31}y_{1i} + a_{32}y_{2i} + a_{33}y_{3i}$.

B.2 The Role of Proxy Exogeneity Restrictions in Shock Identification

The previous section discussed how proxy exogeneity restrictions may point-identify the untargeted shock. In this section, we further explore how these restrictions recover shocks in both cases where the IVs are valid and invalid. In subsection B.2.1, we demonstrate that proxy exogeneity restrictions not only point-identify the untargeted shocks but also perfectly recover the true shocks when the IVs are valid. Conversely, in the case of weak IVs, we illustrate that proxy exogeneity restrictions fail to effectively separate targeted from untargeted shocks. In subsection B.2.2, we show that when the IVs are not exogenous, proxy exogeneity restrictions can introduce bias into shock identification, with the degree of bias increasing to the severity of the violation.

To show the main idea intuitively, we can use a metaphor to compare macro shock identification to dividing a cake. The task of shock identification is to attribute data observations to the correct exogenous shocks. If we think of the data as a whole cake, the proxy exogeneity restrictions are like the first cut, dividing the "cake" between these contributed by targeted and untargeted shocks. If the first cut is precise, meaning the IVs are valid, then dividing the rest of the cake with additional restrictions becomes easier than dividing the whole cake. However, if the first cut is flawed due to a violation of the exogeneity restrictions, no matter how one makes the second cut (to separate between the targeted shocks) with additional identification restrictions, she won't be able to correctly separate the pieces, as the initial cut was incorrect.

B.2.1 (Strong and Weak) Exogenous IVs

We begin by characterizing the relationship between the SVAR-identified shocks, ε^*_{it}, and the true shocks, ε_{it}, by combining Equations (B.1) and (B.9):

$$\tilde{\varepsilon}^*_t = Q'\Sigma_{tr}^{-1}\tilde{B}\tilde{\varepsilon}_t. \tag{B.11}$$

To simplify the expression, we denote the orthonormal coefficient matrix as $D = Q'\Sigma_{tr}^{-1}\tilde{B}$ so that:

$$\begin{bmatrix} \varepsilon^*_{1t} \\ \varepsilon^*_{2t} \\ \varepsilon^*_{3t} \end{bmatrix} = \underbrace{\begin{bmatrix} d_{11} & d_{12} & d_{13} \\ d_{21} & d_{22} & d_{23} \\ d_{31} & d_{32} & d_{33} \end{bmatrix}}_{D} \begin{bmatrix} \varepsilon_{1t} \\ \varepsilon_{2t} \\ \varepsilon_{3t} \end{bmatrix}. \tag{B.12}$$

where each diagonal element of the orthonormal matrix D, d_{ii}, captures the correlation between each true shock, ε_{it}, and its SVAR-identified counterpart, ε^*_{it}, for $i = 1, 2, 3$. Accordingly, the "exogeneity condition" is represented by:

$$E(\varepsilon^*_{1t} m_{1t}) = E((d_{11}\varepsilon_{1t} + d_{12}\varepsilon_{2t} + d_{13}\varepsilon_{3t}) m_{1t}) = E((d_{12}\varepsilon_{2t} + d_{13}\varepsilon_{3t}) m_{1t}) = 0, \tag{B.13}$$

and

$$E(\varepsilon^*_{1t} m_{2t}) = E((d_{11}\varepsilon_{1t} + d_{12}\varepsilon_{2t} + d_{13}\varepsilon_{3t}) m_{2t}) = E((d_{12}\varepsilon_{2t} + d_{13}\varepsilon_{3t}) m_{2t}) = 0. \tag{B.14}$$

Given that matrix D is orthonormal, we have

$$d_{11}^2 + d_{12}^2 + d_{13}^2 = 1. \tag{B.15}$$

In cases of strong IVs, we can solve that $d_{11} = 1$, $d_{12} = 0$ and $d_{13} = 0$ by combining Equations (B.13), (B.14), (B.15) and the sign normalization condition. As $\varepsilon^*_{1t} = \varepsilon_{1t}$, the untargeted shock, ε_{1t}, is not only point-identified but also perfectly recovered conditional on given reduced-form parameters. Correctly distinguishing between targeted and untargeted shocks is crucial for accurately identifying the targeted shocks. If the exogeneity conditions do not effectively separate the two sets of shocks, the targeted shocks may be misidentified and confounded with the untargeted shocks.

When the relevance assumption of the IVs is violated, we have $E(\varepsilon_{2t} m_{1t}) = E(\varepsilon_{3t} m_{1t}) = 0$ and $E(\varepsilon_{2t} m_{2t}) = E(\varepsilon_{3t} m_{2t}) = 0$. In this situation, the proxy exogeneity restrictions do not help identify the untargeted shocks, as Equations (B.13) and (B.14) hold for any values of d_{12} and d_{13}. The theoretical macroeconometrics literature typically defines weak IVs as those for which $E(\varepsilon_{2t} m_{1t}) = E(\varepsilon_{3t} m_{1t}) = 0$ and $E(\varepsilon_{2t} m_{2t}) = E(\varepsilon_{3t} m_{2t}) = 0$ asymptotically hold (Giacomini et al. 2022b Arias et al. 2024). Thus, the identification of untargeted shocks does not hold in the limit. In small samples, the correlations between IVs and true shocks are close to zero due to large measurement errors, leading to significant uncertainty in the estimation of d_{11}, d_{12}, and d_{13}.

In the main text, we also discuss another case of weak IVs, where the two IVs share the same principal component. In this case, $E(\varepsilon_{2t} m_{1t}) / E(\varepsilon_{3t} m_{1t}) = E(\varepsilon_{2t} m_{2t}) / E(\varepsilon_{3t} m_{2t})$, which makes Equations (B.13) and (B.14) equivalent. Again, the exogeneity restriction fails to solve a unique set of d_{12} and d_{13} and cannot determine the untargeted shocks.

B.2.2 Endogenous IVs

This subsection examines the identification performance when the IV exogeneity assumption is violated. Specifically, we assume that the IVs are correlated not only with the targeted shocks (ε_{2t} and ε_{3t}) but also with the untargeted shock (ε_{1t}). We demonstrate that when the exogeneity assumption is not satisfied, the true shocks cannot be fully recovered. There exists an upper bound on the correlation between the true targeted shocks and the corresponding SVAR shocks, which decreases as the IVs become more correlated with the untargeted shock.

The intuition is as follows: The untargeted shocks remain point-identified even with the exogeneity assumption violated. However, the true untargeted shocks cannot be perfectly recovered. The correlation between the true and identified untargeted shocks decreases as the IVs become more correlated with the untargeted shock. This occurs because the identified untargeted shock becomes confounded with the targeted shocks, leading to an incorrect distinction between them. As a result, no matter how the additional restrictions are imposed, there is an upper bound on the correlation between the identified and true targeted shocks, as the differentiation between the targeted and untargeted shocks is fundamentally flawed by the invalid IV. In the following, we demonstrate the idea by mathematically deriving the expression of the upper bounds. The process generating the IVs is described as follows:

$$\begin{bmatrix} m_{1t} \\ m_{2t} \end{bmatrix} = \begin{bmatrix} 1 & \theta_1 \\ \theta_2 & 1 \end{bmatrix} \begin{bmatrix} \varepsilon_{2t} \\ \varepsilon_{3t} \end{bmatrix} + \begin{bmatrix} \delta_1 \varepsilon_{1t} \\ \delta_2 \varepsilon_{1t} \end{bmatrix} + \begin{bmatrix} \xi_1 v_{1t} \\ \xi_2 v_{2t} \end{bmatrix}. \tag{B.16}$$

Parameters δ_1 and δ_2 control the severity of endogeneity issue conditional on other parameters, represented by the correlation between the IVs and the untargeted shocks. Without loss of generality, we assume that δ_1 and δ_2 are positive, though the analysis in this section holds even if these parameters are negative. It should be noted that all the analysis in this subsection assumes the IVs are not strictly weak, meaning $\theta_1\theta_2 \neq 1$.

To facilitate analysis, we rewrite Equation (B.17) that describes the relationship between SVAR-identified and true shocks as:

$$\begin{bmatrix} \varepsilon^*_{1t} \\ \varepsilon^*_{2t} \\ \varepsilon^*_{3t} \end{bmatrix} = \underbrace{\begin{bmatrix} d_{11} & d_{12} & d_{13} \\ d_{21} & d_{22} & d_{23} \\ d_{31} & d_{32} & d_{33} \end{bmatrix}}_{D} \begin{bmatrix} \varepsilon_{1t} \\ \varepsilon_{2t} \\ \varepsilon_{3t} \end{bmatrix}, \tag{B.17}$$

where each diagonal element of the orthonormal matrix D, d_{ii}, captures the correlation between each true shock, ε_{it}, and its SVAR-identified counterpart, ε^*_{it}, for $i = 1, 2, 3$. As in Equations (B.13) and (B.14), the "exogeneity conditions" can be expressed as:

$$E(\varepsilon^*_{1t} m_{1t}) = E((d_{11}\varepsilon_{1t} + d_{12}\varepsilon_{2t} + d_{13}\varepsilon_{3t}) m_{1t}) = 0, \tag{B.18}$$

and

$$E(\varepsilon^*_{1t} m_{2t}) = E((d_{11}\varepsilon_{1t} + d_{12}\varepsilon_{2t} + d_{13}\varepsilon_{3t}) m_{2t}) = 0. \tag{B.19}$$

Substituting the expression of the IVs in Equation (B.16), the "exogeneity conditions" become:

$$E\left[(d_{11}\varepsilon_{1t} + d_{12}\varepsilon_{2t} + d_{13}\varepsilon_{3t})\left(\varepsilon_{2t} + \theta_1\varepsilon_{3t} + \delta_1\varepsilon_{1t} + \xi_1 v_{1t}\right)\right] = d_{11}\delta_1 + d_{12} + d_{13}\theta_1 = 0, \tag{B.20}$$

and

$$E\left[(d_{11}\varepsilon_{1t} + d_{12}\varepsilon_{2t} + d_{13}\varepsilon_{3t})\left(\theta_2\varepsilon_{2t} + \varepsilon_{3t} + \delta_2\varepsilon_{1t} + \xi_2 v_{1t}\right)\right] = d_{11}\delta_2 + d_{12}\theta_2 + d_{13} = 0. \tag{B.21}$$

Combining (B.20), (B.21), the equation $d_{11}^2 + d_{12}^2 + d_{13}^2 = 1$, and the sign normalization condition, we can again solve the values of d_{11}, d_{12} and d_{13}:

$$d_{11} = \sqrt{\frac{(\theta_1\theta_2 - 1)^2}{(\theta_1\theta_2 - 1)^2 + (\delta_1 - \delta_2\theta_1)^2 + (\delta_2 - \delta_1\theta_2)^2}}, \tag{B.22}$$

$$d_{12} = \frac{\delta_1 - \delta_2\theta_1}{\theta_1\theta_2 - 1}\sqrt{\frac{(\theta_1\theta_2 - 1)^2}{(\theta_1\theta_2 - 1)^2 + (\delta_1 - \delta_2\theta_1)^2 + (\delta_2 - \delta_1\theta_2)^2}}, \tag{B.23}$$

and

$$d_{13} = \frac{\delta_2 - \delta_1\theta_2}{\theta_1\theta_2 - 1}\sqrt{\frac{(\theta_1\theta_2 - 1)^2}{(\theta_1\theta_2 - 1)^2 + (\delta_1 - \delta_2\theta_1)^2 + (\delta_2 - \delta_1\theta_2)^2}}. \tag{B.24}$$

This shows that the untargeted shock is still point identified by the proxy exogeneity restriction. However, since d_{12} and d_{13} are not zero, the SVAR-identified shock, ε^*_{1t}, is confounded with the targeted shocks, ε_{2t} and ε_{3t}. As a result, Equation (B.22) shows that the correlation between the true untargeted shock, ε_{1t}, and its SVAR counterpart, ε^*_{1t}, is lower than 1.

Now, we shift the focus to the targeted shock, ε_{2t} ,and the second row of matrix D. As D is an orthonormal matrix, we have

$$d_{21}^2 + d_{22}^2 + d_{23}^2 = 1, \tag{B.25}$$

and

$$d_{11}d_{21} + d_{12}d_{22} + d_{13}d_{23} = 0. \tag{B.26}$$

Combining equations (B.25) and (B.26), we have

$$\left(\frac{d_{12}}{d_{11}}d_{22} + \frac{d_{13}}{d_{11}}d_{23}\right)^2 + d_{22}^2 + d_{23}^2 = 1, \tag{B.27}$$

where d_{11}, d_{12}, and d_{13} are solved coefficients expressed in Equations (B.22) to (B.24). Obviously, we cannot solve two unknown parameters, d_{22} and d_{23}, from a single equation (B.27), and thus the targeted shock, ε_{2t} ,is only set identified. Although we cannot determine d_{22} without additional restrictions, we can obtain an upper bound for this parameter, which represents the correlation between the SVAR-identified shock, ε_{2t}^*, and the respective true targeted shock, ε_{2t}. To achieve this goal, we proceed to rewrite Equation (B.27), grouping the uninterested term d_{23} as follows:

$$\left(\frac{d_{13}^2}{d_{11}^2} + 1\right)\left(d_{23} + \frac{d_{12}d_{13}}{d_{11}^2 + d_{13}^2}d_{22}\right)^2 + d_{22}^2 + \frac{d_{12}^2}{d_{11}^2}d_{22}^2 - \frac{d_{12}^2 d_{13}^2}{d_{11}^2\left(d_{11}^2 + d_{13}^2\right)}d_{22}^2 = 1, \tag{B.28}$$

where we structure the first term to eliminate interaction terms. This enables us to calculate the upper bound of d_{22} as:

$$\begin{aligned} d_{22}^2 &= \frac{1 - \left(\frac{d_{13}^2}{d_{11}^2} + 1\right)\left(d_{23} + \frac{d_{12}d_{13}}{d_{11}^2 + d_{13}^2}d_{22}\right)^2}{1 + \frac{d_{12}^2}{d_{11}^2} - \frac{d_{12}^2 d_{13}^2}{d_{11}^2\left(d_{11}^2 + d_{13}^2\right)}} \\ &\leq \frac{1}{1 + \frac{d_{12}^2}{d_{11}^2} - \frac{d_{12}^2 d_{13}^2}{d_{11}^2\left(d_{11}^2 + d_{13}^2\right)}}, \end{aligned} \tag{B.29}$$

where the upper bound is attained if and only if $d_{23} = -\frac{d_{12}d_{13}}{d_{11}^2 + d_{13}^2}d_{22}$.

To show how the upper bound can be related to the severity of the endogeneity problem controlled by the parameters of the IV generating process, we substitute in the solved coefficients of d_{1i} expressed by Equations (B.22) to (B.24):

$$d_{22}^2 \leq 1 - \frac{(\delta_1 - \delta_2\theta_1)^2}{(\theta_1\theta_2 - 1)^2 + (\delta_1 - \delta_2\theta_1)^2 + (\delta_2 - \delta_1\theta_2)^2}. \tag{B.30}$$

Similarly, we can solve the upper bound for d_{33}:

$$\begin{aligned} d_{33}^2 &\leq \frac{1}{1 + \frac{d_{13}^2}{d_{11}^2} - \frac{d_{12}^2 d_{13}^2}{d_{11}^2(d_{11}^2 + d_{12}^2)}} \\ &= 1 - \frac{(\delta_2 - \delta_1\theta_2)^2}{(\theta_1\theta_2 - 1)^2 + (\delta_1 - \delta_2\theta_1)^2 + (\delta_2 - \delta_1\theta_2)^2}. \end{aligned} \tag{B.31}$$

Equations (B.30) and (B.31) show that the upper bounds for d_{22} and d_{33} cannot simultaneously reach 1 unless $\delta_1 = \delta_2 = 0$. Thus, when the exogeneity restrictions are violated, at least one targeted shock cannot be perfectly identified, even with strong and precise additional identification restrictions.

In the general case, the relationship between the upper bounds and the δ parameters is complicated by the interactions among δ_1, δ_2, θ_1, and θ_2. To illustrate how the correlation between SVAR-identified and true shocks changes with the severity of the endogeneity problem, we consider a simpler case with symmetric settings where $\delta_1 = \delta_2 = \delta$. In this case, Equations (B.22), (B.30) and (B.31) simplify to:

$$d_{11} = \sqrt{\frac{(\theta_1\theta_2 - 1)^2}{(\theta_1\theta_2 - 1)^2 + ((1-\theta_1)^2 + (1-\theta_2)^2)\,\delta^2}}, \tag{B.32}$$

$$d_{22} \leq \sqrt{\frac{(1-\theta_2)^2}{(1-\theta_1)^2 + (1-\theta_2)^2}} \sqrt{1 + \frac{(\theta_1\theta_2 - 1)^2 \frac{(1-\theta_1)^2}{(1-\theta_2)^2}}{(\theta_1\theta_2 - 1)^2 + ((1-\theta_1)^2 + (1-\theta_2)^2)\,\delta^2}}, \tag{B.33}$$

$$d_{33} \leq \sqrt{\frac{(1-\theta_1)^2}{(1-\theta_1)^2 + (1-\theta_2)^2}} \sqrt{1 + \frac{(\theta_1\theta_2 - 1)^2 \frac{(1-\theta_2)^2}{(1-\theta_1)^2}}{(\theta_1\theta_2 - 1)^2 + ((1-\theta_1)^2 + (1-\theta_2)^2)\,\delta^2}}. \tag{B.34}$$

We observe that d_{11} and the upper bounds of d_{22} and d_{33} decrease as δ increases, since δ

appears only in the denominators of these expressions. Notably, the correlation between the IVs and untargeted shocks positively depends on δ. For instance, the correlation between m_{1t} and ε_{1t} is $\delta_1 / \sqrt{1 + \theta_1^2 + \delta_1^2 + \xi_1^2}$. Thus, as the endogeneity problem worsens — represented by higher correlations between the IVs and the untargeted shocks — the identification of all three shocks deteriorates, at least in this symmetric case.

In the above analysis, we focus solely on identification uncertainty, assuming the reduced-form parameters are given and ignoring estimation uncertainty. In the following, we conclude this section with a series of Monte Carlo simulations that account for both types of uncertainty. We examine three different sets of values for δ_1 and δ_2, corresponding to: (1) $\delta_1 = \delta_2 = 0$, suggesting the absence of an endogeneity problem, as discussed in our main text; (2) $\delta_1 = \delta_2 = 0.3$, indicating a mild endogeneity problem; and (3) $\delta_1 = \delta_2 = 0.9$, signaling a severe endogeneity problem. We set the values of other parameters to the same values as the benchmark case. Table B.1 reports the identification performance by combining the IV exogeneity restrictions with: (1) four shock-sign restrictions (SS_4); (2) one shock rank restriction (SR_1); and (3) zero restriction (ZR). We also report the identification results with only narrative sign restrictions (NSS_4). The identification performance deteriorates when the IV exogeneity assumption is violated, particularly in the presence of a severe endogeneity problem. Nonetheless, the identification performance remains satisfactory under a mild endogeneity issue. Additionally, the IV exogeneity restrictions enhance the identification performance, as evidenced by comparing the relative statistics between SS_4 and NSS_4.

Table B.1: Evaluating the Influence of Endogenous IVs with Monte Carlo Simulations

	Panel A: Median correlation for ε_{2t}						Panel B: Median $RMSE(\hat{b}_{.2})$					
	1	2	3	4	5	6	1	2	3	4	5	6
IV generating parameters												
ξ	1.60	1.60	1.60	5.00	5.00	5.00	1.60	1.60	1.60	5.00	5.00	5.00
θ_1	0.00	0.90	0.90	0.00	0.90	0.90	0.00	0.90	0.90	0.00	0.90	0.90
θ_2	0.00	0.90	-0.90	0.00	0.90	-0.90	0.00	0.90	-0.90	0.00	0.90	-0.90
Identification performance with $\delta_1 = \delta_2 = 0$												
SS_4	0.93	0.85	0.93	0.80	0.83	0.84	0.44	0.56	0.39	0.65	0.58	0.65
SR_1	0.93	0.89	0.94	0.87	0.88	0.88	0.43	0.50	0.39	0.56	0.56	0.56
ZR	0.95	0.52	0.71	0.56	0.47	0.50	0.39	1.40	0.59	1.21	1.39	1.05
NSS_4	0.77	0.77	0.77	0.77	0.77	0.77	0.72	0.72	0.72	0.72	0.72	0.72
Identification performance with $\delta_1 = \delta_2 = 0.3$												
SS_4	0.90	0.85	0.91	0.81	0.83	0.81	0.45	0.52	0.48	0.58	0.63	0.64
SR_1	0.91	0.89	0.94	0.87	0.87	0.86	0.47	0.51	0.41	0.58	0.54	0.56
ZR	0.91	0.51	0.73	0.52	0.48	0.49	0.37	1.38	0.70	1.29	1.31	1.15
NSS_4	0.77	0.77	0.77	0.77	0.77	0.77	0.70	0.70	0.70	0.70	0.70	0.70
Identification performance with $\delta_1 = \delta_2 = 0.9$												
SS_4	0.70	0.72	0.86	0.71	0.77	0.78	0.64	0.66	0.59	0.75	0.66	0.62
SR_1	0.75	0.80	0.91	0.80	0.80	0.80	0.58	0.58	0.52	0.61	0.60	0.59
ZR	0.54	0.54	0.80	0.36	0.46	0.38	0.87	1.16	0.76	1.43	1.34	1.40
NSS_4	0.77	0.77	0.77	0.77	0.77	0.77	0.73	0.73	0.73	0.73	0.73	0.73

Notes: The table reports Monte Carlo simulation results based on 1000 replications. "Median correlation for ε_{2t}" in panel A assesses the correlation between ε_{2t} and the corresponding shocks identified by different SVAR-identification methods. "Median $RMSE(\hat{b}_{.2})$" in panel B corresponds to the median of the root mean square error evaluated by $\sqrt{\sum_{j=1}^{3}\sum_{i=1}^{1000}\left(b_{j2}-\hat{b}_{j2}(i)\right)^2/1000}$, where $\hat{b}_{j2}(i)$ is the impulse response of ε_{2t} on the j-th endogenous variable implied by the i-th accepted draw.

B.3 The Role of Shock-sign Restrictions in Shock Identification

In this subsection, we assess how effectively our approach recovers the true targeted shocks by examining the correlation between the true shocks and the SVAR-identified shocks. We demonstrate how applying sharp shock-sign restrictions can narrow the admissible set of rotation angles, increasing the correlation between the true targeted shocks and their SVAR counterparts toward one. Additionally, our analysis reveals that the sharpness of each shock-sign restriction depends on the periods to which they are applied. Sharper identification is achieved when restrictions are imposed on periods with smaller shocks, while the admissible set broadens when applied to periods with larger shock realizations.

Given that the untargeted shocks have been identified by the proxy exogeneity restrictions, we can rewrite the relationship between the SVAR-identified shocks and the true shocks, as defined in Equation (B.12), as follows:

$$\begin{bmatrix} \varepsilon^*_{1t} \\ \varepsilon^*_{2t} \\ \varepsilon^*_{3t} \end{bmatrix} = \underbrace{\begin{bmatrix} 1 & 0 & 0 \\ 0 & cos\vartheta & sin\vartheta \\ 0 & -sin\vartheta & cos\vartheta \end{bmatrix}}_{D} \begin{bmatrix} \varepsilon_{1t} \\ \varepsilon_{2t} \\ \varepsilon_{3t} \end{bmatrix}, \tag{B.35}$$

where $-\pi \leq \vartheta \leq \pi$. The reason that we can express matrix D in this form is that D is orthonormal. We write it this way to simplify the analysis. The correlation between the true shocks and the SVAR-identified shocks is given by:

$$E\left(\varepsilon^*_{2t}\varepsilon_{2t}\right) = \cos\vartheta, \quad E\left(\varepsilon^*_{3t}\varepsilon_{3t}\right) = \cos\vartheta. \tag{B.36}$$

Notably. the correlation equals 1 when $\vartheta = 0$. Consequently, identification performance is optimal when only draws with ϑ close to zero are accepted by the identification restrictions. Without loss of generality, we consider the imposition of positive shock-sign restrictions at period t_i for the second shock and at period t_j for the third shock, i.e., $\varepsilon^*_{2,t_i} > 0$ and $\varepsilon^*_{3,t_j} > 0$. These shock-sign restrictions can be further expressed as:

$$\begin{cases} \varepsilon_{2,t_i}\cos\vartheta + \varepsilon_{3,t_i}\sin\vartheta > 0 \\ -\varepsilon_{2,t_j}\sin\vartheta + \varepsilon_{3,t_j}\cos\vartheta > 0. \end{cases} \tag{B.37}$$

Without loss of generality, we assume that ε_{3,t_i} and ε_{2,t_j} are positive. Solving the above

equation, we obtain the admissible set of ϑ under the sign normalization condition $\cos\vartheta > 0$:

$$-\frac{\varepsilon_{2,t_i}}{\varepsilon_{3,t_i}} < \tan\vartheta < \frac{\varepsilon_{3,t_j}}{\varepsilon_{2,t_j}}. \tag{B.38}$$

When imposing shock-sign restrictions on periods with the largest values of true shocks ε_{2,t_i} and ε_{3,t_j}, the interval defined by $-\frac{\varepsilon_{2,t_i}}{\varepsilon_{3,t_i}}$ and $\frac{\varepsilon_{3,t_j}}{\varepsilon_{2,t_j}}$ is wide. Consequently, draws with low correlations between the identified and true shocks (i.e., low $\cos\vartheta$) can fall within this interval and be accepted into the admissible set. Conversely, when restrictions are imposed on periods with smaller shock realizations, sharper inferences are possible, as only draws with ϑ close to zero (i.e., high $\cos\vartheta$) will be accepted.

Finally, a set of intervals, as in (B.38), will be obtained when imposing multiple shock sign restrictions. The admissible set of ϑ should be the intersection of these intervals. If the set of restrictions is sharp, the identification will closely recover the true shocks, as only draws with ϑ close to zero will be accepted.

C Supplementary Tables for Monte Carlo Simulations

C.1 F-statistics Reported in Selected Papers: A Review

Olea et al. (2021) introduce methods for testing weak instruments within a single IV framework, recommending the use of the Wald statistic or a heteroskedasticity-robust first-stage F statistic. Building on this, subsequent studies such as Lakdawala (2019) and Kim et al. (2020) have adapted the F test for use with multiple proxies by regressing the reduced-form disturbances of target equations against the chosen IVs. In our Monte Carlo simulations, the F statistics range from 16.49 to 28.01 for scenarios with strong IVs. For weak IV scenarios, the F statistics vary between 2.28 and 5.98. Stock et al. (2002) and Stock and Yogo (2005) suggest a threshold of 10 to distinguish between strong and weak IVs. In this Appendix, we aim to demonstrate that our parameter settings are intended to ensure that the F statistics from our simulated data align closely with those reported for strong and weak IVs in the literature. Table C.1 displays the F statistics for strong and weak IVs as documented in previous studies.

Table C.1: F-statistics in the Proxy SVAR Literature

Panel A: Strong IVs		Panel B: Weak IVs	
Paper	F-statistics	Paper	F-statistics
Our simulation	16.49, 28.01	Our simulation	2.28, 3.66, 5.98
Stock and Watson (2018)	20.50	Lakdawala and Sengupta (2021)	7.00
Lakdawala (2019)	18.91, 14.73	Olea et al. (2021)	1.60, 3.20
Mertens and Ravn (2019)	11.09; 9.15; 22.30	Noh (2024)	3.10
Cesa-Bianchi et al. (2020)	40.30		
Miranda-Agrippino and Rey (2020)	17.93, 10.95		
Rüth (2020)	21.86		
Klein and Linnemann (2021)	821.48, 17.34		
gregory2022us	9.94, 24.47, 10.56		
Lagerborg et al. (2023)	19.30		

Notes: This table presents the F-statistics from applications in the literature. Our objective is to demonstrate that the strong and weak IV scenarios in our Monte Carlo simulations are comparable to those observed in various applications documented in the literature. Some entries contain multiple values to accommodate studies that feature multiple SVAR models or utilize several IVs.

C.2 Identification Performance with Varying Number of Narrative Sign Restrictions

Table C.2 evaluates the identification performance with varying number of shock-sign restrictions. The data generating process is consistent with those described in the main text. SS_i, where $i = 1, 2, 3, 4, 5$, combines the IV exogeneity restriction with i shock-sign restrictions based on the sign of true shock realizations. NSS_i, for $i = 1, 2, 3, 4, 5$, employs only shock-sign restrictions based on the signs of true shocks. As expected, identification performance improves with an increase in the number of shock-sign restrictions. The IV exogeneity restrictions continue to enhance identification performance with up to five shock-sign restrictions, particularly with strong IVs.

We also assess the identification performance with ten and twenty shock-sign restrictions based on the sign of IVs. SS_i^{B*}, where $i = 10, 20$, combines the IV exogeneity restrictions with i shock-sign restrictions based on the IVs' signs, while $SS_i^{B,SC}$, where $i = 10, 20$, integrates these exogeneity restrictions with i sign concordance restrictions. The counterparts without IV exogeneity restrictions, NSS_i^{B*} and $NSS_i^{B,SC}$, for $i = 10, 20$, follow a similar setup. The identification performance improves only when the IVs are strong and each IV uniquely correlates with one of the shocks. In other scenarios, the benefits are minimal as the number of shock-sign restrictions increases, due to a significant likelihood of imposing incorrect restrictions. Particularly, when the number of incorrect restrictions is large, no acceptable results are obtained in the admissible sets with weak IVs for both SS_i^{B*} and NSS_i^{B*} when $i = 20$ (marked by "NAN" in the table).

We explore identification through various numbers of shock rank (SR_i and NSR_i for $i = 1, 2, 3$) and historical decomposition restrictions (HD_i and NHD_i for $i = 1, 2, 3$). The notation's initial "N" represents identification using only narrative sign restrictions. The fundamental insight is that shock rank restrictions are stringent, as they require not only the knowledge of the periods when the restrictions are imposed but also of the information about the shocks in other periods. Imposing three shock rank restrictions, the narrative sign-only approach alone can achieve satisfactory identification performance. In such cases, the additional benefit of the IV exogeneity restriction becomes minimal when combined with shock rank restrictions. Consequently, our approach is most useful in scenarios where information about the narrative sign restrictions is available but not strong enough to recover the true shocks, which is often the case in practice.

Table C.2: Evaluating Identification Performances for various number of narrative sign restrictions

	Panel A: Median correlation for ε_{2t}						Panel B: Median $RMSE(\hat{b}_{.2})$					
	1	2	3	4	5	6	1	2	3	4	5	6
IV generating parameters												
ξ	1.60	1.60	1.60	5.00	5.00	5.00	1.60	1.60	1.60	5.00	5.00	5.00
θ_1	0.00	0.90	0.90	0.00	0.90	0.90	0.00	0.90	0.90	0.00	0.90	0.90
θ_2	0.00	0.90	-0.90	0.00	0.90	-0.90	0.00	0.90	-0.90	0.00	0.90	-0.90
Shock-sign restrictions based on the sign of true shock realizations												
SS_0	0.61	0.55	0.62	0.44	0.51	0.51	0.95	1.07	0.89	1.33	1.20	1.18
SS_1	0.74	0.63	0.76	0.55	0.58	0.61	0.81	0.80	0.66	1.17	1.11	1.04
SS_2	0.85	0.75	0.84	0.65	0.71	0.71	0.59	0.66	0.54	0.97	0.93	0.86
SS_3	0.88	0.82	0.90	0.77	0.79	0.79	0.50	0.57	0.46	0.70	0.69	0.78
SS_4	0.93	0.85	0.93	0.80	0.83	0.84	0.44	0.56	0.39	0.65	0.58	0.65
SS_5	0.94	0.90	0.94	0.86	0.85	0.88	0.40	0.51	0.37	0.53	0.55	0.54
NSS_1	0.46	0.46	0.46	0.46	0.46	0.46	1.33	1.33	1.33	1.33	1.33	1.33
NSS_2	0.59	0.59	0.59	0.59	0.59	0.59	1.11	1.11	1.11	1.11	1.11	1.11
NSS_3	0.69	0.69	0.69	0.69	0.69	0.69	0.87	0.87	0.87	0.87	0.87	0.87
NSS_4	0.77	0.77	0.77	0.77	0.77	0.77	0.72	0.72	0.72	0.72	0.72	0.72
NSS_5	0.82	0.82	0.82	0.82	0.82	0.82	0.64	0.64	0.64	0.64	0.64	0.64
Shock-sign restrictions based on the sign of IVs												
SS_{10}^{B*}	0.93	0.80	0.72	0.67	0.67	0.61	0.44	0.57	0.54	0.79	0.75	0.68
SS_{20}^{B*}	0.94	0.81	0.71	NaN	NaN	NaN	0.43	0.72	0.60	NaN	NaN	NaN
$SS_{10}^{B,SC}$	0.87	0.80	0.66	0.62	0.66	0.55	0.59	0.68	0.59	0.93	0.82	0.76
$SS_{20}^{B,SC}$	0.90	0.82	0.69	0.73	0.73	0.59	0.52	0.66	0.54	0.76	0.73	0.69
NSS_{10}^{B*}	0.83	0.65	0.63	0.71	0.53	0.56	0.60	0.79	0.70	0.71	0.80	0.71
NSS_{20}^{B*}	0.90	0.68	0.70	NaN	NaN	NaN	0.43	0.72	0.60	NaN	NaN	NaN
$NSS_{10}^{B,SC}$	0.74	0.66	0.62	0.58	0.53	0.47	0.85	0.85	0.80	1.04	0.93	0.91
$NSS_{20}^{B,SC}$	0.84	0.68	0.66	0.68	0.59	0.56	0.67	0.78	0.72	0.85	0.78	0.80
Shock rank restrictions												
SR_1	0.93	0.89	0.94	0.87	0.88	0.88	0.43	0.50	0.39	0.56	0.56	0.56
SR_2	0.96	0.95	0.97	0.94	0.95	0.95	0.33	0.37	0.30	0.38	0.40	0.39
SR_3	0.98	0.97	0.98	0.96	0.96	0.97	0.28	0.31	0.28	0.30	0.32	0.32
NSR_1	0.84	0.84	0.84	0.84	0.84	0.84	0.64	0.64	0.64	0.64	0.64	0.64
NSR_2	0.92	0.92	0.92	0.92	0.92	0.92	0.46	0.46	0.46	0.46	0.46	0.46
NSR_3	0.95	0.95	0.95	0.95	0.95	0.95	0.36	0.36	0.36	0.36	0.36	0.36
Historical decomposition restrictions												
HD_1	0.88	0.80	0.88	0.76	0.77	0.80	0.54	0.59	0.51	0.64	0.62	0.58
HD_2	0.93	0.89	0.94	0.88	0.87	0.88	0.40	0.46	0.38	0.48	0.47	0.47
HD_3	0.95	0.92	0.95	0.92	0.93	0.92	0.32	0.41	0.34	0.40	0.39	0.37
NHD_1	0.71	0.71	0.71	0.71	0.71	0.71	0.69	0.69	0.69	0.69	0.69	0.69
NHD_2	0.84	0.84	0.84	0.84	0.84	0.84	0.54	0.54	0.54	0.54	0.54	0.54
NHD_3	0.88	0.88	0.88	0.88	0.88	0.88	0.47	0.47	0.47	0.47	0.47	0.47

Notes: This table compares the identification performance across different numbers of narrative sign restrictions. The notations for the identification methods are as described in the main text.

C.3 Monte Carlo Simulation with Additional Information about the True Shocks

In the main text, we examine scenarios where proxy exogeneity restrictions are combined with shock-sign restrictions, both based on the signs of true shocks and the signs of proxies. As expected, using true shock-sign restrictions yields more efficient identification compared to cases where shock signs are inferred only from the signs of instruments. This highlights the risks of mechanically imposing shock-sign restrictions based on instrument signs. We encourage researchers to explore information from multiple sources when imposing narrative sign restrictions.

In the spirit of this, we explore in this appendix a scenario where researchers have additional proxies for each true shock for selected periods. In particular, the proxy generating process can be formulated by:

$$m_{3t} = \varepsilon_{2t} + \xi_3 v_{3t}, \tag{C.1}$$

and

$$m_{4t} = \varepsilon_{3t} + \xi_4 v_{4t}, \tag{C.2}$$

where ε_{2t} and ε_{3t} are the targeted shocks, as described in the main text. $v_{it} \sim N(0,1)$ for $i = 3, 4$ so that parameters ξ_3 and ξ_4 control the size of measurement errors. Proxies m_{3t} and m_{4t} are used solely to induce shock-sign restrictions with m_{1t} and m_{2t} in the main text. We impose shock-sign restrictions using the same strategy as in our technology shock applications, where the shock-sign restrictions are imposed on periods based on the sign of multiple proxies. Specifically, we apply shock-sign restrictions to ε_{2t} only when the signs of m_{1t} and m_{3t} align and their absolute values exceed the average. Similarly, we impose shock-sign restrictions on ε_{3t} only during periods when the signs of m_{2t} and m_{4t} are aligned and their absolute values are above the average.

We do not use m_{3t} and m_{4t} as IVs, considering scenarios where additional proxies are unavailable for the entire sample period. For instance, proxies may only be available for a specific consecutive subsample period, as seen in technology shock applications. Alternatively, additional proxies may be sparse, providing information on the signs of true shocks only for certain periods. In such cases, the shock-sign restrictions are based on true shock signs when ξ_3 and ξ_4 approach zero, and on the sign of a single instrument

when ξ_3 and ξ_4 approach infinity so that the alternative proxies are uninformative.

Table C.3 reports the identification performance when setting ξ_3 and ξ_4 to 1. Row NSS_{miv} reports the identification performance when shock-sign restrictions, induced solely by multiple proxies, are implemented. Row SS_{miv} displays the identification results when shock-sign restrictions are combined with the IV exogeneity restrictions. The combination of IV exogeneity restrictions and shock-sign restrictions leads to valid inferences. We acknowledge that the identification performance can be different when the proxy strength controlled by the parameter ξ_3 and ξ_4 becomes higher or lower. [1]

Table C.3: Evaluating Identification Performances when shock signs are Induced by Multiple Sources

	Panel A: Median correlation for ε_{2t}						Panel B: Median $RMSE(b_{.2})$					
	1	2	3	4	5	6	1	2	3	4	5	6
IV generating parameters												
ξ_1 and ξ_2	1.60	1.60	1.60	5.00	5.00	5.00	1.60	1.60	1.60	5.00	5.00	5.00
θ_1	0.00	0.90	0.90	0.00	0.90	0.90	0.00	0.90	0.90	0.00	0.90	0.90
θ_2	0.00	0.90	-0.90	0.00	0.90	-0.90	0.00	0.90	-0.90	0.00	0.90	-0.90
Narra	16.3	15.5	15.9	11.4	11.2	11.3	16.3	15.5	15.9	11.4	11.2	11.3
Correct	15.7	14.8	15.2	10.7	10.5	10.4	15.7	14.8	15.2	10.7	10.5	10.4
SS_{miv}	0.93	0.90	0.89	0.87	0.89	0.86	0.41	0.46	0.41	0.56	0.52	0.49
NSS_{miv}	0.89	0.87	0.85	0.86	0.86	0.85	0.57	0.54	0.56	0.56	0.56	0.56

Notes: The table reports Monte Carlo simulation results based on 1000 replications. "Median correlation for ε_{2t}" assesses the correlation between ε_{2t} and the corresponding shocks identified by different SVAR-identification methods. Median $RMSE(\hat{b}_{.2})$ corresponds to the median of the root mean square error evaluated by $\sqrt{\sum_{j=1}^{3}\sum_{i=1}^{1000}\left(b_{j2}-\hat{b}_{j2}(i)\right)^2/1000}$, where $\hat{b}_{j2}(i)$ is the i-th accepted draw of b_{j2}. Row "Narr" reports the average number of shock-sign restrictions imposed, while row "Correct" details the alignment of these restrictions with the sign of true shocks.

[1] Row "Narr" reports the average number of shock-sign restrictions imposed, while row "Correct" details the alignment of these restrictions with the sign of true shocks. On average, fewer than one of the shock-sign restrictions is incorrectly imposed across all six data-generating processes. As the proxies become less informative with increases in ξ_3 and ξ_4, identification performance may deteriorate, caused by an increase in the number of incorrectly imposed restrictions.

C.4 Additional Evaluation of Identification Performance for the Identification in Main Text

In the main text, we evaluate identification performance using two primary metrics: (1) median correlation for ε_{2t}; and (2) $RMSE(\hat{b}_{.2})$. In this Appendix, we expand our evaluation using the same identification strategies, incorporating additional metrics, including: (1) the median correlation for ε_{3t} and the Median RMSE of $\hat{b}_{.3}$ (see Table C.4); (2) the Median RMSE of each individual parameter in the identified columns of B matrix, specifically $\hat{b}_{ij}$ for $i = 1, 2, 3$ and $j = 2, 3$ (see Tables C.5 to C.7); and (3) the bias and standard deviations of individual parameters (see Tables C.8 to C.13). The results generally align with those presented in the main text, offering consistent insights.

Table C.4: Evaluating Identification Performances for ε_{3t} and $\hat{b}_{.3}$

	Panel A: Median correlation for ε_{3t}						Panel B: Median $RMSE(\hat{b}_{.3})$					
	1	2	3	4	5	6	1	2	3	4	5	6
IV generating parameters and strength												
ξ	1.60	1.60	1.60	5.00	5.00	5.00	1.60	1.60	1.60	5.00	5.00	5.00
θ_1	0.00	0.90	0.90	0.00	0.90	0.90	0.00	0.90	0.90	0.00	0.90	0.90
θ_2	0.00	0.90	-0.90	0.00	0.90	-0.90	0.00	0.90	-0.90	0.00	0.90	-0.90
IV and narrative sign restrictions												
SS_4	0.93	0.86	0.93	0.81	0.82	0.85	0.41	0.49	0.41	0.70	0.59	0.60
SS_{10}^{B*}	0.93	0.80	0.72	0.71	0.64	0.60	0.38	0.56	1.11	0.64	0.72	1.04
$SS_{10}^{B,SC}$	0.87	0.80	0.66	0.62	0.65	0.55	0.61	0.67	1.31	0.89	0.77	1.26
SR_1	0.94	0.89	0.94	0.86	0.88	0.88	0.42	0.51	0.41	0.56	0.54	0.56
HD_2	0.92	0.89	0.94	0.88	0.87	0.87	0.43	0.46	0.37	0.49	0.51	0.48
Related identification strategies												
SS_0	0.61	0.51	0.61	0.48	0.49	0.53	1.19	1.32	1.23	1.42	1.38	1.33
NSS_4	0.77	0.77	0.77	0.77	0.77	0.77	0.74	0.74	0.74	0.74	0.74	0.74
ZR	0.96	0.63	0.71	0.63	0.53	0.57	0.38	0.68	1.18	1.16	1.14	1.35

Notes: The table reports Monte Carlo simulation results based on 1000 replications. Median correlation for ε_{3t} assesses the correlation between ε_{3t} and the corresponding shocks identified by different SVAR-identification methods. Median $RMSE(\hat{b}_{.3})$ corresponds to the median of the root mean square error evaluated by $\sqrt{\sum_{j=1}^{3}\sum_{i=1}^{1000}\left(b_{j3}-\hat{b}_{j3}(i)\right)^2/1000}$, where $\hat{b}_{j3}(i)$ is the i-th accepted draw of b_{j3}.

Table C.5: Evaluating Identification Performances for $\hat{b}_{12}$ and $\hat{b}_{13}$

	Panel A: Median $RMSE(\hat{b}_{12})$						Panel B: Median $RMSE(\hat{b}_{13})$					
	1	2	3	4	5	6	1	2	3	4	5	6
IV generating parameters and strength												
ξ	1.60	1.60	1.60	5.00	5.00	5.00	1.60	1.60	1.60	5.00	5.00	5.00
θ_1	0.00	0.90	0.90	0.00	0.90	0.90	0.00	0.90	0.90	0.00	0.90	0.90
θ_2	0.00	0.90	-0.90	0.00	0.90	-0.90	0.00	0.90	-0.90	0.00	0.90	-0.90
IV and narrative sign restrictions												
SS_4	0.26	0.35	0.20	0.41	0.39	0.41	0.23	0.30	0.22	0.46	0.38	0.37
SS_{10}^{B*}	0.25	0.43	0.21	0.51	0.53	0.36	0.22	0.41	0.48	0.40	0.50	0.42
$SS_{10}^{B,SC}$	0.30	0.44	0.24	0.55	0.50	0.41	0.31	0.43	0.56	0.54	0.47	0.63
SR_1	0.25	0.31	0.22	0.36	0.37	0.37	0.25	0.32	0.23	0.39	0.36	0.34
HD_2	0.22	0.27	0.20	0.29	0.31	0.30	0.24	0.26	0.20	0.33	0.33	0.28
Related identification strategies												
SS_0	0.43	0.59	0.37	0.77	0.68	0.66	0.53	0.66	0.53	0.75	0.72	0.70
NSS_4	0.49	0.49	0.49	0.49	0.49	0.49	0.47	0.47	0.47	0.47	0.47	0.47
ZR	0.26	0.79	0.23	0.74	0.81	0.62	0.24	0.28	0.55	0.64	0.57	0.66

Notes: The table reports Monte Carlo simulation results based on 1000 replications. Median $RMSE(\hat{b}_{jk})$ corresponds to the median of the root mean square error evaluated by $\sqrt{\sum_{i=1}^{1000}(b_{jk} - \hat{b}_{jk}(i))^2/1000}$, where $\hat{b}_{jk}(i)$ is the i-th accepted draw of b_{jk}.

Table C.6: Evaluating Identification Performances for $\hat{b}_{22}$ and $\hat{b}_{23}$

	Panel A: Median $RMSE(\hat{b}_{22})$						Panel B: Median $RMSE(\hat{b}_{23})$					
	1	2	3	4	5	6	1	2	3	4	5	6
IV generating parameters and strength												
ξ	1.60	1.60	1.60	5.00	5.00	5.00	1.60	1.60	1.60	5.00	5.00	5.00
θ_1	0.00	0.90	0.90	0.00	0.90	0.90	0.00	0.90	0.90	0.00	0.90	0.90
θ_2	0.00	0.90	-0.90	0.00	0.90	-0.90	0.00	0.90	-0.90	0.00	0.90	-0.90
IV and narrative sign restrictions												
SS_4	0.21	0.24	0.18	0.33	0.26	0.31	0.28	0.31	0.28	0.37	0.35	0.35
SS_{10}^{B*}	0.18	0.20	0.15	0.31	0.27	0.18	0.25	0.30	0.80	0.40	0.38	0.71
$SS_{10}^{B,SC}$	0.28	0.32	0.22	0.57	0.45	0.41	0.43	0.40	0.89	0.53	0.45	0.83
SR_1	0.19	0.22	0.18	0.26	0.27	0.27	0.27	0.32	0.29	0.32	0.32	0.33
HD_2	0.17	0.19	0.16	0.21	0.20	0.20	0.29	0.28	0.27	0.30	0.30	0.31
Related identification strategies												
SS_0	0.54	0.62	0.50	0.85	0.72	0.72	0.80	0.83	0.82	0.81	0.80	0.79
NSS_4	0.36	0.36	0.36	0.36	0.36	0.36	0.42	0.42	0.42	0.42	0.42	0.42
ZR	0.18	0.82	0.13	0.74	0.87	0.63	0.24	0.55	0.83	0.66	0.68	0.88

Notes: The table reports Monte Carlo simulation results based on 1000 replications. Median $RMSE(\hat{b}_{jk})$ corresponds to the median of the root mean square error evaluated by $\sqrt{\sum_{i=1}^{1000}(b_{jk} - \hat{b}_{jk}(i))^2/1000}$, where $\hat{b}_{jk}(i)$ is the i-th accepted draw of b_{jk}.

Table C.7: Evaluating Identification Performances for $\hat{b}_{32}$ and $\hat{b}_{33}$

	Panel A: Median $RMSE(\hat{b}_{32})$						Panel B: Median $RMSE(\hat{b}_{33})$					
	1	2	3	4	5	6	1	2	3	4	5	6
IV generating parameters and strength												
ξ	1.60	1.60	1.60	5.00	5.00	5.00	1.60	1.60	1.60	5.00	5.00	5.00
θ_1	0.00	0.90	0.90	0.00	0.90	0.90	0.00	0.90	0.90	0.00	0.90	0.90
θ_2	0.00	0.90	-0.90	0.00	0.90	-0.90	0.00	0.90	-0.90	0.00	0.90	-0.90
IV and narrative sign restrictions												
SS_4	0.28	0.35	0.27	0.39	0.35	0.38	0.17	0.20	0.18	0.39	0.29	0.30
SS_{10}^{B*}	0.28	0.28	0.46	0.43	0.40	0.42	0.16	0.24	0.61	0.25	0.21	0.59
$SS_{10}^{B,SC}$	0.41	0.40	0.47	0.55	0.46	0.46	0.30	0.30	0.77	0.53	0.41	0.76
SR_1	0.27	0.30	0.27	0.31	0.33	0.31	0.18	0.20	0.18	0.27	0.26	0.25
HD_2	0.26	0.29	0.28	0.31	0.28	0.28	0.18	0.19	0.17	0.22	0.22	0.22
Related identification strategies												
SS_0	0.65	0.63	0.63	0.69	0.69	0.65	0.71	0.80	0.73	0.87	0.85	0.81
NSS_4	0.42	0.42	0.42	0.42	0.42	0.42	0.37	0.37	0.37	0.37	0.37	0.37
ZR	0.23	0.78	0.52	0.61	0.72	0.54	0.16	0.31	0.67	0.69	0.70	0.81

Notes: The table reports Monte Carlo simulation results based on 1000 replications. Median $RMSE(\hat{b}_{jk})$ corresponds to the median of the root mean square error evaluated by $\sqrt{\sum_{i=1}^{1000}(b_{jk} - \hat{b}_{jk}(i))^2/1000}$, where $\hat{b}_{jk}(i)$ is the i-th accepted draw of b_{jk}.

Table C.8: Evaluating Median Biases for $\hat{b}_{12}$ and $\hat{b}_{13}$

	Panel A: Median $Bias(\hat{b}_{12})$						Panel B: Median $Bias(\hat{b}_{13})$					
	1	2	3	4	5	6	1	2	3	4	5	6
IV generating parameters and strength												
ξ	1.60	1.60	1.60	5.00	5.00	5.00	1.60	1.60	1.60	5.00	5.00	5.00
θ_1	0.00	0.90	0.90	0.00	0.90	0.90	0.00	0.90	0.90	0.00	0.90	0.90
θ_2	0.00	0.90	-0.90	0.00	0.90	-0.90	0.00	0.90	-0.90	0.00	0.90	-0.90
IV and narrative sign restrictions												
SS_4	-0.11	-0.07	-0.05	-0.19	-0.10	-0.21	-0.01	-0.01	-0.05	-0.24	-0.13	-0.17
SS_{10}^{B*}	-0.06	0.05	0.12	-0.22	-0.14	0.10	0.00	-0.00	-0.44	-0.13	0.16	-0.36
$SS_{10}^{B,SC}$	-0.07	-0.03	0.13	-0.26	-0.20	-0.07	-0.09	-0.02	-0.46	-0.33	-0.15	-0.45
SR_1	-0.09	-0.07	-0.01	-0.13	-0.14	-0.17	-0.01	-0.04	-0.07	-0.14	-0.07	-0.11
HD_2	-0.04	-0.01	-0.01	-0.05	-0.05	-0.09	-0.03	-0.03	-0.03	-0.08	-0.05	-0.07
Related identification strategies												
SS_0	-0.17	-0.21	-0.14	-0.52	-0.36	-0.41	-0.24	-0.33	-0.28	-0.53	-0.38	-0.46
NSS_4	-0.14	-0.14	-0.14	-0.14	-0.14	-0.14	-0.14	-0.14	-0.14	-0.14	-0.14	-0.14
ZR	-0.07	-0.57	0.17	-0.46	-0.49	-0.30	-0.01	0.06	-0.53	-0.42	-0.29	-0.50

Notes: The table reports Monte Carlo simulation results based on 1000 replications. Median $Bias\left(\hat{b}_{jk}\right)$ corresponds to the median of the bias evaluated by $\hat{b}_{jk} - b_{jk}$, where $\hat{b}_{jk}$ is average of the accepted draws for each replication.

Table C.9: Evaluating the Median Biases for $\hat{b}_{22}$ and $\hat{b}_{23}$

	Panel A: Median $Bias(\hat{b}_{22})$						Panel B: Median $Bias(\hat{b}_{23})$					
	1	2	3	4	5	6	1	2	3	4	5	6
IV generating parameters and strength												
ξ	1.60	1.60	1.60	5.00	5.00	5.00	1.60	1.60	1.60	5.00	5.00	5.00
θ_1	0.00	0.90	0.90	0.00	0.90	0.90	0.00	0.90	0.90	0.00	0.90	0.90
θ_2	0.00	0.90	-0.90	0.00	0.90	-0.90	0.00	0.90	-0.90	0.00	0.90	-0.90
IV and narrative sign restrictions												
SS_4	-0.11	-0.11	-0.07	-0.22	-0.15	-0.24	-0.02	0.04	-0.01	-0.18	-0.04	-0.10
SS_{10}^{B*}	-0.08	-0.07	0.01	-0.28	-0.23	-0.09	-0.03	0.04	-0.76	-0.11	0.23	-0.69
$SS_{10}^{B,SC}$	-0.12	-0.14	-0.04	-0.40	-0.29	-0.27	-0.14	0.01	-0.75	-0.22	-0.07	-0.73
SR_1	-0.10	-0.07	-0.04	-0.16	-0.16	-0.17	0.01	-0.01	-0.05	-0.08	-0.02	-0.08
HD_2	-0.07	-0.08	-0.04	-0.10	-0.10	-0.11	-0.04	0.02	-0.04	-0.04	-0.02	-0.07
Related identification strategies												
SS_0	-0.35	-0.39	-0.32	-0.64	-0.52	-0.55	-0.33	-0.31	-0.32	-0.54	-0.38	-0.49
NSS_4	-0.20	-0.20	-0.20	-0.20	-0.20	-0.20	-0.14	-0.14	-0.14	-0.14	-0.14	-0.14
ZR	-0.06	-0.72	0.03	-0.56	-0.71	-0.37	-0.02	0.38	-0.81	-0.44	-0.10	-0.73

Notes: The table reports Monte Carlo simulation results based on 1000 replications. Median $Bias\left(\hat{b}_{jk}\right)$ corresponds to the median of the bias evaluated by $\hat{b}_{jk} - b_{jk}$, where $\hat{b}_{jk}$ is average of the accepted draws for each replication.

Table C.10: Evaluating the Median Bias for $\hat{b}_{32}$ and $\hat{b}_{33}$

	Panel A: Median $Bias(\hat{b}_{32})$						Panel B: Median $Bias(\hat{b}_{33})$					
	1	2	3	4	5	6	1	2	3	4	5	6
IV generating parameters and strength												
ξ	1.60	1.60	1.60	5.00	5.00	5.00	1.60	1.60	1.60	5.00	5.00	5.00
θ_1	0.00	0.90	0.90	0.00	0.90	0.90	0.00	0.90	0.90	0.00	0.90	0.90
θ_2	0.00	0.90	-0.90	0.00	0.90	-0.90	0.00	0.90	-0.90	0.00	0.90	-0.90
IV and narrative sign restrictions												
SS_4	-0.09	-0.05	-0.05	-0.12	-0.07	-0.21	-0.07	-0.08	-0.08	-0.24	-0.16	-0.17
SS_{10}^{B*}	-0.07	0.06	0.45	-0.17	0.02	0.39	-0.05	-0.05	-0.56	-0.22	-0.09	-0.58
$SS_{10}^{B,SC}$	-0.04	0.01	0.41	-0.20	-0.14	0.26	-0.15	-0.15	-0.61	-0.40	-0.26	-0.68
SR_1	-0.08	-0.02	0.00	-0.13	-0.08	-0.14	-0.04	-0.10	-0.09	-0.13	-0.10	-0.12
HD_2	-0.02	-0.04	-0.00	-0.07	-0.01	-0.02	-0.09	-0.08	-0.06	-0.13	-0.11	-0.13
Related identification strategies												
SS_0	-0.09	-0.09	-0.05	-0.34	-0.20	-0.27	-0.45	-0.53	-0.46	-0.69	-0.58	-0.62
NSS_4	-0.11	-0.11	-0.11	-0.11	-0.11	-0.11	-0.22	-0.22	-0.22	-0.22	-0.22	-0.22
ZR	-0.04	-0.74	0.52	-0.38	-0.48	0.08	-0.05	-0.07	-0.65	-0.54	-0.44	-0.70

Notes: The table reports Monte Carlo simulation results based on 1000 replications. Median $Bias\left(\hat{b}_{jk}\right)$ corresponds to the median of the bias evaluated by $\hat{b}_{jk} - b_{jk}$, where $\hat{b}_{jk}$ is average of the accepted draws for each replication.

Table C.11: Evaluating the Median Standard Deviations of $\hat{b}_{12}$ and $\hat{b}_{13}$

	Panel A: Median $Std(\hat{b}_{12})$						Panel B: Median $Std(\hat{b}_{13})$					
	1	2	3	4	5	6	1	2	3	4	5	6
IV generating parameters and strength												
ξ	1.60	1.60	1.60	5.00	5.00	5.00	1.60	1.60	1.60	5.00	5.00	5.00
θ_1	0.00	0.90	0.90	0.00	0.90	0.90	0.00	0.90	0.90	0.00	0.90	0.90
θ_2	0.00	0.90	-0.90	0.00	0.90	-0.90	0.00	0.90	-0.90	0.00	0.90	-0.90
IV and narrative sign restrictions												
SS_4	0.19	0.28	0.16	0.32	0.30	0.30	0.19	0.25	0.16	0.33	0.29	0.29
SS_{10}^{B*}	0.15	0.17	0.13	0.12	0.11	0.12	0.15	0.16	0.16	0.14	0.11	0.13
$SS_{10}^{B,SC}$	0.24	0.39	0.17	0.36	0.39	0.33	0.25	0.36	0.32	0.39	0.37	0.34
SR_1	0.19	0.24	0.16	0.28	0.29	0.28	0.19	0.25	0.16	0.30	0.30	0.27
HD_2	0.18	0.21	0.15	0.23	0.22	0.22	0.18	0.20	0.14	0.24	0.23	0.20
Related identification strategies												
SS_0	0.36	0.53	0.33	0.55	0.56	0.50	0.43	0.56	0.45	0.54	0.58	0.50
NSS_4	0.40	0.40	0.40	0.40	0.40	0.40	0.40	0.40	0.40	0.40	0.40	0.40
ZR	0.20	0.55	0.14	0.54	0.60	0.50	0.17	0.23	0.16	0.44	0.47	0.37

Notes: The table reports Monte Carlo simulation results based on 1000 replications. Median $Std\left(\hat{b}_{jk}\right)$ corresponds to the median standard deviation of $\hat{b}_{jk}$.

Table C.12: Evaluating the Standard Deviations of $\hat{b}_{22}$ and $\hat{b}_{22}$

	Panel A: Median $Std(\hat{b}_{22})$						Panel B: Median $Std(\hat{b}_{23})$					
	1	2	3	4	5	6	1	2	3	4	5	6
IV generating parameters and strength												
ξ	1.60	1.60	1.60	5.00	5.00	5.00	1.60	1.60	1.60	5.00	5.00	5.00
θ_1	0.00	0.90	0.90	0.00	0.90	0.90	0.00	0.90	0.90	0.00	0.90	0.90
θ_2	0.00	0.90	-0.90	0.00	0.90	-0.90	0.00	0.90	-0.90	0.00	0.90	-0.90
IV and narrative sign restrictions												
SS_4	0.15	0.18	0.12	0.25	0.20	0.23	0.22	0.24	0.20	0.31	0.28	0.26
SS_{10}^{B*}	0.11	0.11	0.10	0.11	0.10	0.10	0.13	0.12	0.18	0.13	0.10	0.12
$SS_{10}^{B,SC}$	0.21	0.27	0.19	0.32	0.31	0.27	0.38	0.36	0.46	0.38	0.37	0.38
SR_1	0.14	0.16	0.12	0.19	0.19	0.19	0.20	0.23	0.22	0.26	0.27	0.24
HD_2	0.13	0.13	0.11	0.16	0.14	0.14	0.22	0.20	0.19	0.22	0.22	0.19
Related identification strategies												
SS_0	0.39	0.48	0.38	0.53	0.51	0.46	0.72	0.74	0.75	0.61	0.68	0.63
NSS_4	0.29	0.29	0.29	0.29	0.29	0.29	0.34	0.34	0.34	0.34	0.34	0.34
ZR	0.14	0.34	0.10	0.51	0.48	0.44	0.18	0.31	0.15	0.47	0.62	0.39

Notes: The table reports Monte Carlo simulation results based on 1000 replications. Median $Std\left(\hat{b}_{jk}\right)$ corresponds to the median standard deviation of $\hat{b}_{jk}$.

Table C.13: Evaluating the Median Standard Deviations of $\hat{b}_{32}$ and $\hat{b}_{33}$

	Panel A: Median $Std(\hat{b}_{32})$						Panel B: Median $Std(\hat{b}_{33})$					
	1	2	3	4	5	6	1	2	3	4	5	6
IV generating parameters and strength												
ξ	1.60	1.60	1.60	5.00	5.00	5.00	1.60	1.60	1.60	5.00	5.00	5.00
θ_1	0.00	0.90	0.90	0.00	0.90	0.90	0.00	0.90	0.90	0.00	0.90	0.90
θ_2	0.00	0.90	-0.90	0.00	0.90	-0.90	0.00	0.90	-0.90	0.00	0.90	-0.90
IV and narrative sign restrictions												
SS_4	0.22	0.25	0.20	0.30	0.27	0.27	0.14	0.17	0.12	0.27	0.22	0.24
SS_{10}^{B*}	0.14	0.13	0.11	0.11	0.10	0.10	0.11	0.11	0.17	0.11	0.10	0.11
$SS_{10}^{B,SC}$	0.37	0.36	0.23	0.38	0.37	0.31	0.25	0.25	0.42	0.33	0.30	0.36
SR_1	0.21	0.22	0.19	0.26	0.25	0.25	0.13	0.15	0.13	0.21	0.20	0.19
HD_2	0.21	0.20	0.19	0.22	0.22	0.21	0.14	0.14	0.12	0.15	0.16	0.14
Related identification strategies												
SS_0	0.63	0.62	0.61	0.60	0.64	0.58	0.53	0.60	0.56	0.52	0.58	0.52
NSS_4	0.33	0.33	0.33	0.33	0.33	0.33	0.29	0.29	0.29	0.29	0.29	0.29
ZR	0.17	0.29	0.10	0.48	0.52	0.51	0.13	0.31	0.15	0.43	0.53	0.37

Notes: The table reports Monte Carlo simulation results based on 1000 replications. Median $Std\left(\hat{b}_{jk}\right)$ corresponds to the median standard deviation of $\hat{b}_{jk}$.

D Supplementary Tables and Figures for Empirical Application

This section provides supplementary results for our empirical application of technology shocks. Section D.1 presents evidence on the correlation between technology proxies and various economic shocks identified in the literature. Section D.2 examines the robustness of our identification by exploring alternative numbers of shock-sign restrictions, reporting the effects and contributions when proxy exogeneity restrictions are combined with 6 or 10 shock-sign restrictions. In Section D.3, we evaluate whether our VAR model contains sufficient information to recover the technology shocks using the fundamentalness test by Forni and Gambetti (2014). Section D.4 compares our estimated peak technology shock effects and contributions with those reported in recent SVAR papers. Section D.5 compares our benchmark results with those from the max-share methods of Barsky and Sims (2011) and Chahrour et al. (2023). Section D.6 explores the identification performance when replacing the narrative sign restrictions in our benchmark identification with zero-correlation restrictions between technology shocks and IVs. Section D.7 documents the results when shocks are identified by proxy exogeneity restrictions using the Sign Concordance method of Budnik and Rünstler (2023), which explicitly models the probability that shock-sign restrictions are imposed incorrectly. Section D.8 re-estimates these effects using a robust prior, as described in Section A.2, and assesses the impact of the prior using the method from Giacomini and Kitagawa (2021). Section D.9 performs joint inference under a uniform prior over impulse responses using the method detailed in Section 2.3 and Online Appendix A.3. Section D.10 examines whether the identified technology shocks are supply-side or demand-side shocks by including the inflation rate in the benchmark model. Section D.11 explores whether our approach identifies technology shocks primarily by truncating the reduced-form parameters or by truncating the identified set for the structural parameters, conditional on the reduced-form parameters. Section D.12 evaluates the robustness of our empirical findings by imposing additional inequality restrictions on the correlations between IVs and structural shocks, as Piffer and Podstawski (2018) suggest.

D.1 The Correlation between the Technology Proxies and Alternative Shock Measures

In this section, we assess IV exogeneity by examining the correlation between the IVs and various economic shocks identified in the literature. As shown in the following tables, the technology proxies show no significant correlation with shocks related to monetary policy, government spending, taxes, oil supply, sentiment, or financial markets.

Table D.1: Correlation of the Patent Series with Alternative Shock Measures

Shock	Source	ρ	p-value	Sample
Monetary policy	Gertler and Karadi (2015)	-0.012	0.908	1990M1–2012M6
	Bu et al. (2021)	0.093	0.362	1994M1–2018M6
	Jarociński and Karadi (2020)	0.144	0.128	1990M2–2018M6
Government spending	Ramey (2011)	0.033	0.632	1960Q1–2013Q4
	Ben Zeev and Pappa (2017)	0.024	0.741	1960Q1–2007Q4
Tax	Leeper et al. (2012)	0.032	0.667	1960Q1–2005Q4
	Mertens and Ravn (2014)	-0.065	0.371	1960Q1–2007Q4
Oil supply news	Känzig (2021)	0.076	0.318	1974M1–2017M12
Sentiment	Lagerborg et al. (2023)	0.071	0.344	1973M1–2018M6
Financial	TED spread	-0.079	0.373	1986M1–2018M6
	Cesa-Bianchi and Sokol (2022)	-0.009	0.914	1980M7–2016M12

Notes: The table presents the correlation between the patent series and various shock measures from existing literature. The correlation coefficient, denoted as ρ, measures the strength and direction of the relationship, while the accompanying p-value indicates whether the correlation is statistically significant. In cases where the shock measure is only accessible monthly, it is aggregated by summing across months.

Table D.2: Correlation of the TFP Series with Alternative Shock Measures

Shock	Source	ρ	p-value	Sample
Monetary policy	Gertler and Karadi (2015)	-0.008	0.944	1990M1–2012M6
	Bu et al. (2021)	-0.165	0.105	1994M1–2018M6
	Jarociński and Karadi (2020)	0.031	0.745	1990M2–2018M6
Government spending	Ramey (2011)	0.090	0.188	1960Q1–2013Q4
	Ben Zeev and Pappa (2017)	0.012	0.873	1960Q1–2007Q4
Tax	Leeper et al. (2012)	-0.046	0.533	1960Q1–2005Q4
	Mertens and Ravn (2014)	-0.061	0.397	1960Q1–2007Q4
Oil supply news	Känzig (2021)	0.009	0.904	1974M1–2017M12
Sentiment	Lagerborg et al. (2023)	-0.054	0.468	1973M1–2018M6
Financial	TED spread	0.084	0.340	1986M1–2018M6
	Cesa-Bianchi and Sokol (2022)	0.008	0.919	1980M7–2016M12

Notes: The table presents the correlation between TFP series and various shock measures from existing literature. The correlation coefficient, denoted as ρ, measures the strength and direction of the relationship, while the accompanying p-value indicates whether the correlation is statistically significant. In cases where the shock measure is only accessible monthly, it is aggregated by summing across months.

D.2 Alternative Number of Narrative Sign Restrictions

In our benchmark analysis, we impose shock-sign restrictions during periods when proxies from different sources align in sign and exceed their respective averages. We identify nine periods that meet the criteria for unanticipated technology shocks and eight periods for anticipated technology shocks. In this section, we test the robustness of our findings by varying the number of restrictions imposed. Specifically, we present the results when restrictions are applied to ten periods for both shocks in Figures D.1 and D.2, and to six periods for both shocks in Figures D.3 and D.4. The selection of these periods is again based on the size and values of the proxies, but with different thresholds than in the benchmark. The results remain robust when using an alternative number of narrative sign restrictions, although the credible bands are slightly wider when fewer restrictions are imposed.

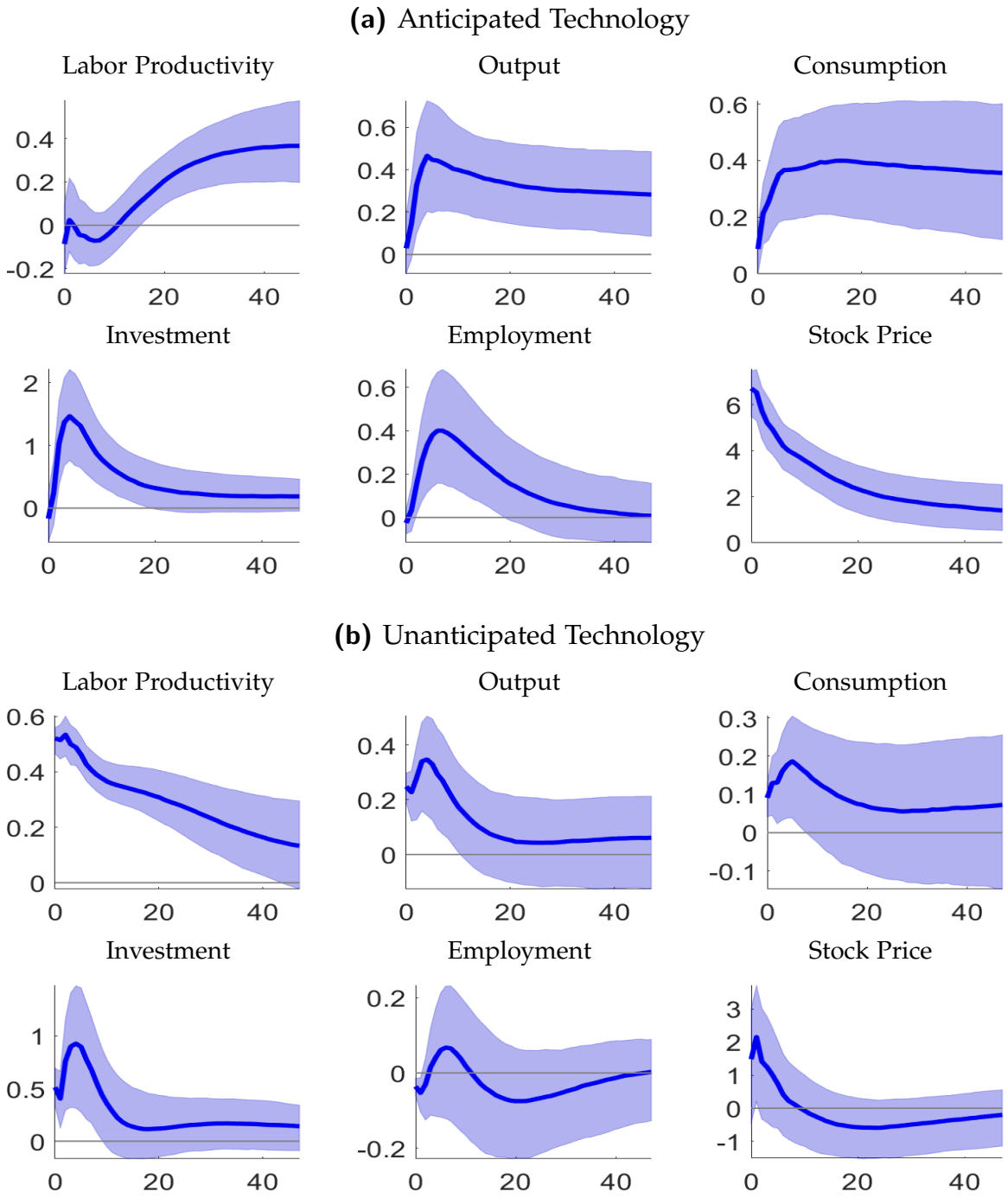

Figure D.1: Impulse Responses by Imposing 10 Narrative Sign Restrictions

Notes: The blue solid lines and shaded areas represent, respectively, the median and 68% (point-wise) credible bands for impulse responses.

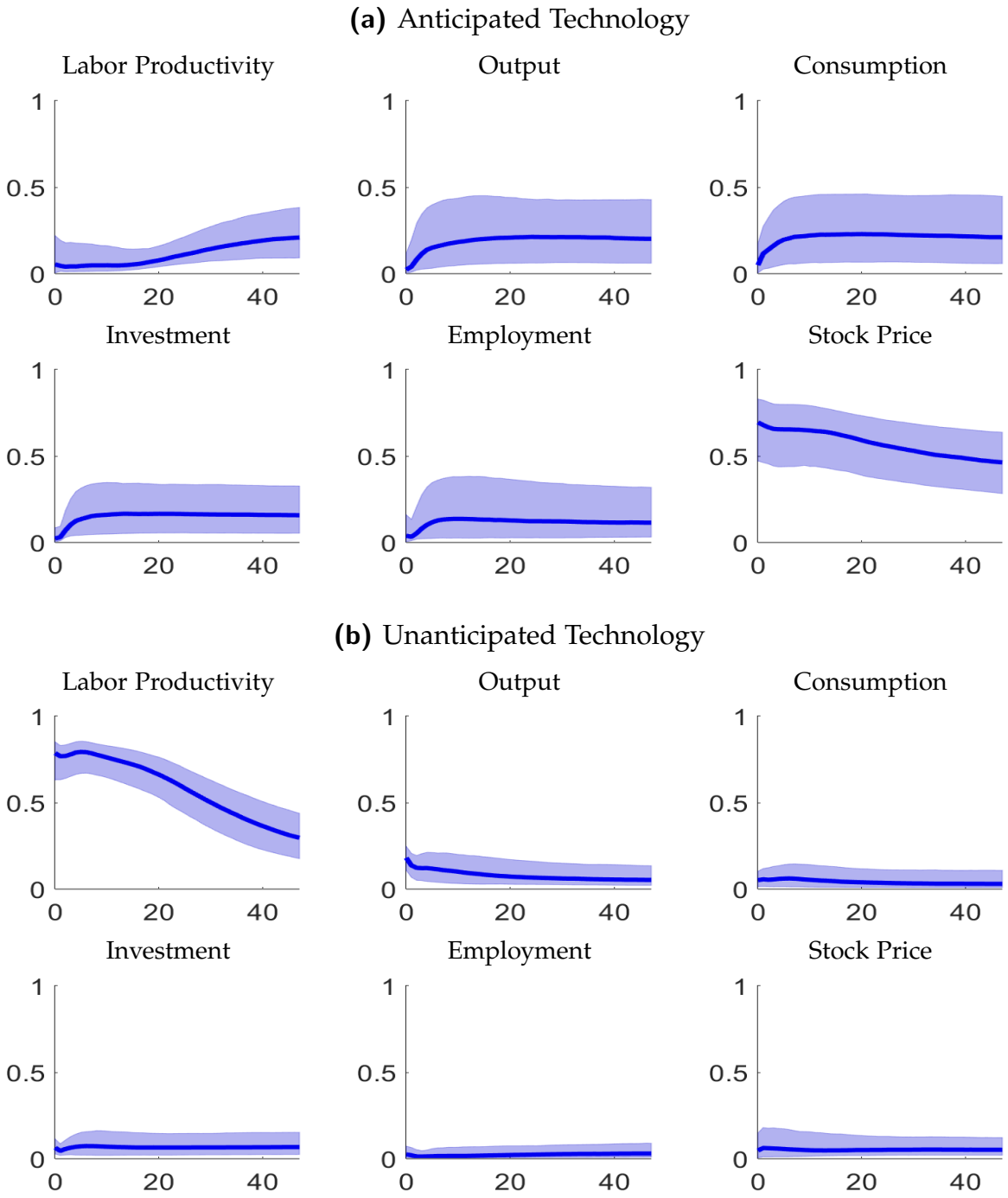

Figure D.2: Forecast Error Variance Decomposition by Imposing 10 Narrative Sign Restrictions

Notes: The blue solid lines and shaded areas represent, respectively, the median and 68% (point-wise) credible bands for forecast error variance decompositions.

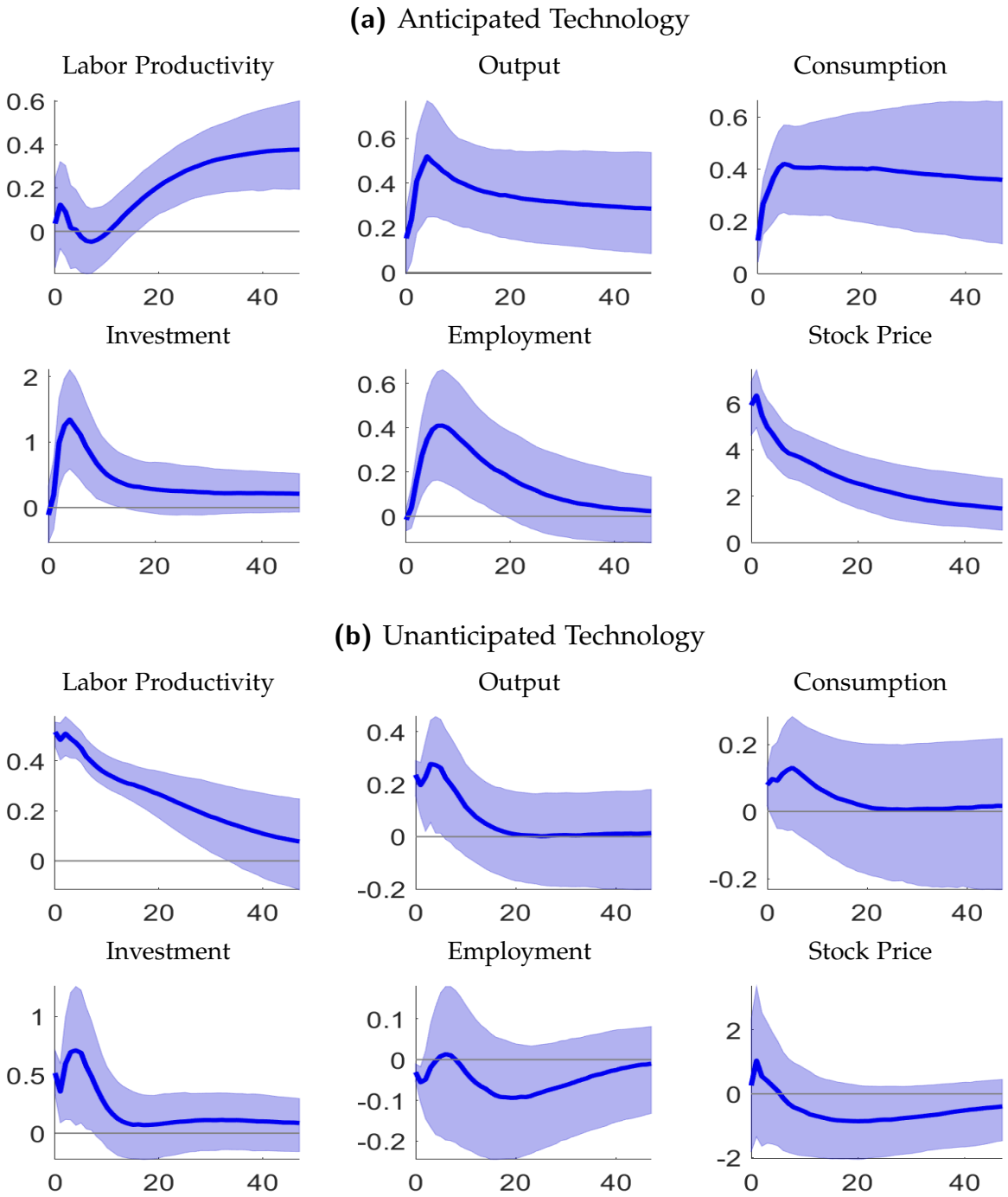

Figure D.3: Impulse Responses by Imposing 6 Narrative Sign Restrictions

Notes: The blue solid lines and shaded areas represent, respectively, the median and 68% (point-wise) credible bands for impulse responses.

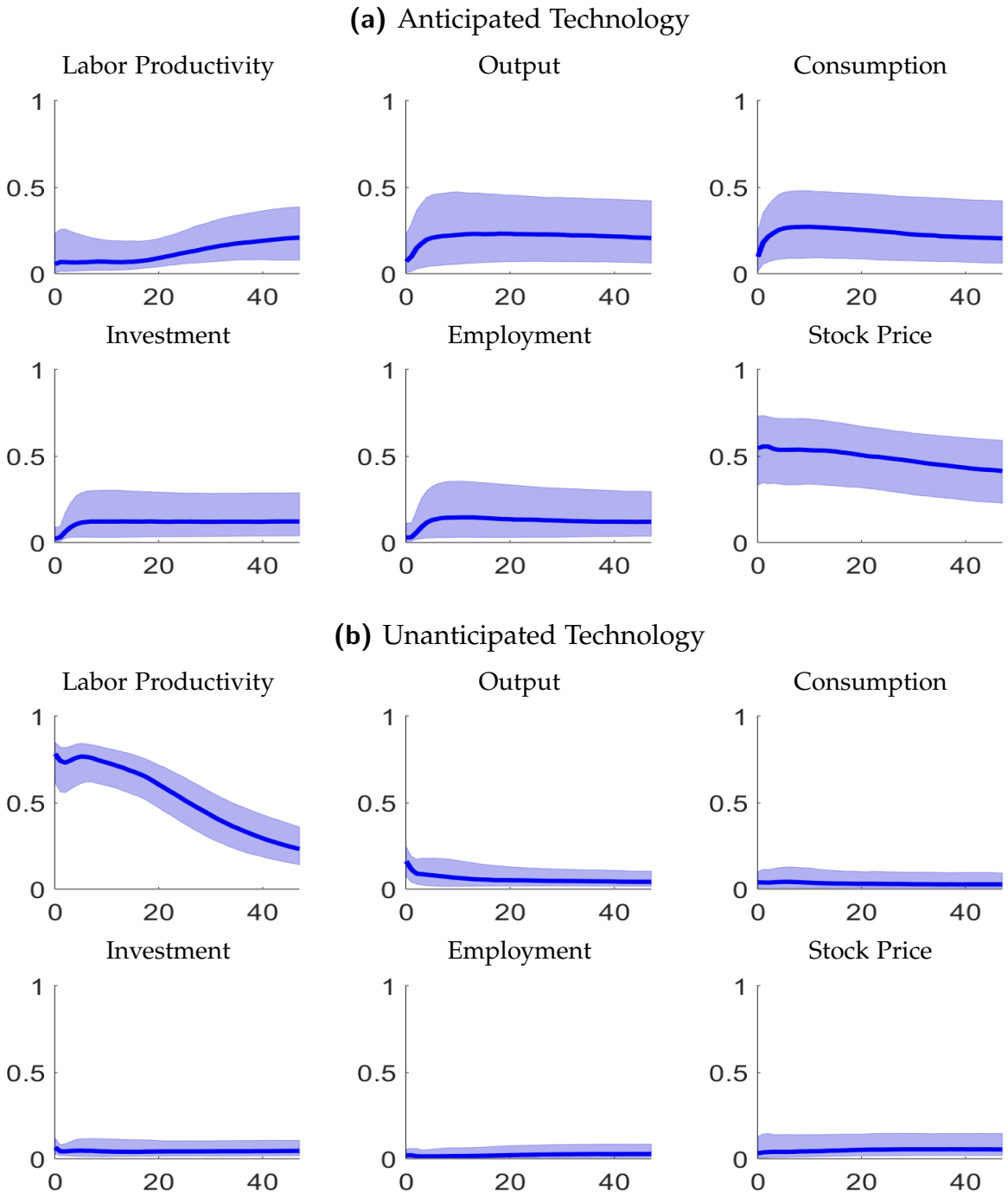

Figure D.4: Forecast Error Variance Decomposition by Imposing 6 Narrative Sign Restrictions

Notes: The blue solid lines and shaded areas represent, respectively, the median and 68% (point-wise) credible bands for forecast error variance decompositions.

D.3 Fundamentalness Test of Forni and Gambetti (2014)

The standard SVAR-identification method assumes that the structural shocks can be expressed as linear combinations of the residuals of the linear projection of a vector of variables onto their past values. However, if the information set contained in the VAR model does not span that of the agents, the structural shocks cannot be obtained from a VAR and the identification method fails.

In this section, we apply the procedure proposed by Forni and Gambetti (2014) to test whether our VAR model contains sufficient information. The information sufficiency testing procedure can be summarized as follows. First, estimate the reduced-form VAR model and identify the structural shocks of interest. Second, collect a large macroeconomic data set and compute the first P principal components. Finally, test for orthogonality of the estimated structural shocks with respect to L lags of the principal components by using a standard F-test.

We perform the information sufficiency test for $P = 1, 2, \ldots, 8$ and $L = 1, 2, 3, 4$. The large data set is the same as that used by Forni and Gambetti (2014), covering 107 US quarterly macroeconomic series. The results of the information sufficiency test are reported in Table D.3.

Table D.3: Test of orthogonality: p-values of the F-test of the structural shocks

	Number of lags			
Regressor	1 lag	2 lags	3 lags	4 lags
Anticipated Technology				
f(1,1)	0.50	0.52	0.48	0.47
f(1,2)	0.32	0.26	0.28	0.37
f(1,3)	0.39	0.30	0.28	0.45
f(1,4)	0.28	0.13	0.18	0.27
f(1,5)	0.31	0.16	0.22	0.31
f(1,6)	0.19	0.15	0.17	0.24
f(1,7)	0.21	0.16	0.22	0.26
f(1,8)	0.19	0.20	0.27	0.20
Unanticipated Technology				
f(1,1)	0.52	0.60	0.58	0.59
f(1,2)	0.57	0.63	0.63	0.75
f(1,3)	0.64	0.60	0.66	0.74
f(1,4)	0.61	0.64	0.75	0.80
f(1,5)	0.57	0.49	0.59	0.63
f(1,6)	0.60	0.52	0.61	0.70
f(1,7)	0.58	0.56	0.68	0.74
f(1,8)	0.63	0.66	0.75	0.74

Notes: The table presents the p-values for F test for orthogonality of the estimated structural shocks with respect to $L = 1, 2, 3, 4$ lags of the first $P = 1, 2, \ldots, 8$ principal components.

D.4 Comparing Technology Shock Effects and Contributions With Established Literature

This section compares the peak technology shock effects and contributions with those reported in six recent SVAR papers. Four of these papers use various max-share approaches and identify technology shocks by imposing restrictions on variance decompositions. The other two papers, Klein and Linnemann (2021) and Cascaldi-Garcia and Vukotić (2022), employ the single IV method for identification. We calculate these effects based on replication packages available on the journal's or the author's website and cross-check our replication against the results reported in the papers. Our findings indicate smaller effects and contributions than those reported in most of the existing literature. Our estimates of anticipated technology shock effects are most closely aligned with those of Klein and Linnemann (2021), but we estimate lower contributions and effects for unanticipated technology shocks.

Table D.4: The Effects and Contributions of Anticipated technology shocks

Paper	Method, Sample	Technology	Output	Consumption	Stock Prices
Panel A: Median Peak Effects					
Our paper	60Q1–18Q2	0.37	0.46	0.39	6.59
Barsky and Sims (2011)	MS, 60Q1–07Q4	0.22	0.4	0.38	NA
Kurmann and Otrok (2013)	MS, 59Q2–05Q2	0.57	0.71	0.84	1.50
Klein and Linnemann (2021)	IV, 73Q1–19Q1	0.27	0.43	0.50	6.54
Görtz et al. (2022)	MS, 84Q1–17Q1	0.44	0.60	0.56	5.02
Cascaldi-Garcia and Vukotić (2022)	IV, 61Q1–10Q4	0.34	0.36	0.23	4.88
Chahrour et al. (2023)	MS, 60Q1–18Q4	0.35	0.88	0.89	4.76
Panel B: Median Peak Shock Contributions					
Our paper	60Q1–18Q2	22%	21%	22%	68%
Barsky and Sims (2011)	MS, 60Q1–07Q4	45%	43%	52%	NA
Kurmann and Otrok (2013)	MS, 59Q2–05Q2	47%	42%	51%	31%
Klein and Linnemann (2021)	IV, 73Q1–19Q1	18%	21%	26%	41%
Görtz et al. (2022)	MS, 84Q1–17Q1	38%	62%	71%	63%
Cascaldi-Garcia and Vukotić (2022)	IV, 61Q1–10Q4	4%	12%	20%	46%
Chahrour et al. (2023)	MS, 60Q1–18Q4	35%	87%	95%	40%

Notes: "MS" stands for the Max-share approach, while "IV" denotes the instrumental variable method. Some entries are marked as "NA" because the related variable or shock is not examined in the corresponding paper.

Table D.5: The Effects and Contributions of Unanticipated technology shocks

Paper	Method, Sample	Technology	Output	Consumption	Stock Prices
Panel A: Median Peak Effects					
Our paper	60Q1–18Q2	0.52	0.33	0.18	2.04
Barsky and Sims (2011)	MS, 60Q1–07Q4	0.70	NA	NA	NA
Kurmann and Otrok (2013)	MS, 59Q2–05Q2	0.77	0.34	0.43	0.51
Klein and Linnemann (2021)	IV, 73Q1–19Q1	0.45	0.30	0.40	3.24
Görtz et al. (2022)	MS, 84Q1–17Q1	0.60	0.34	NA	2.07
Cascaldi-Garcia and Vukotić (2022)	IV, 61Q1–10Q4	NA	NA	NA	NA
Chahrour et al. (2023)	MS, 60Q1–18Q4	0.68	0.22	0.04	0.10
Panel B: Median Peak Shock Contributions					
Our paper	60Q1–18Q2	79%	17%	6%	6%
Barsky and Sims (2011)	MS, 60Q1–07Q4	100%	NA	NA	NA
Kurmann and Otrok (2013)	MS, 59Q2–05Q2	100%	11%	17%	5%
Klein and Linnemann (2021)	IV, 73Q1–19Q1	95%	18%	15%	11%
Görtz et al. (2022)	MS, 84Q1–17Q1	100%	17%	17%	11%
Cascaldi-Garcia and Vukotić (2022)	IV, 61Q1–10Q4	NA	NA	NA	NA
Chahrour et al. (2023)	MS, 60Q1–18Q4	94%	11%	2%	19%

Notes: "MS" stands for the Max-share approach, while "IV" denotes the instrumental variable method. Some entries are marked as "NA" because the related variable or shock is not examined in the corresponding paper.

D.5 Max-share Approach

A prevalent strategy to identify technology shocks is the max-share approach. This section compares our benchmark results with those obtained using the max-share methods proposed by Barsky and Sims (2011) and Chahrour et al. (2023). Barsky and Sims (2011) assume that only unanticipated technology shocks immediately impact productivity. They identify anticipated technology shocks by maximizing their contributions to productivity, conditioned on unanticipated technology shocks, over a predetermined horizon.[2] The identification scheme of Chahrour et al. (2023) also proceeds in two steps but with reverse identification ordering. It is worth noting that the max-share identification hinges on researchers' subjective belief in shock contributions without referring to any historical observations. As a result, a preponderant share of posterior draws implies shock realizations with signs at odds with the IVs, as documented in the "BS" and "CCP" columns of Table 2.

Figures D.5 and D.6 delineate the effects and contributions of the technology shocks identified using the procedures of Barsky and Sims (2011) (represented by black dashed lines) and Chahrour et al. (2023) (represented by red dash-dotted lines). Similar to the benchmark results, both max-share methods demonstrate substantial comovements in macroeconomic variables following favorable anticipated technology shocks. However, there are notable differences between the results from the max-share method and our benchmark model. The credible bands of the effects and contributions of Barsky and Sims (2011) anticipated technology shocks are remarkably wider. Moreover, both max-share methods predict quantitatively larger effects and contributions of anticipated technology shocks compared to the benchmark estimation. For instance, the Chahrour et al. (2023) anticipated technology shocks are held accountable for 73%, 85%, and 94% of the variations in labor productivity, output, and consumption, respectively. The inference of unanticipated technology shocks broadly concurs with our benchmark estimation. Nevertheless, it is noteworthy that the unanticipated technology shocks identified by Chahrour et al. (2023) exert suppressing effects on output and consumption at long horizons.

[2]It is worth noting that, in implementing the Barsky and Sims (2011) scheme, we adopt TFP as the measure of productivity, although the results remain robust when using labor productivity instead.

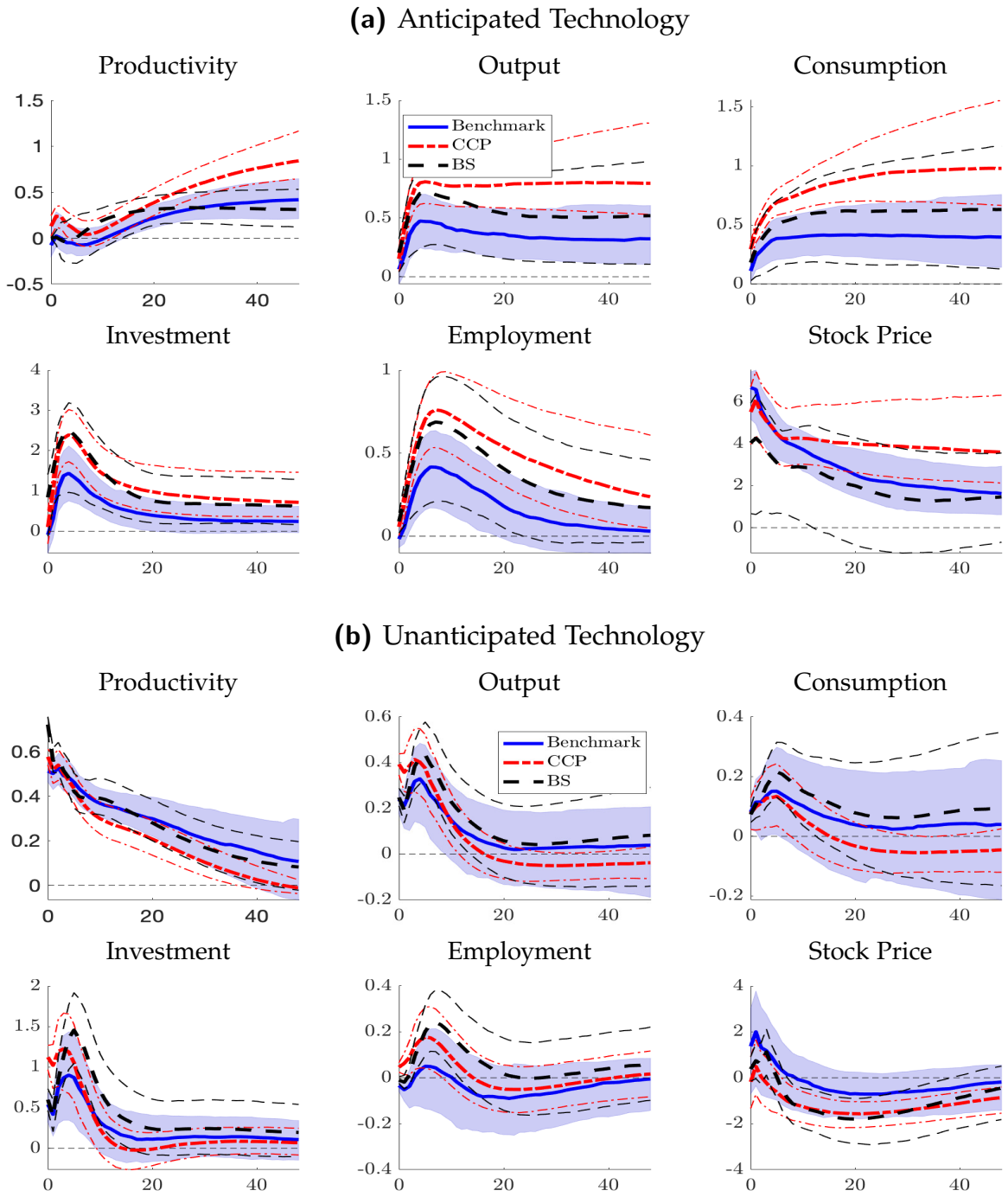

Figure D.5: Impulse Responses by Max-Share Approach

Notes: The blue solid lines and the shaded areas represent, respectively, the median and the 68% (pointwise) credible bands for impulse responses when technology shocks are identified with both IVs and narrative sign restrictions. The black dashed lines and the red dash-dotted lines plot impulse responses to the shocks identified, respectively, using Barsky and Sims (2011) and Chahrour et al. (2023) methods, with thick lines indicating the median and thin lines informing 68% credible bands.

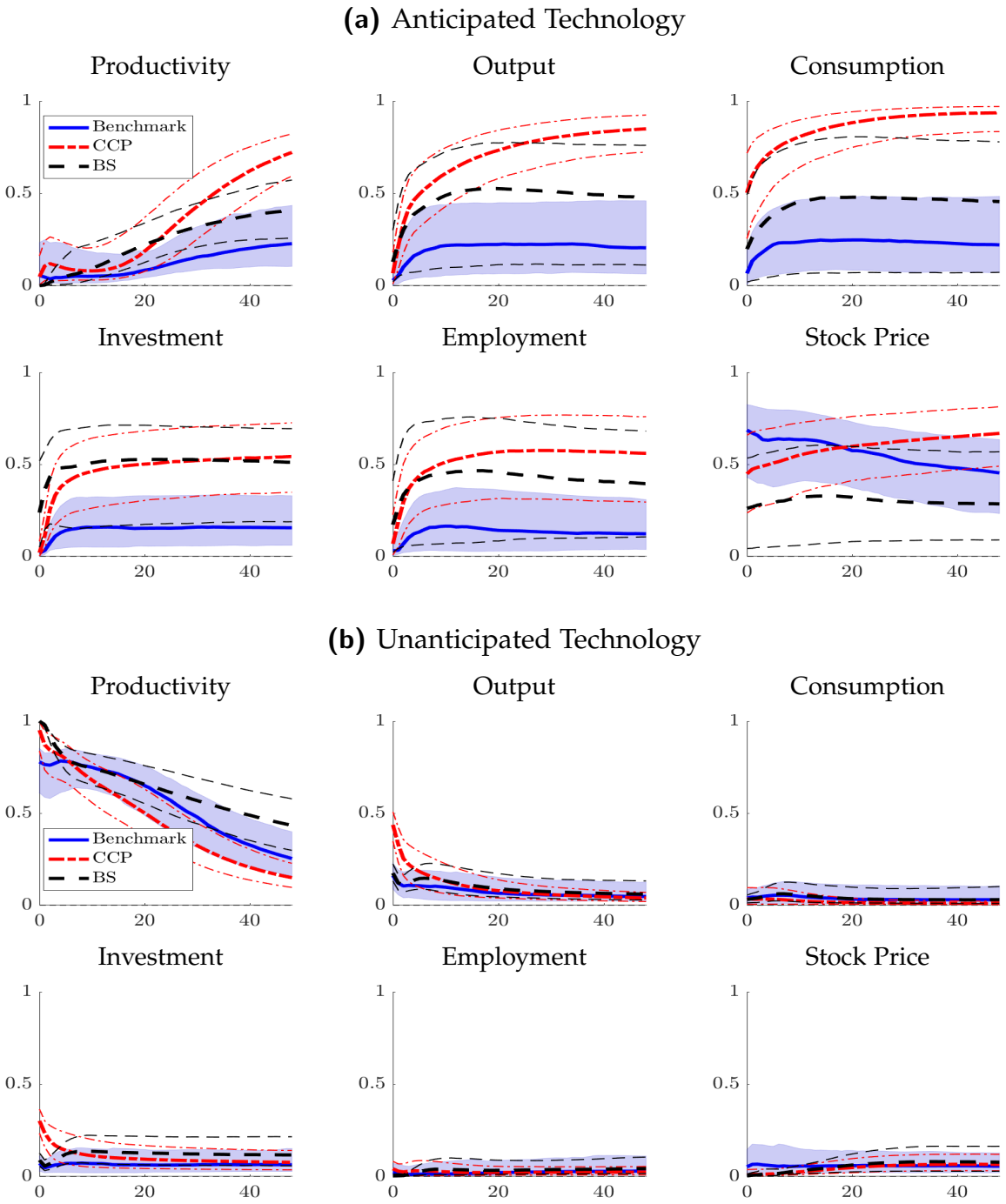

Figure D.6: Variance Decompositions by Max-Share Approach

Notes: The blue solid lines and shaded areas represent, respectively, the median and the 68% (point-wise) credible bands for variance decompositions when technology shocks are identified with both IVs and narrative sign restrictions. The black dashed lines and the red dash-dotted lines plot impulse responses to the shocks identified, respectively, using Barsky and Sims (2011) and Chahrour et al. (2023) methods, with thick lines indicating the median and thin lines informing 68% credible bands.

D.6 Combining IVs and Zero Restrictions

In this Section, we conduct robustness checks by introducing zero-correlation restrictions between technology shocks and IVs as an alternative to the narrative sign restrictions in our benchmark model. We consider two specific strategies: (i) assuming that the patent-based IV is uncorrelated with unanticipated technology shocks ("zero-anticipated"); and (ii) assuming that TFP growth is uncorrelated with anticipated technology shocks ("zero-unanticipated").

The results, presented in Figures D.7 and D.8, show that both zero-correlation restriction strategies yield similar shock effects and contributions as the benchmark model, with the exception of lower contributions of anticipated technology shocks to stock prices and labor productivity. However, it is noteworthy that introducing additional zero restrictions may lead to distinct implications compared to our benchmark model in at least two aspects. Firstly, as detailed in Table 2, both "zero-anticipated" and "zero-unanticipated" strategies accept more than half of the posterior draws with opposite signs for instrumental variables (IVs) in specific quarters, such as 91Q2, 00Q1, and 03Q3 for anticipated technology shocks, and 96Q2 and 15Q3 for unanticipated technology shocks. Secondly, both "zero-anticipated" and "zero-unanticipated" strategies suggest a low correlation between IVs and shock realizations. As illustrated in Figure D.9, the benchmark model indicates that 37.4% of posterior draws imply correlations between anticipated technology shocks and Total Factor Productivity (TFP) growth with absolute values exceeding 0.2. In contrast, when applying "zero-anticipated" restrictions, only 8 out of 10,000 posterior draws exhibit correlations beyond the range of [-0.2, 0.2].

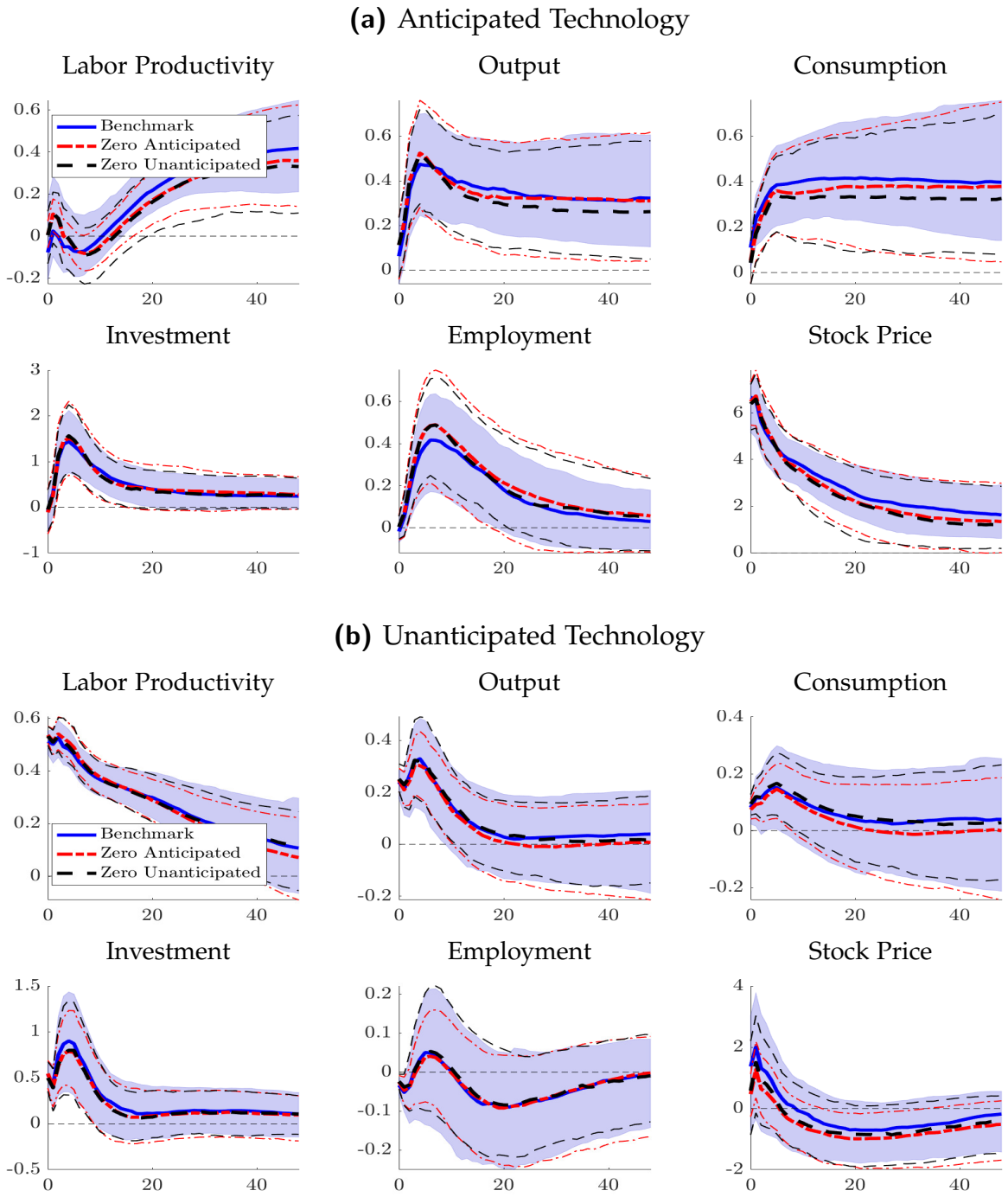

Figure D.7: Impulse Responses by IVs and Zero Restrictions

Notes: The blue solid lines and the shaded areas represent, respectively, the median and the 68% (point-wise) credible bands for impulse responses when technology shocks are identified with both IVs and narrative sign restrictions. The red dash-dotted lines and the black dashed lines plot impulse responses, to shocks identified, respectively, using IVs together with zero-correlation restriction between patent-based IV growth and unanticipated technology shocks, and IVs together with zero-correlation restriction between TFP growth and anticipated technology shocks.

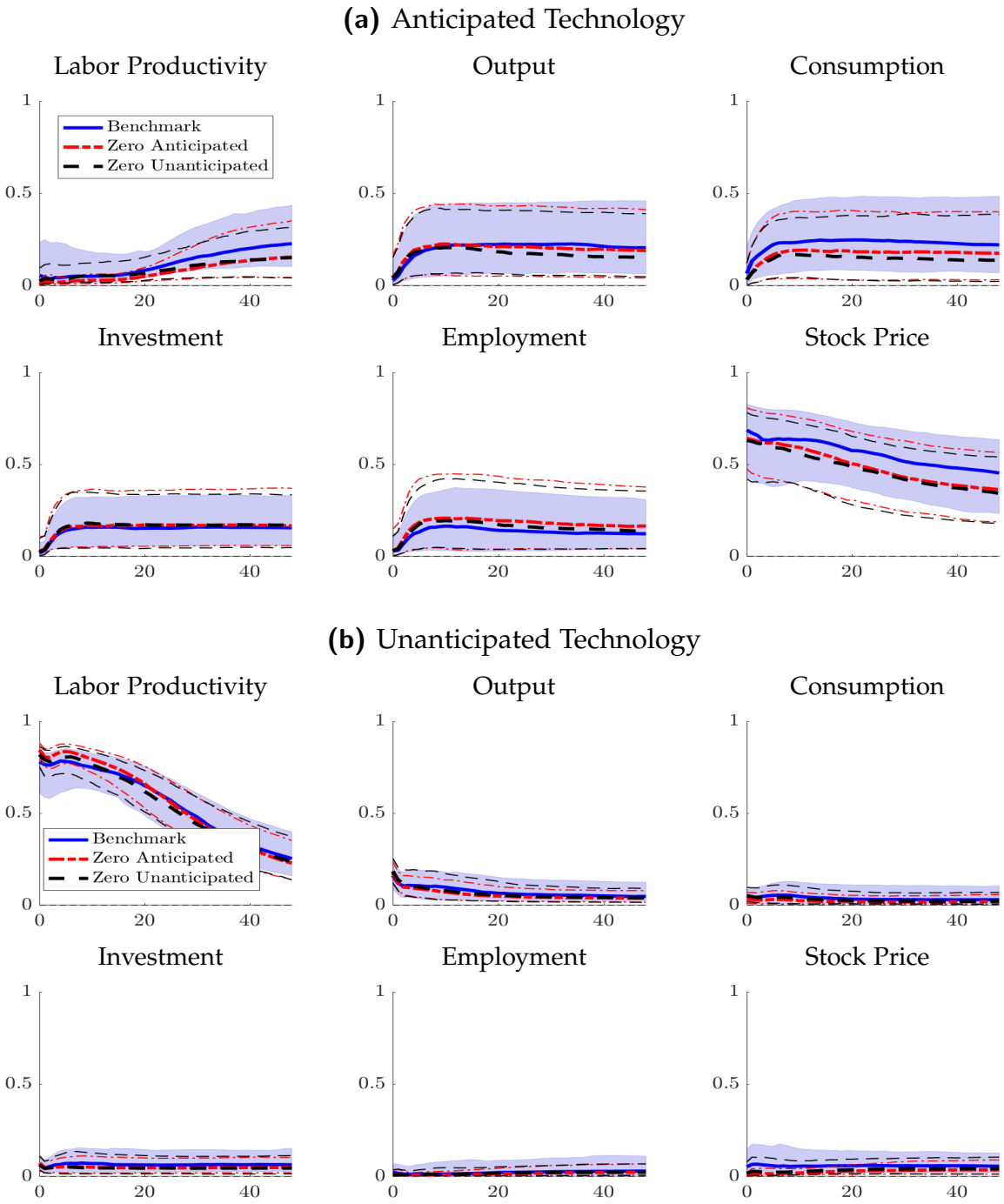

Figure D.8: Forecast Error Variance Decomposition by IVs and Zero Restrictions

Notes: The blue solid lines and the shaded areas represent, respectively, the median and the 68% (pointwise) credible bands for forecast error variance decompositions when technology shocks are identified with both IVs and narrative sign restrictions. The red dash-dotted lines and the black dashed lines plot variance decomposition, by shocks identified, respectively, using IVs together with zero-correlation restriction between patent-based IV growth and unanticipated technology shocks, and IVs together with zero-correlation restriction between TFP growth and anticipated technology shocks.

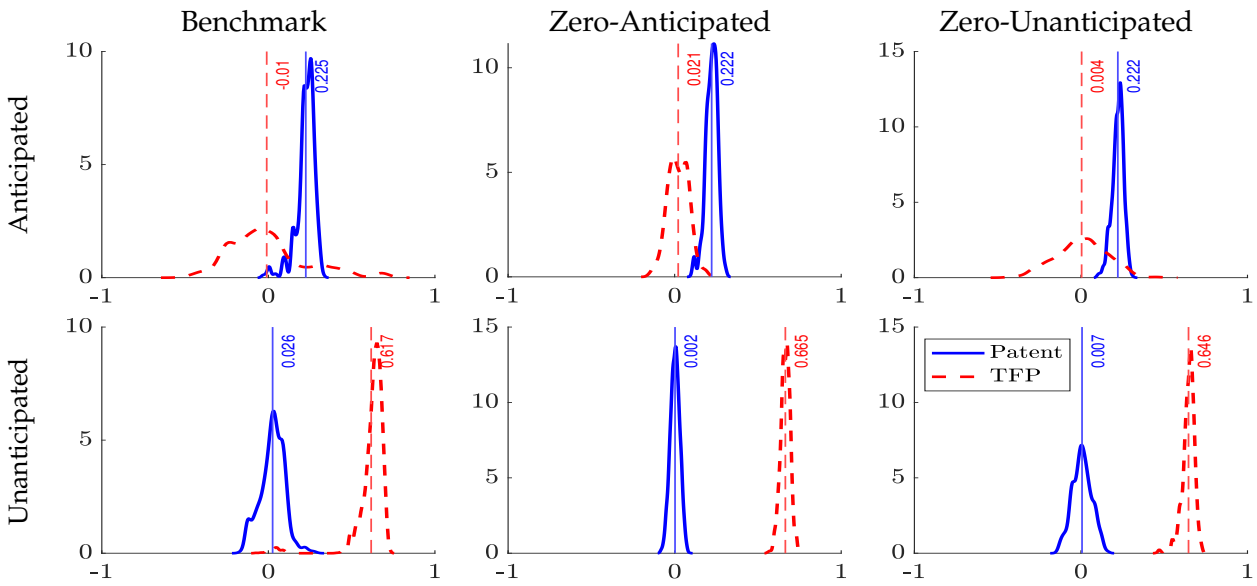

Figure D.9: The Posterior Distribution of Realized Correlation between Shocks and Proxies

Notes: The figure plots the posterior distribution of the correlation between each of the two identified SVAR shocks and IVs based on 10000 posterior draws under three different identification strategies, with anticipated shocks in the upper panel and unanticipated shocks in the lower panel. Each of the three columns (from left to right) corresponds, respectively, to the identification approach with shocks identified with IVs and narrative sign restrictions, with IVs and the restriction that unanticipated technology shocks are uncorrelated with the patent-based IV, and with IVs as well as the restriction that anticipated technology shocks are uncorrelated with current TFP growth.

D.7 Combining IVs and Sign Concordance Approach

In this section, we make the first attempt in the literature to combine the IV approach with the Sign Concordance (SC) method of Budnik and Rünstler (2023), allowing for incorrect imposition of shock-sign restrictions. In the following, We explain how to integrate the IV with the SC approach, followed by an analysis of the shock effects and contributions when SC restrictions are applied. Our primary findings remain robust, although the range of uncertainty increases, particularly when the hyperparameter governing the possibility of incorrect imposition, denoted as Λ, to values such as 0.8 and 0.9.

D.7.1 Combining IV with SC approach

To account for potential errors in the econometrician's beliefs, we adopt the Sign Concordance (SC) method proposed by Budnik and Rünstler (2023), which addresses imperfect sign concordance under narrative sign restrictions. Our paper discusses three types of narrative sign restrictions: shock-sign restrictions, historical decomposition restrictions, and shock rank restrictions. When applying the SC method, we follow Budnik and Rünstler (2023) and assume that only shock-sign restrictions are imposed to identify structural shocks.

We define the share of instances where the signs of structural shocks align with shock-sign restrictions as $\xi = N_{\text{TRUE}}/s$, where s is the total number of narrative sign restrictions and N_{TRUE} is the number of instances for which the signs of structural shocks coincide with narrative sign restrictions. The number of correct signs follows a binomial distribution:

$$p\left(s\xi|\,\tilde{A}_0, \tilde{A}_+\right) = f\left(s\xi; s, \lambda\right), \tag{D.1}$$

where λ is the unknown probability of the correct classification of a single event. If $\lambda = 1$, we accept the draw of the structural parameter only when all narrative sign restrictions are satisfied. However, if we believe that narrative restrictions may contain errors, we accept the draw of the structural parameter with a certain probability $f\left(s\xi; s, \lambda\right)$, which depends on the value of λ. Following Budnik and Rünstler (2023), we assume $\lambda \sim \beta(p, q)$ over support $[\Lambda, 1]$, where $\beta(p, q)$ is a beta distribution. In the empirical analysis, we set $p = q = 1$ and let Λ vary between 0.8 and 0.9, as suggested by Budnik and Rünstler (2023).

The SC method is implemented using the following algorithm:

Algorithm D.1 1. *Use the Algorithm from Arias et al. (2021) to independently draw* $(\tilde{A}_0, \tilde{A}_+)$.

2. *Calculate the number of instances where the signs of structural shocks align with narrative sign restrictions:* $N_{TRUE} = s\xi$.

3. *Draw* λ *from a beta distribution:* $\lambda \sim \beta(p, q)$ *over support* $[\Lambda, 1]$.

4. *Accept the draw of* $(\tilde{A}_0, \tilde{A}_+)$ *with probability* $f(s\xi; s, \lambda)$.

5. *Repeat Steps 1–4 until the required number of draws is obtained.*

6. *Re-sample* $(\tilde{A}_0, \tilde{A}_+)$ *with replacement using the importance weights* $NGN_{(\tilde{v},\tilde{\Phi},\tilde{\Psi},\tilde{\Omega})}\left(\tilde{A}_0, \tilde{A}_+\right) / p\left(\tilde{A}_0, \tilde{A}_+\right)$.

D.7.2 Identification Results

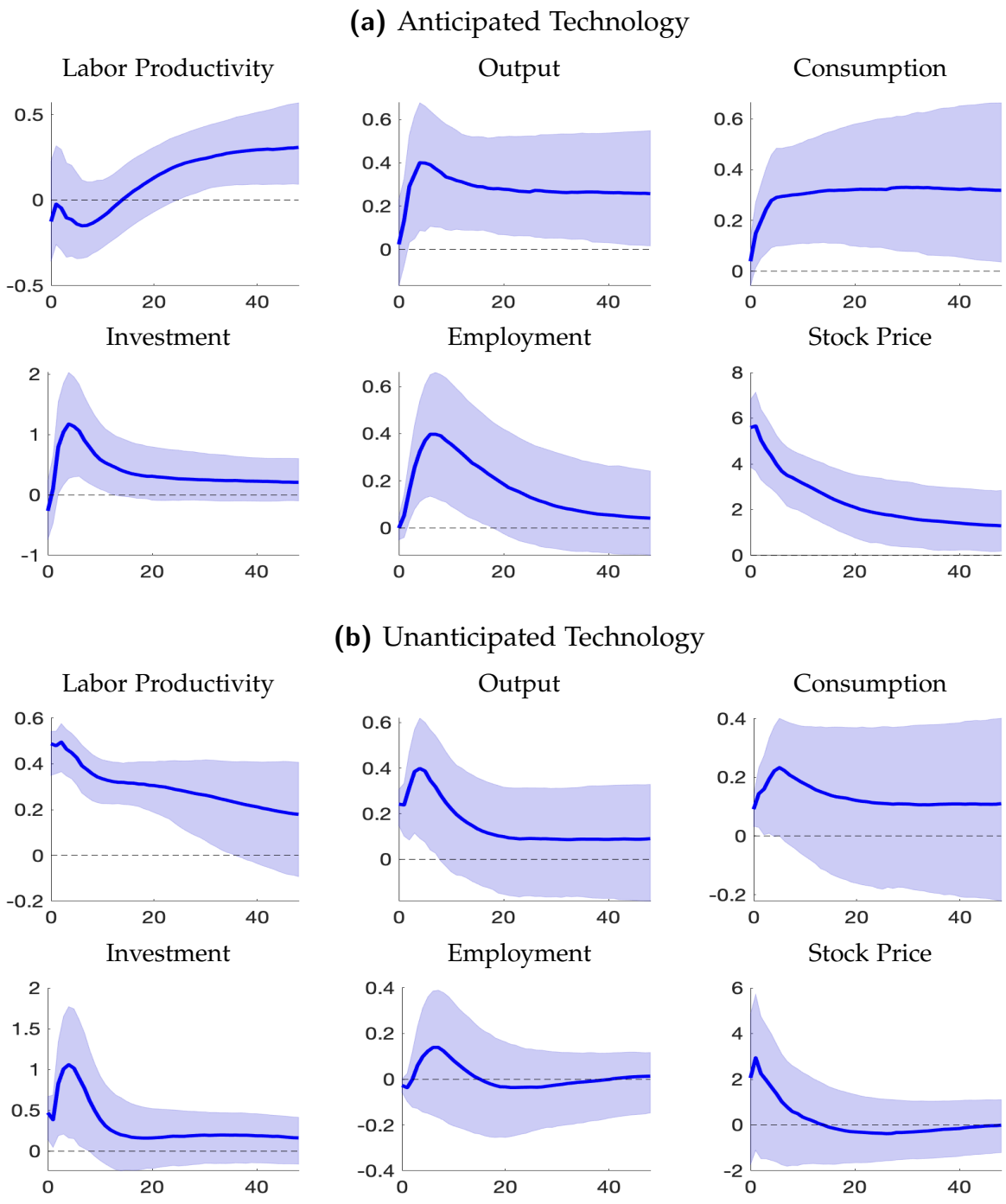

Figure D.10: Impulse Responses by IVs and Sign Concordance Criterion ($\Lambda = 0.9$)

Notes: The blue solid lines and the shaded areas represent, respectively, the median and the 68% (pointwise) credible bands for impulse responses when technology shocks are identified with both IVs and sign concordance criterion.

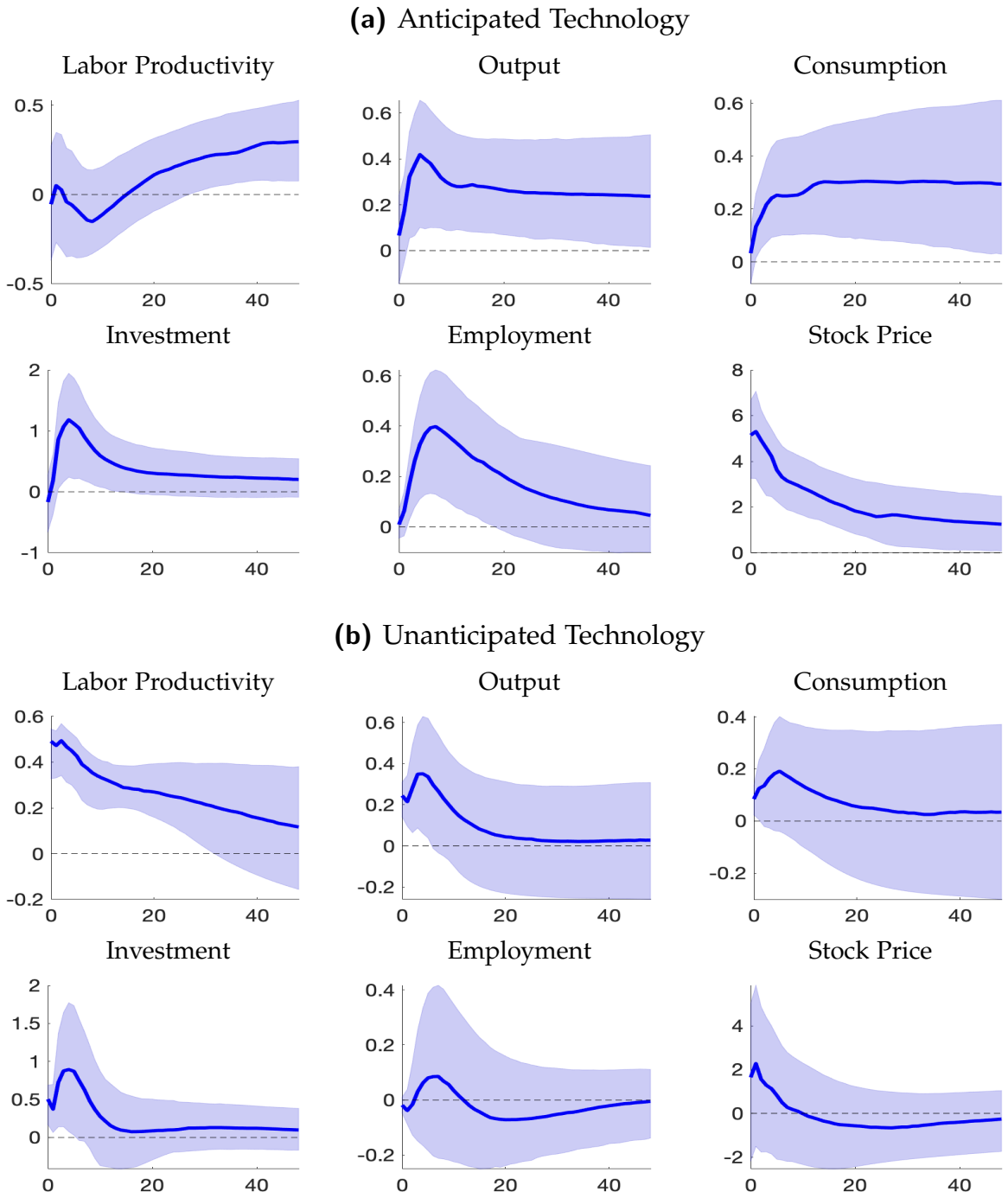

Figure D.11: Impulse Responses by IVs and Sign Concordance Criterion ($\Lambda = 0.8$)

Notes: The blue solid lines and the shaded areas represent, respectively, the median and the 68% (point-wise) credible bands for impulse responses when technology shocks are identified with both IVs and sign concordance criterion.

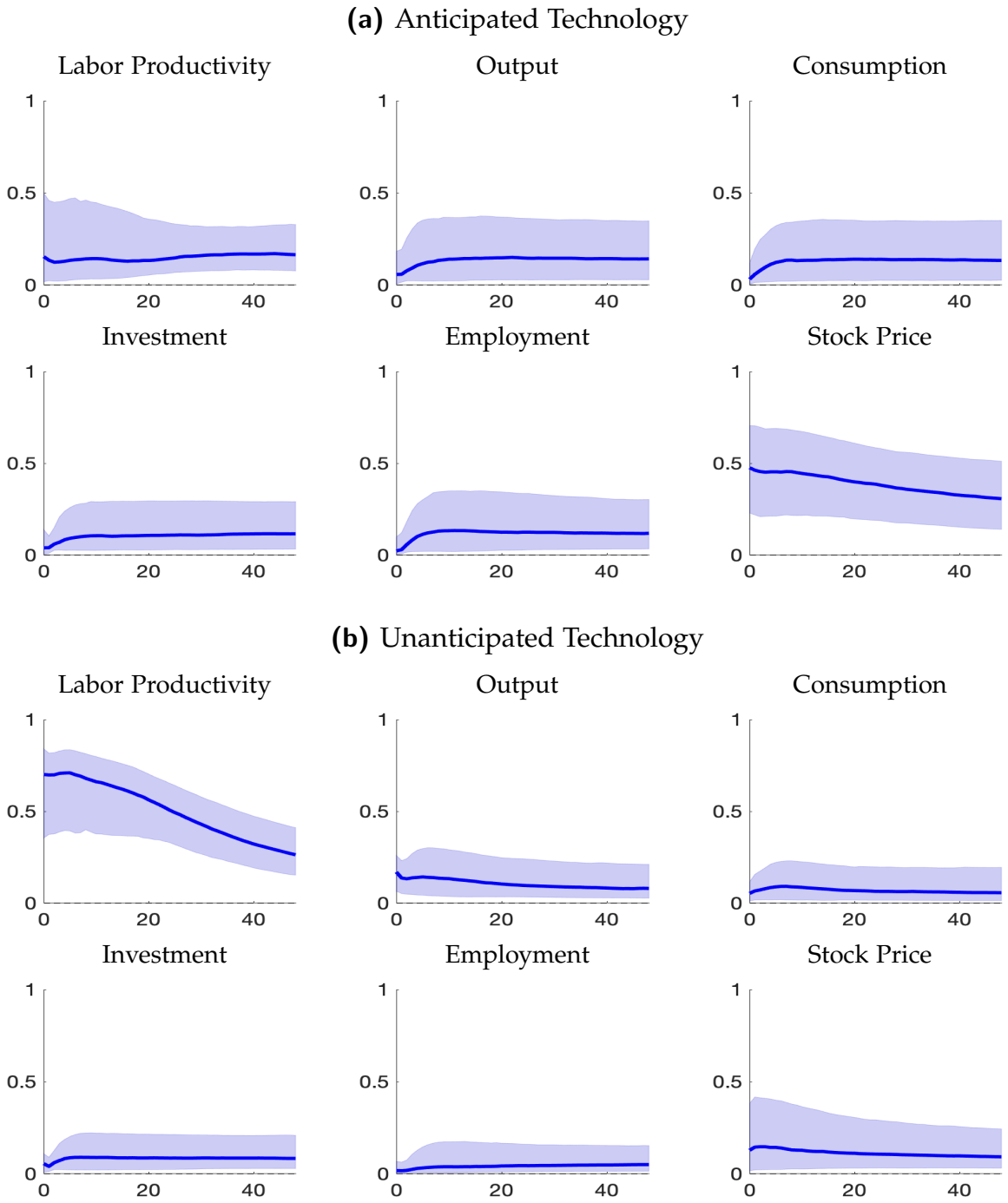

Figure D.12: Forecast Error Variance Decomposition by IVs and Sign Concordance Criterion ($\Lambda = 0.9$)

Notes: The blue solid lines and the shaded areas represent, respectively, the median and the 68% (pointwise) credible bands for forecast error variance decomposition when technology shocks are identified with both IVs and sign concordance criterion.

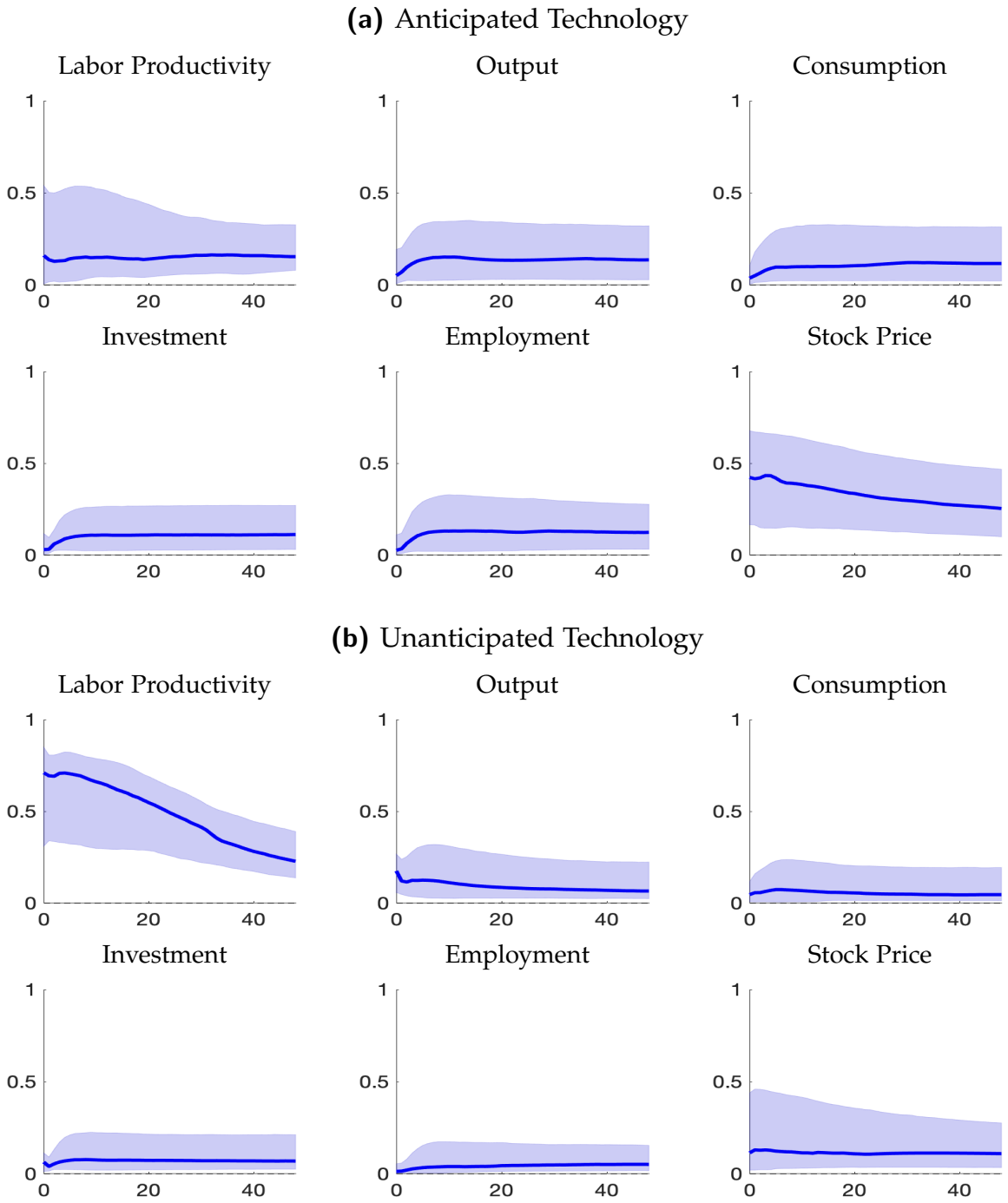

Figure D.13: Forecast Error Variance Decomposition by IVs and Sign Concordance Criterion ($\Lambda = 0.8$)

Notes: The blue solid lines and the shaded areas represent, respectively, the median and the 68% (pointwise) credible bands for forecast error variance decomposition when technology shocks are identified with both IVs and sign concordance criterion.

D.8 Impulse Responses with Robust Prior

We re-evaluate the effects of technology shocks under a robust prior using the algorithms detailed in Appendix A.2. The lower and upper bounds of the impulse responses are computed from the identified sets by solving the optimization problem with Algorithm A.3. To ensure convergence to the global optimum, we employ 25 different initial values. Figures D.14 and D.15 present the set of posterior means for the impulse responses (vertical bars) and the smallest robust credible region with 68% credibility (solid curve) for the robust multiple prior Bayesian approach. We display the posterior mean (point) and the 68% highest posterior density region (dashed curve) for the standard single prior Bayesian approach. The effects of technology shocks using robust multiple prior Bayesian approach are very similar to those using standard single prior Bayesian approach.

We further use diagnostic tools to measure the informativeness of the prior choice. Following Giacomini and Kitagawa (2021) and Giacomini et al. (2022b), the informativeness is defined as:

$$1 - \frac{\text{width of a single prior Bayesian credible region of } \eta_{ij,h} \text{ with credibility } \alpha}{\text{width of a multiple prior Bayesian credible region of } \eta_{ij,h} \text{ with credibility } \alpha}. \quad \text{(D.2)}$$

This measure captures how much the credible region of $\eta_{ij,h}$ is tightened by selecting a specific prior for the rotation matrix. The results, shown in Figures D.16 and D.17 and Table D.6, demonstrate the diagnostic statistic is mostly below 0.2. We conclude that imposing a uniform prior for the rotation matrix does not significantly affect posterior inference in our empirical application.

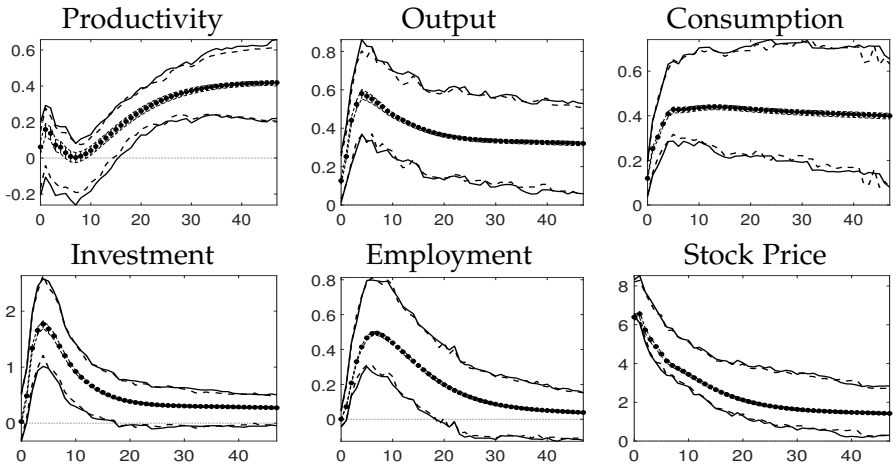

Figure D.14: IRFs to Anticipated Technology shock

Notes: In each figure, the points are the single prior Bayesian posterior means, the vertical bars are the set of multiple prior posterior means, the dashed curves are the upper and lower bounds of the single prior Bayesian highest posterior density regions with credibility 68%, and the solid curves are the upper and lower bounds of the multiple prior credible regions with credibility 68%.

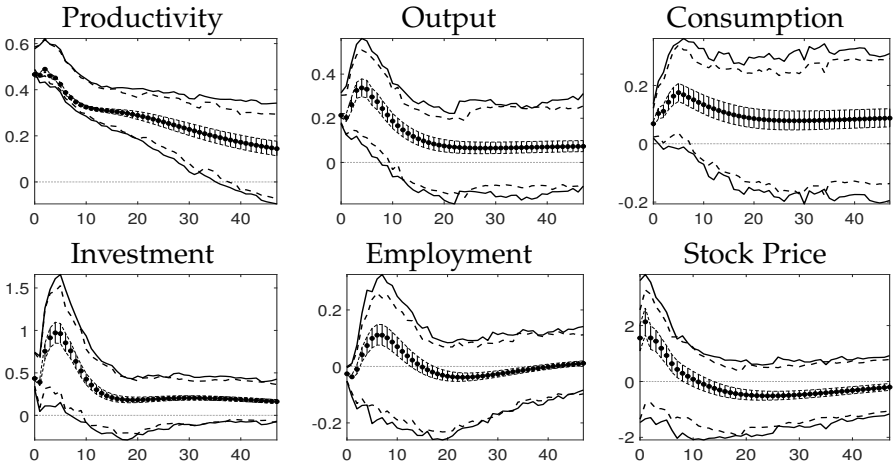

Figure D.15: IRFs to Unanticipated Technology shock

Notes: In each figure, the points are the single prior Bayesian posterior means, the vertical bars are the set of multiple prior posterior means, the dashed curves are the upper and lower bounds of the single prior Bayesian highest posterior density regions with credibility 68%, and the solid curves are the upper and lower bounds of the multiple prior credible regions with credibility 68%.

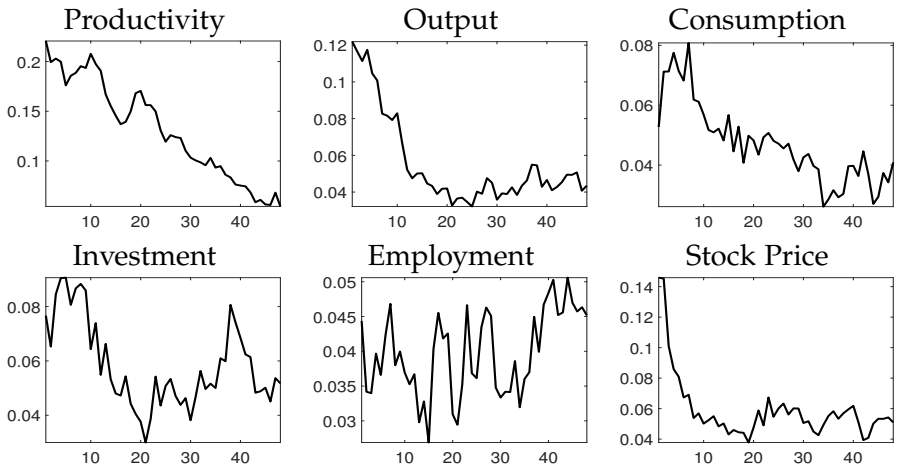

Figure D.16: Informativeness of the choice of prior for Anticipated Technology shock

Notes: Informativeness of the choice of prior is calculated using equation (D.2).

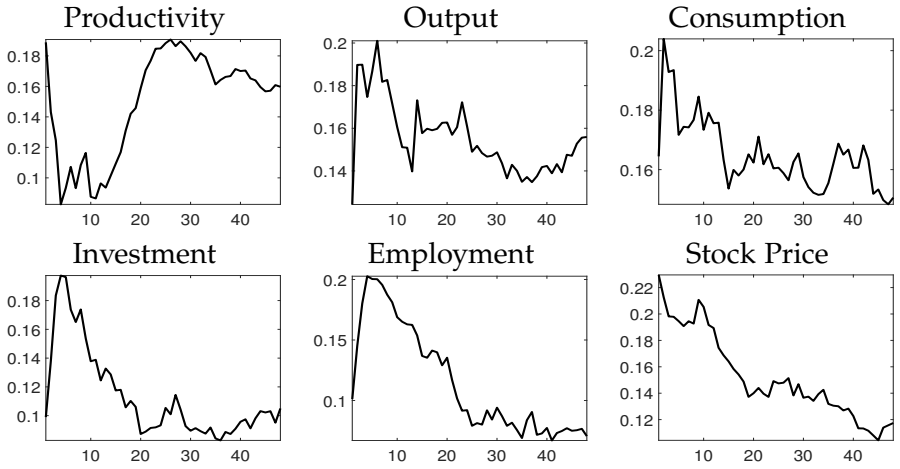

Figure D.17: Informativeness of the choice of prior for Unanticipated Technology shock

Notes: Informativeness of the choice of prior is calculated using equation (D.2).

Table D.6: Informativeness of the choice of prior

	Productivity	Output	Consumption	Investment	Employment	Stock Price
			Anticipated Technology Shock			
Average	0.13	0.06	0.05	0.06	0.04	0.06
Minimum	0.05	0.03	0.03	0.03	0.03	0.04
Maximum	0.22	0.12	0.08	0.09	0.05	0.15
			Unanticipated Technology Shock			
Average	0.15	0.16	0.16	0.11	0.11	0.15
Minimum	0.08	0.12	0.15	0.08	0.07	0.10
Maximum	0.19	0.20	0.20	0.20	0.20	0.23

Notes: Informativeness of the choice of prior is calculated using equation (D.2).

D.9 Inferences with Uniform Priors over Impulse Responses

In this section, we present the impulse responses obtained by imposing a uniform prior over impulse responses, following the method described in Section A.3. Figure D.18 displays the traditional impulse responses with 68% credible sets, representing the uncertainty using the marginal density of the impulse responses. The marginal inference is similar to our benchmark results, providing further evidence that the prior on the orthonormal matrix plays a minimal role in our analysis. Figure D.19 shows the joint posterior impulse responses using the approach of Inoue and Kilian (2022), indicating that the credible limits are qualitatively similar to the pointwise error bands, though with a wider range.

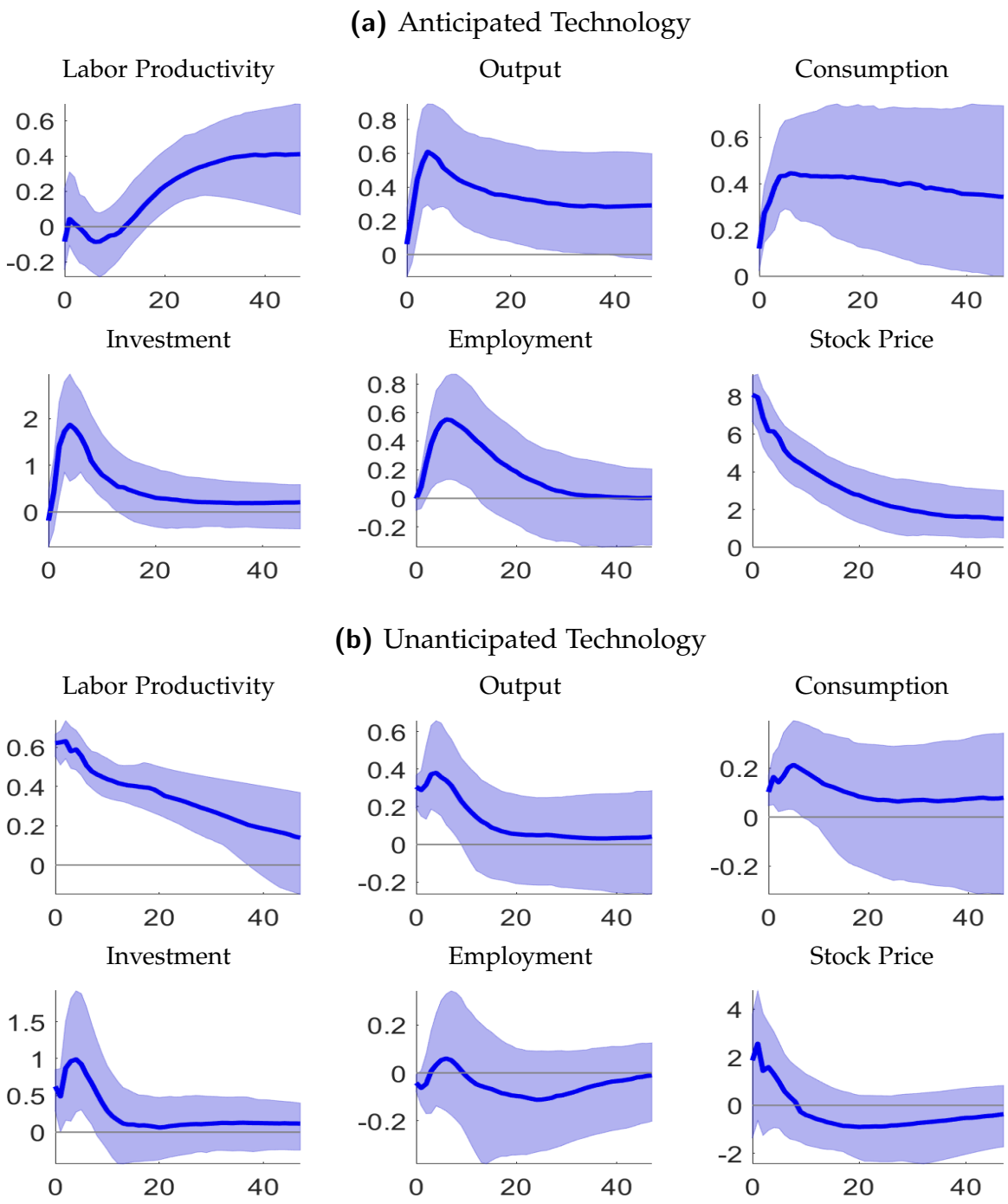

Figure D.18: Impulse Responses with 68% Pointwise Credible Bands under a Uniform Prior for Impulse Responses

Notes: The blue solid lines and the shaded areas represent, respectively, the median and the 68% (pointwise) credible bands.

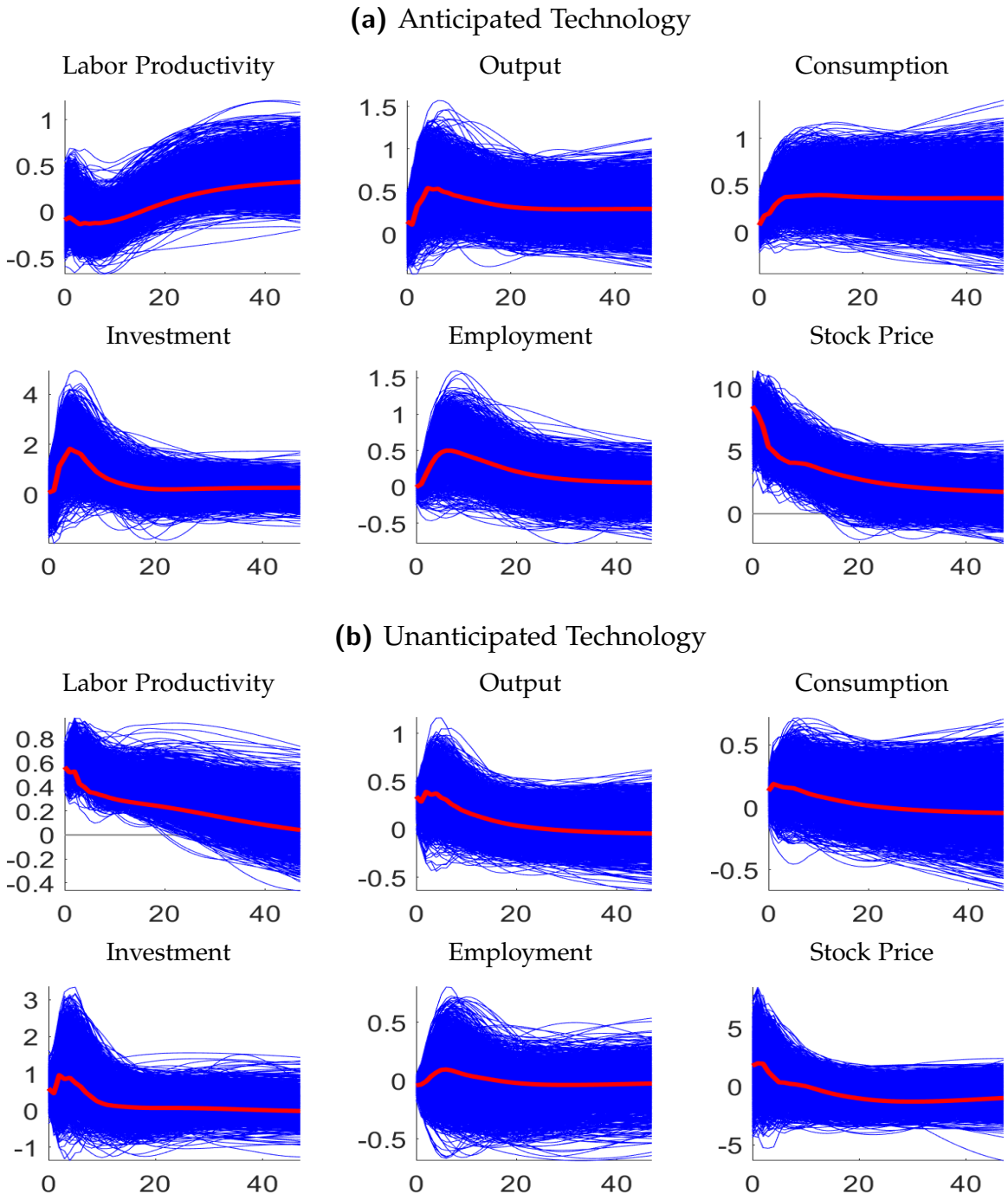

Figure D.19: Joint Posterior Impulse Responses under Uniform Priors for Impulse Responses

Notes: The red thick lines indicate the estimator of the impulse responses using Equation (A.24) and the blue thin lines represent the 68% joint credible set using Equation (A.25).

D.10 Robustness Check: Including the Inflation Rate in the Model

An intriguing question is whether our identification method reveals a supply-side or demand-side nature of technology shocks. To investigate this question, we include the inflation rate as an additional endogenous variable in our model. Figures D.20 and D.21 present the impulse responses and variance decompositions of all the endogenous variables. Most of our benchmark results remain robust with the inclusion of the inflation rate. In addition, an anticipated technology shock induces a persistent decline in inflation, while an unanticipated technology shock leads to a decrease in inflation within the first six quarters post-shock. Thus, in the short to medium term, both types of technology shocks behave like aggregate supply shocks, causing opposite movements in output and inflation.

There are three key observations to highlight. First, unlike stock prices, the inflation rate responds to anticipated technology shocks with a lag, with the effects most pronounced when the positive technology news materializes. Second, unanticipated technology shocks cause the inflation rate to increase over longer horizons, beyond six quarters. This suggests that the general equilibrium effects of unanticipated technology shocks, through their interactions with other endogenous variables, can be complex. We leave a formal analysis of these results to future research. Third, both types of technology shocks contribute minimally to the inflation rate.

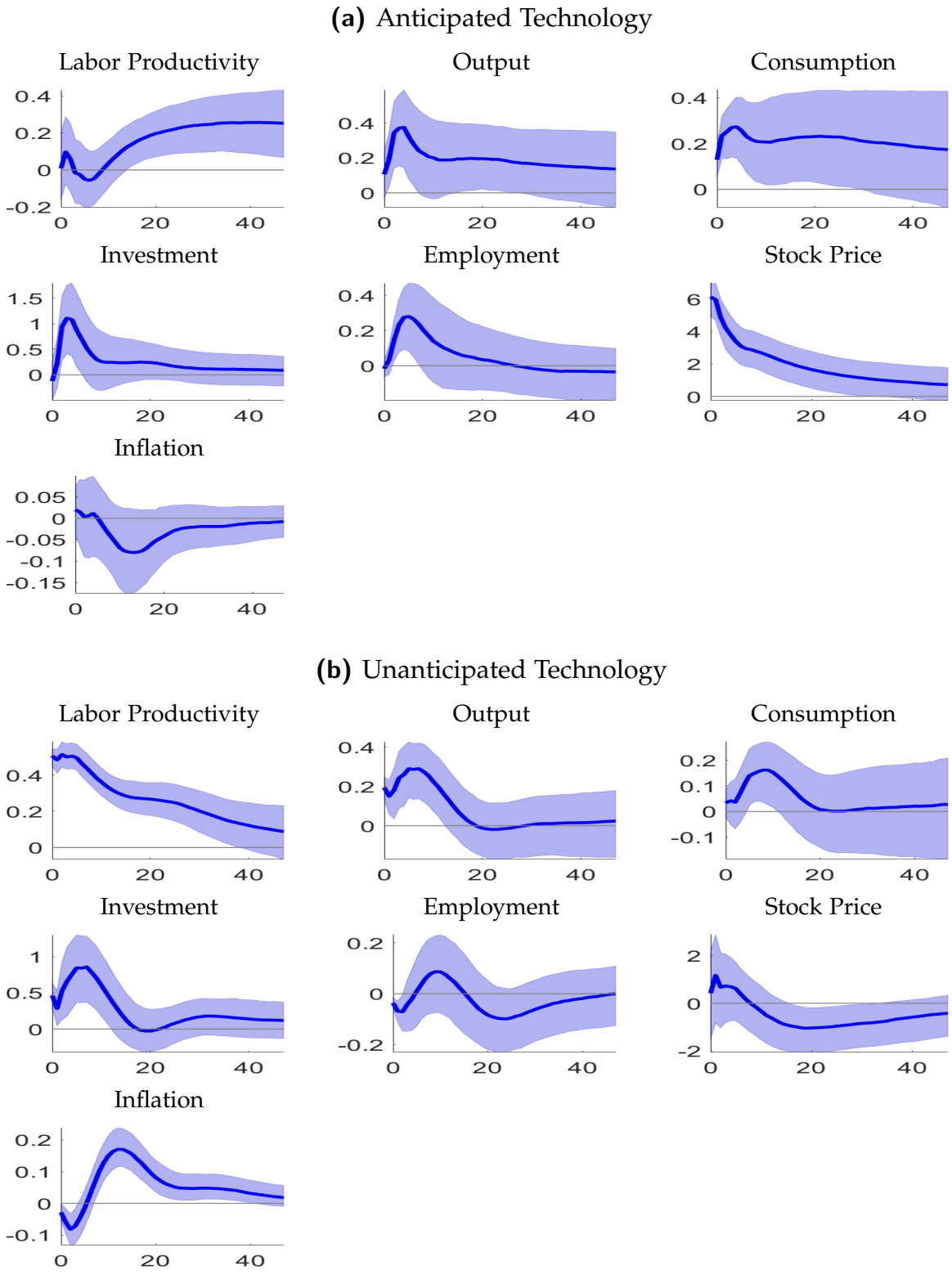

Figure D.20: Impulse Responses when Inflation Rate is Included in the SVAR Model

Notes: The blue solid lines and shaded areas represent, respectively, the median and 68% (point-wise) credible bands for impulse responses.

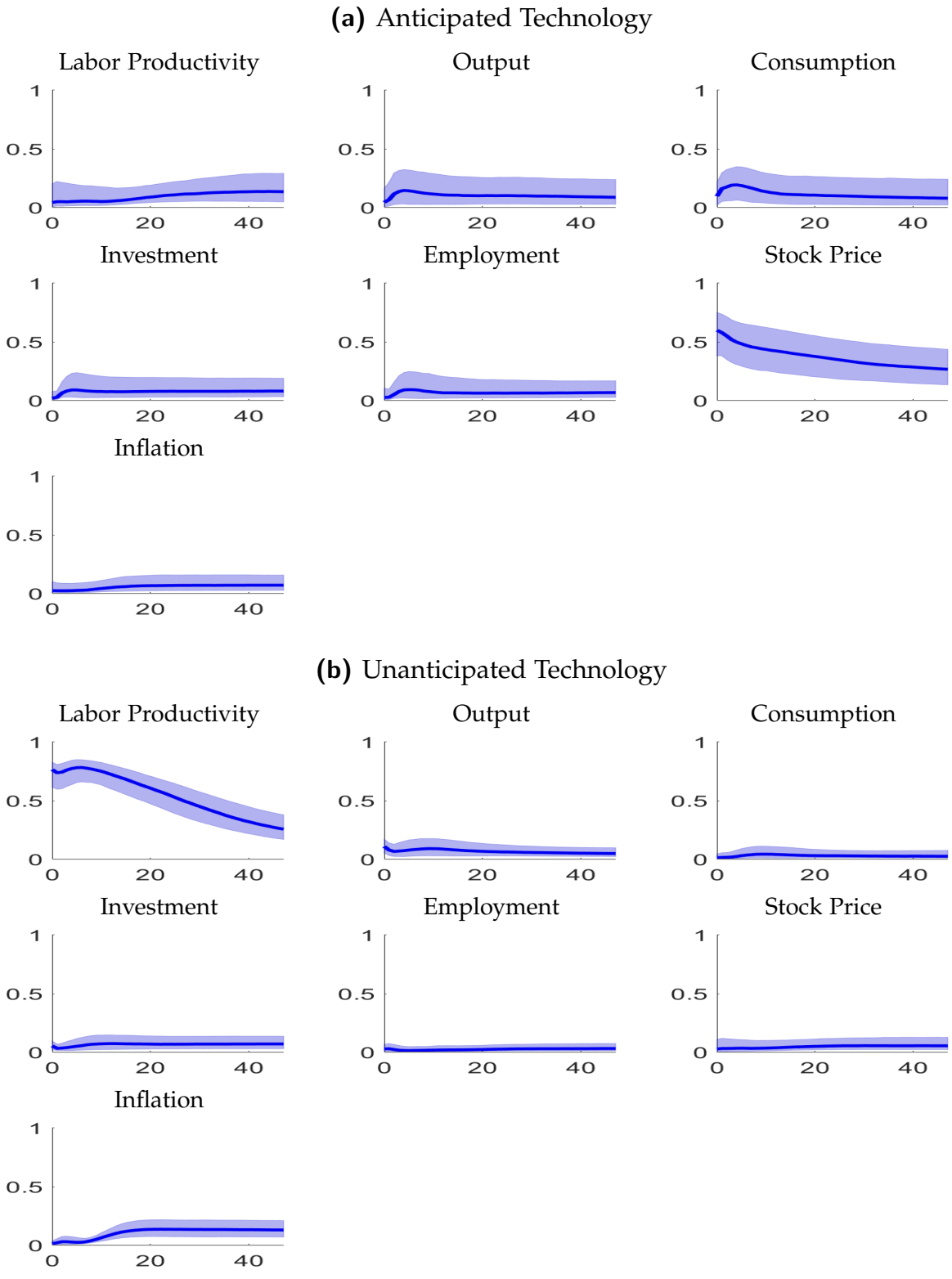

Figure D.21: Variance Decomposition when Inflation Rate is Included in the SVAR Model

Notes: The blue solid lines and shaded areas represent, respectively, the median and 68% (point-wise) credible bands for forecast error variance decompositions.

D.11 Inference versus Identification

Giacomini et al. (2022a) argue that combining proxy identification with narrative sign restrictions can influence the posterior in two ways. First, it can truncate the identified set for the structural parameters conditional on the reduced-form parameters, a process known as sharpening identification. Second, it can truncate the space of reduced-form parameters that yield a non-empty identified set, referred to as sharpening inference. It would be valuable to explore which of the two effects drives the "more informative inference" about the impacts of shocks.

In this Appendix, we begin by examining whether narrative sign restrictions primarily influence the posterior through sharpening identification. To do this, we compare the confidence bands of the impulse responses while keeping reduced-form parameters fixed. Next, we evaluate whether the narrative sign restrictions have altered the posterior distributions of the reduced-form parameters, using related statistical measures from Inoue and Kilian (2020) and Inoue and Kilian (2022). Both approaches suggest that, in our technology shock application, narrative sign restrictions primarily sharpen identification rather than inference.

D.11.1 Assessing the Role of Narrative Sign Restrictions in Sharpening Identification

To evaluate the role of narrative sign restrictions in enhancing identification, we fix the set of reduced-form parameter draws that yield a non-empty identified set under these narrative sign restrictions. We then compare the widths of the sets of posterior means (under robust priors) with and without narrative sign restrictions.[3] Specifically, we denote

$$P^N = \left\{ \tilde{\Lambda}_0^{(i),N}, \tilde{\Lambda}_+^{(i),N}, \text{diag}\left(Q_1^{(i),N}, Q_2^{(i),N}\right), i = 1, 2, \ldots, M \right\}$$

as the posterior draws of the reduced-form parameters and orthonormal matrices under narrative sign restrictions. We then fix the reduced-form parameters $(\tilde{\Lambda}_0^{(i),N}, \tilde{\Lambda}_+^{(i),N})$ and draw the orthonormal matrices without narrative sign restrictions (i.e., with only proxy exogeneity restrictions). We denote the set of accepted posterior draws with the fixed reduced-form parameters as

[3] We thank one of the referees for suggesting this method to quantify the role of narrative sign restrictions in improving the precision of identification.

$$P^{R*} = \left\{ \tilde{\Lambda}_0^{(i),N}, \tilde{\Lambda}_+^{(i),N}, \text{diag}\left(Q_1^{(i),R*}, Q_2^{(i),R*} \right), i = 1, 2, \ldots, M \right\}.$$

The statistic used to quantify the role of narrative sign restrictions in "sharpening identification" is defined as:

$$\begin{aligned} &\text{Role of "sharpening identification"} = \\ &1 - \frac{\text{The width of the set of posterior means of } \eta_{ij,h} \text{ using} P^N}{\text{The width of the set of posterior means of } \eta_{ij,h} \text{using} P^{R*}}, \end{aligned} \tag{D.3}$$

where $\eta_{ij,h}$ denotes the impulse response of the i-th variable to the j-th shock at horizon h.

This statistic ranges between zero and one, with values close to one indicating that the restrictions significantly sharpen the identification. The results of this statistic for our application to technology shocks are presented in Figure D.22 and Table D.12. The values of the statistic for all impulse responses are close to one, indicating that narrative sign restrictions play a crucial role in enhancing identification.

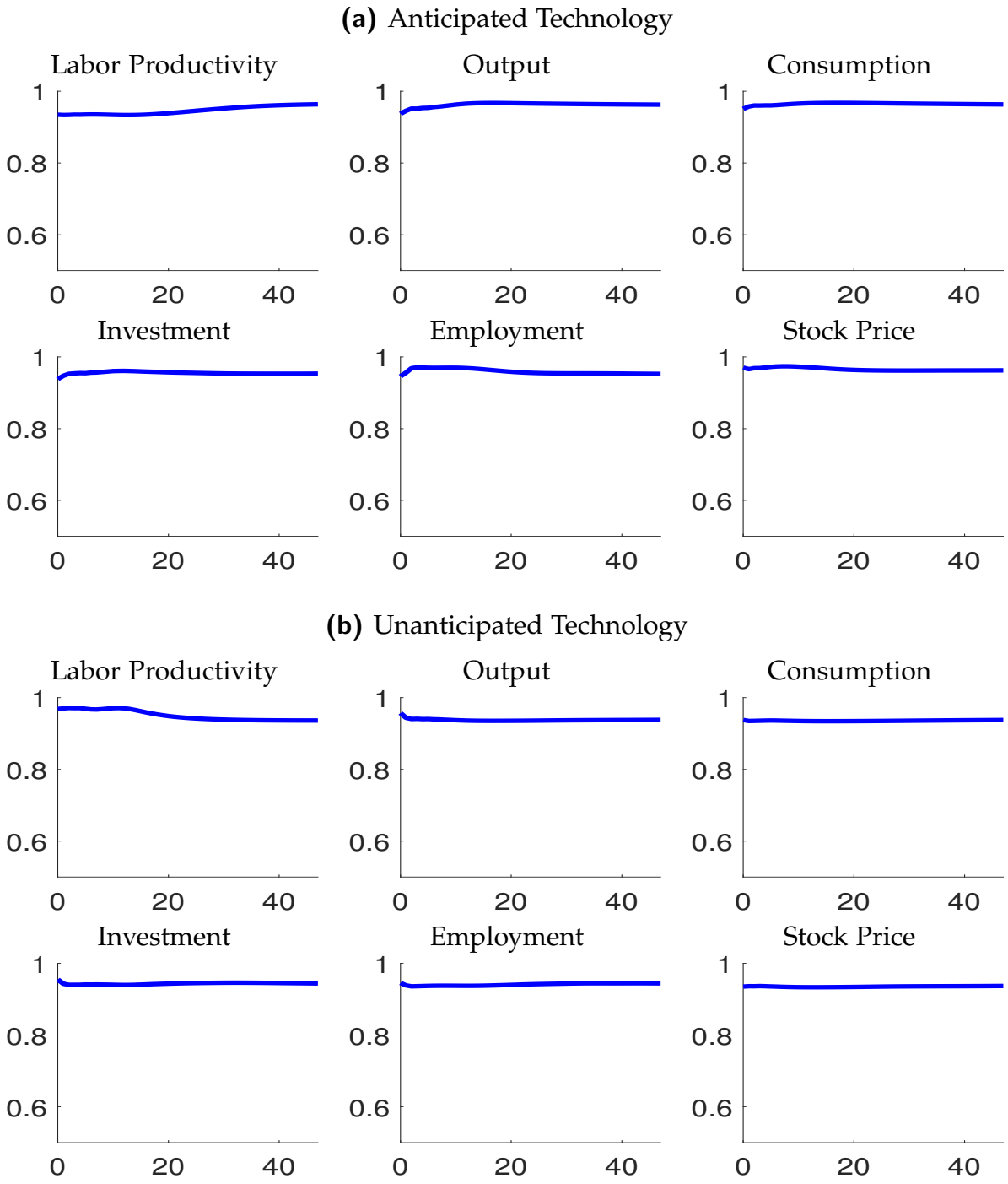

Figure D.22: Role of "sharpening identification"

Notes: In each figure, the lines plot the statistics of the role of "sharpening identification" using equation (D.3).

Table D.12: Role of "sharpening identification"

	Productivity	Output	Consumption	Investment	Employment	Stock Price
			Anticipated Technology Shock			
Average	0.95	0.96	0.96	0.96	0.96	0.97
Minimum	0.93	0.94	0.95	0.94	0.95	0.96
Maximum	0.96	0.97	0.97	0.96	0.97	0.97
			Unanticipated Technology Shock			
Average	0.95	0.94	0.94	0.94	0.94	0.94
Minimum	0.94	0.94	0.93	0.94	0.94	0.93
Maximum	0.97	0.96	0.94	0.96	0.95	0.94

Notes: The table shows the statistics of the role of "sharpening identification" using equation (D.3).

D.11.2 The Shifts in Reduced-form Parameters

We also test whether imposing additional narrative restrictions significantly shifts the posterior distribution of the reduced-form parameters. The test results indicate that the shifts are statistically insignificant. Specifically, we evaluated the average change in the central tendency and the changes in the concentration of probability mass around the reduced-form parameter, as proposed by Inoue and Kilian (2020). The change in the central tendency of the distribution is formulated as follows:

$$d_L = \sum_{i=1}^{n_\theta} \left| \hat{\bar{\theta}}^N_{M,i} - \hat{\bar{\theta}}^R_{M,i} \right| / n_\theta, \tag{D.4}$$

where n_θ represents the number of parameters in θ, M denotes the number of Bayesian draws (10,000 in our estimation), $\hat{\bar{\theta}}^N_{M,i}$ is the i-th element of the estimated central tendency of the reduced-form parameter distribution under narrative sign restrictions, and $\hat{\bar{\theta}}^R_{M,i}$ is the corresponding estimate without such restrictions.

Next, the concentration of the probability mass around the reduced-form parameter within α credible intervals is evaluated by:

$$d_C = 100 \left(\frac{C^N - C^R}{C^R} \right), \tag{D.5}$$

where $C^N = \frac{\sum_{j=1}^{M(1-\alpha)} \sum_{i=1}^{n_\theta} \left| \theta_i^{(j),N} - \hat{\bar{\theta}}^N_{M,i} \right|}{M(1-\alpha) n_\theta}$, $C^R = \frac{\sum_{j=1}^{M(1-\alpha)} \sum_{i=1}^{n_\theta} \left| \theta_i^{(j),R} - \hat{\bar{\theta}}^R_{M,i} \right|}{M(1-\alpha) n_\theta}$, and $\theta_i^{(j),N}$ contains the parameters in the (1- α)×100% (set to 68%) joint credible sets evaluated using the approach of Inoue and Kilian (2022).

Table D.13 confirms that both d_L and d_C fall within the 95% credible bands as assessed by the resampling method. We therefore conclude that there is no significant evidence to suggest that narrative sign restrictions influence the distribution of reduced-form parameters.

Table D.13: Testing for the shifts in reduced-form parameter distribution

Statistics	Value	95% Credible Bands
d_L	0.170	(0.156,0.197)
d_C	0.358	(-2.537,1.358)

Notes: The credible set is produced using the resampling approach in three steps: Step 1. Draw reduced-form parameters under narrative sign restrictions M times, denoted as $\Theta_M^{\text{Narrative}}$. Draw reduced-form parameters without narrative sign restrictions M times, denoted as $\Theta_M^{\text{NoNarrative}}$. Calculate d_L and d_C using $\Theta_M^{\text{Narrative}}$ and $\Theta_M^{\text{NoNarrative}}$. Step 2. Draw additional reduced-form parameters without narrative sign restrictions M times, denoted as $\overline{\Theta}_{M,1}^{\text{NoNarrative}}$. Calculate the test statistics using $\Theta_M^{\text{NoNarrative}}$ and $\overline{\Theta}_{M,1}^{\text{NoNarrative}}$, denoted as $d_L^{(1)}$ and $d_C^{(1)}$. Step 3. Repeat Step 2 1000 times to obtain $d_L^{(i)}$ and $d_C^{(i)}$, where $i = 1, 2, \ldots, 1000$. Calculate credible bands using $d_L^{(i)}$ and $d_C^{(i)}$, where $i = 1, 2, \ldots, 1000$.

D.12 Robustness Checks with Additional Correlation Restrictions

In this section, we assess the robustness of our empirical findings by imposing additional inequality restrictions on the correlations between IVs and structural shocks, as proposed by Piffer and Podstawski (2018).

Consider the case where we use two IVs to identify two structural shocks. Equation (7) implies that:

$$E\left[\begin{pmatrix} m_{1t} \\ m_{2t} \end{pmatrix}\begin{pmatrix} \varepsilon_{n-1,t} & \varepsilon_{n,t} \end{pmatrix}\right] = \begin{bmatrix} E(m_{1t}\varepsilon_{n-1,t}) & E(m_{1t}\varepsilon_{n,t}) \\ E(m_{2t}\varepsilon_{n-1,t}) & E(m_{2t}\varepsilon_{n,t}) \end{bmatrix} = \underbrace{\begin{bmatrix} V_{11} & V_{12} \\ V_{21} & V_{22} \end{bmatrix}}_{V}. \tag{D.6}$$

Piffer and Podstawski (2018) propose imposing sign restrictions on the matrix V. Specifically, they suggest the following restrictions:

$$V_{11} > 0; \quad V_{22} > 0, \tag{D.7}$$

$$V_{11} - V_{12} > \psi; \quad V_{22} - V_{21} > \psi. \tag{D.8}$$

In their study, Piffer and Podstawski (2018) set ψ to 0.1. We incorporate these additional sign restrictions into our baseline model, and the results are presented in Figures D.23 and D.24. Our findings indicate that the results remain robust when these additional sign restrictions are imposed. The results are also similar when setting ψ to 0 or 0.2.

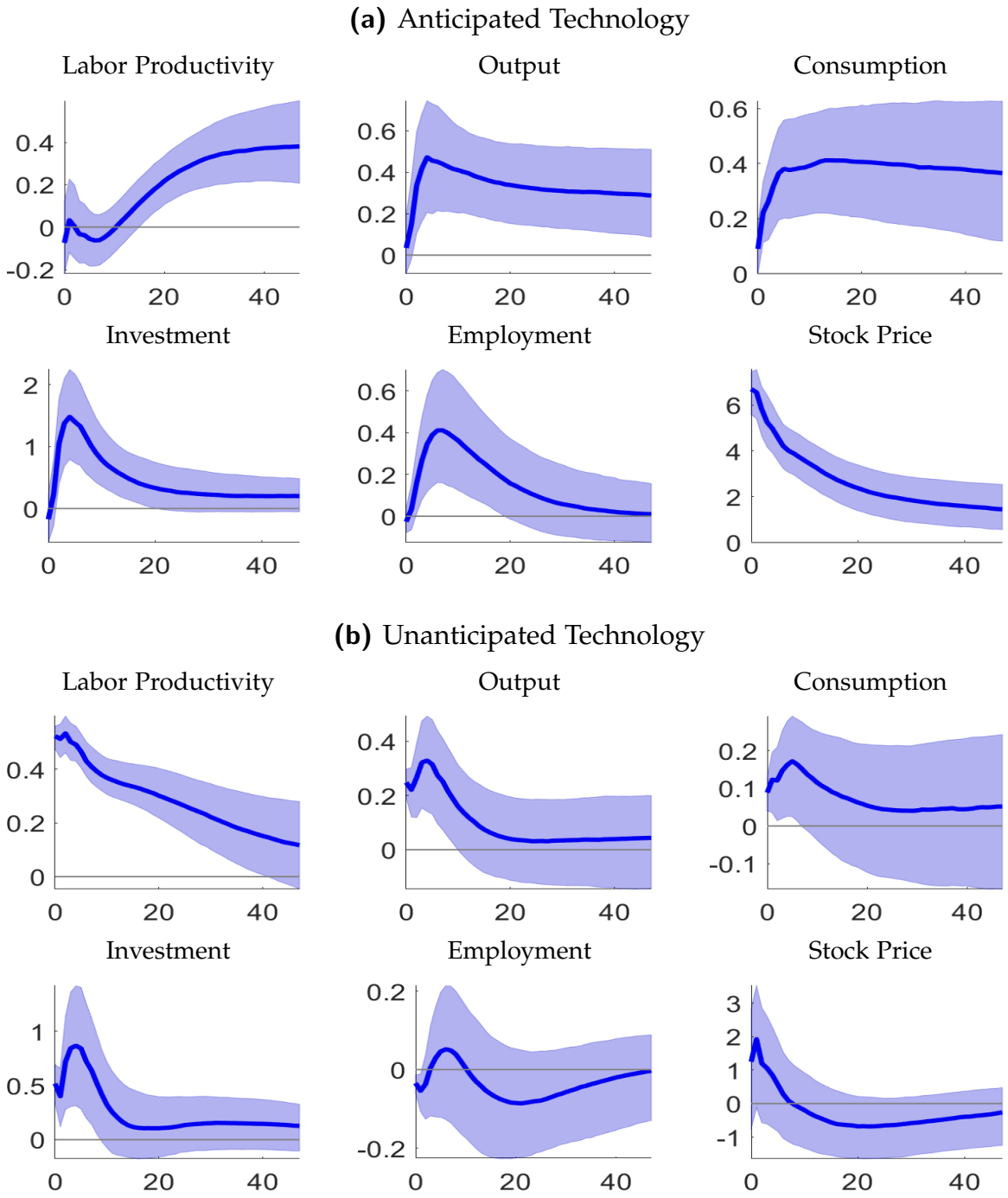

Figure D.23: Impulse Responses by Imposing Additional Sign Restrictions

Notes: The blue solid lines and shaded areas represent, respectively, the median and 68% (point-wise) credible bands for impulse responses.

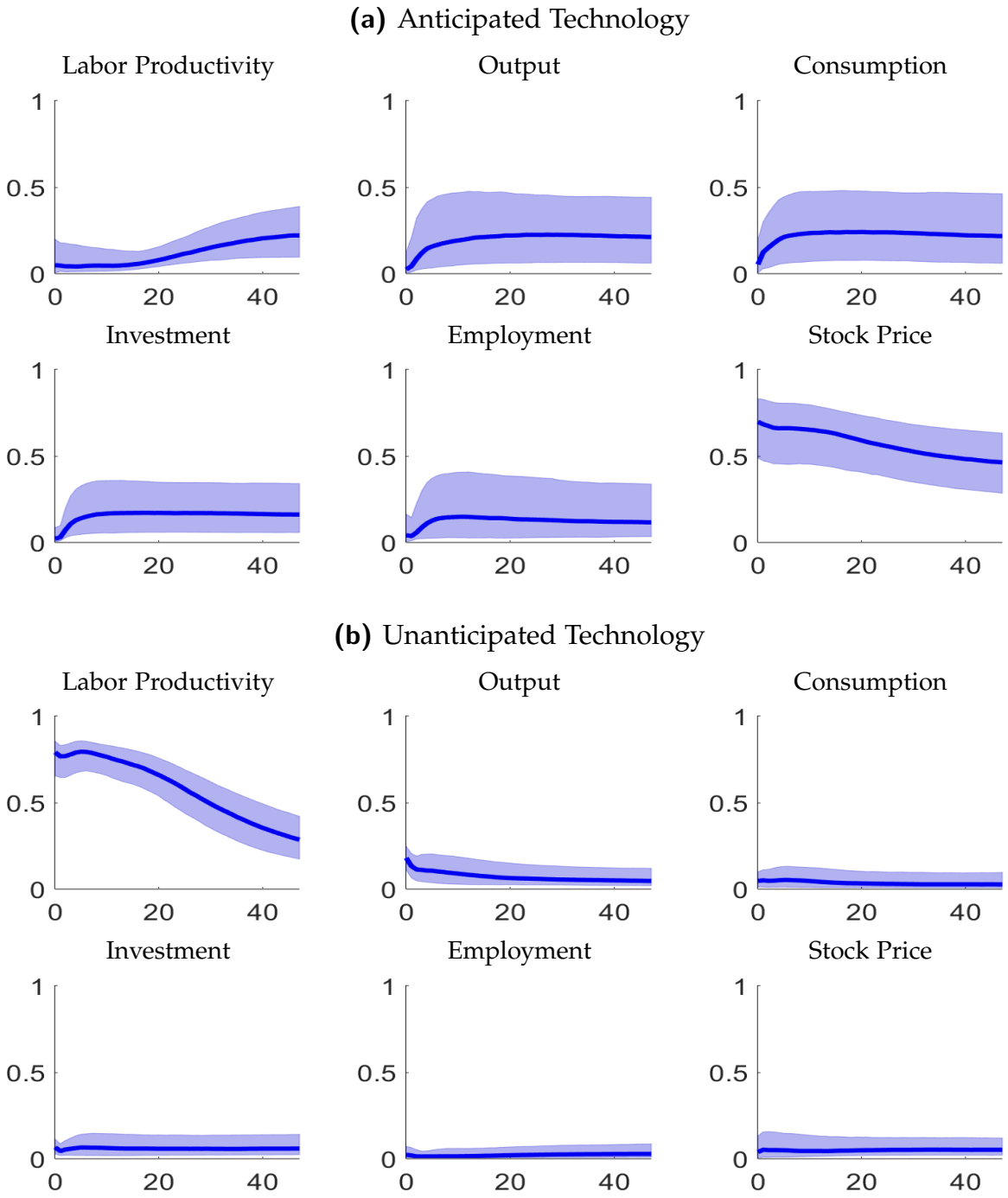

Figure D.24: Forecast Error Variance Decomposition by Imposing Additional Sign Restrictions

Notes: The blue solid lines and shaded areas represent, respectively, the median and 68% (point-wise) credible bands for forecast error variance decompositions.

E Labor Search and Matching Model

The empirical exercise in the main text establishes a plethora of empirical evidence about the effects of technology shocks based on our novel identification strategy. To check the theoretical coherence of the empirical findings, we turn to explore to what extent a micro-founded structural model can be tuned to replicate the SVAR shock effects. In particular, we modify the labor search and matching model of Chahrour et al. (2023) to allow for variable capital utilization and then estimate structural parameters to replicate the empirical responses to anticipated technology shocks. We place anticipated technology shocks in the limelight since unanticipated technology shocks have been estimated to be of little empirical relevance to business cycle fluctuations. The exercise entitles us to evaluate several critical parameters that facilitate the replication of empirical dynamics. It also serves as a litmus test to understand the theoretical implications delivered by different SVAR-identification procedures.

The search and matching model is featured with three types of agents: households, firms, and the government. Households derive utility from consumption and leisure from non-participation in labor. They are either employed, searching for work, or not in the labor force. In each period, a portion of the households search for a job and get matched. Previous matches dissolve with an exogenous probability. Households own capital and choose capital utilization rate optimally. Firms produce output with non-stationary technology. Each period, firms post vacancies and pay costs for posting vacancies, which include both steady-state costs and adjustment costs. The stock price of a firm depends on both the value of the firm and leverage. The government runs a balanced budget and resorts to lump-sum taxes to finance its spending and unemployment benefit transfers.

In the sections that follow, we outline the components of our study as follows: the model environment is described in Section E.1; the stationary equilibrium conditions are presented in Section E.2; parameter calibration is discussed in Section E.3; and the implications of the model are analyzed in Section E.4.

E.1 Model Environment

The representative households are ex-ante identical with preference in the form of Greenwood et al. (1988) adjusted as in Akıncı and Chahrour (2018) and Chahrour et al.

(2023) to allow for balanced growth. This type of preference eliminates the wealth effects on labor supply that may cause labor supply to fall in response to positive news shocks. Households derive utility from consumption (C_t) and leisure from non-participation in labor force in the form of:

$$U\left(C_t, F_t\right) = \frac{\left(C_t - \psi X_t F_t^{\theta}\right)^{1-\sigma}}{1-\sigma}, \tag{E.1}$$

where F_t denotes the measure of household members in the labor force, X_t represents a non-stationary labor-augmenting technology shock, σ symbolizes the inverse of intertemporal elasticity of substitution, θ stands for labor supply elasticity, and ψ is the preference parameter that governs the disutility from participating in labor force.

The households are either employed, searching for work, or not in the labor force. Each period, a portion (S_t) of the households search for a job and get matched with a probability, p_t. The labor force participation (F_t) is defined as the sum of currently employed households (N_t) and the portion of searching households who fail to get matched ($(1-p_t)S_t$) :

$$F_t = N_t + (1-p_t)\, S_t. \tag{E.2}$$

In each period, previous matches dissolve with an exogenous probability λ so that the law of motion of employment follows:

$$N_t = (1-\lambda)N_{t-1} + p_t S_t. \tag{E.3}$$

We assume that households own the capital stock (K_t) which evolves according to:

$$K_{t+1} = (1-\delta(u_t))K_t + I_t, \tag{E.4}$$

where I_t is investment and u_t represents the level of utilization. The depreciation of capital depends on capital utilization in a quadratic form:

$$\delta(u_t) = \delta_0 + \phi_1(u_t - 1) + \frac{\phi_2}{2}(u_t - 1)^2. \tag{E.5}$$

The households' budget constraint is given by:

$$C_t + I_t + \tau_t = R_t u_t K_t + W_t N_t + (1-p_t)\, S_t \kappa W_t + D_t, \tag{E.6}$$

where R_t is the rental rate of capital, $u_t K_t$ indicates the capital services, and D_t represents the lump-sum tax received from firms. The households also pay a lump-sum tax (τ_t) and receive unemployment benefits (κW_t). The households' problem can be summarized as:

$$\max_{C_t, I_t, K_{t+1}, S_t, N_t} E_0 \sum_{t=0}^{\infty} \beta^t \frac{\left(C_t - \psi X_t F_t^{\theta}\right)^{1-\sigma}}{1-\sigma} \qquad \text{s.t. (E.2), (E.3), (E.4) , (E.5)and (E.6).}$$

Firms produce output with a production form of:

$$F\left(K_t, X_t N_t\right) = \left(u_t K_t\right)^{\alpha} \left(X_t N_t\right)^{1-\alpha}, \tag{E.7}$$

where technology, X_t, is assumed as an I(1) process. We assume that technology growth, defined as $\gamma_{x,t} = X_t / X_{t-1}$, follows an AR(1) process in the form of:

$$\log(\gamma_{x,t}/\gamma_x) = \rho_x \log\left(\gamma_{x,t-1}/\gamma_x\right) + \varepsilon_{x,t-h}, \tag{E.8}$$

where $\varepsilon_{x,t-h}$ denotes the technology news received at period $t-h$ but realized at time t. We follow Chahrour et al. (2023) and choose the time horizon of the anticipated technology shocks, h as 7. However, the results are robust when switching to other time horizons. The labor productivity is accordingly defined as:

$$F\left(K_t, X_t N_t\right) / N_t = \left(u_t K_t / N_t\right)^{\alpha} \left(X_t\right)^{1-\alpha}. \tag{E.9}$$

Each period, firms post vacancies, V_t ,with a probability q_t returning a match so that the employed labor evolves according to:

$$N_t = (1-\lambda) N_{t-1} + q_t V_t. \tag{E.10}$$

Firms incur costs for posting vacancies, which include both steady-state costs, a_n, and adjustment costs, $\nu\left(\frac{V_t}{V_{t-1}}\right)$. The total cost is scaled by X_t to induce stationarity of the models:

$$\left(a_n + \nu\left(\frac{V_t}{V_{t-1}}\right)\right) X_t V_t, \tag{E.11}$$

with

$$\nu\left(\frac{V_t}{V_{t-1}}\right) = \frac{\xi}{2}\left(\frac{V_t}{V_{t-1}} - 1\right)^2. \tag{E.12}$$

To summarize, firms maximize the present value of their profits (output less its payments to workers, capital, and for the posting of vacancies) by solving:

$$V_t^{firm} = \max_{V_t, N_t, K_t} E_0 \sum_{t=0}^{\infty} \beta^t \frac{U_{C,t}}{U_{C,0}} \left[Y_t - W_t N_t - u_t R_t K_t - \left(a_n + \nu\left(\frac{V_t}{V_{t-1}}\right)\right) X_t V_t \right]$$
$$\text{s.t. (E.7) (E.10) and (E.12)}, \tag{E.13}$$

where V_t^{firm} denotes the value of the firm. Stock prices, SP_t, depend on both the value of the firm and leverage represented by ϕ_{lev} in the form of:

$$\Delta SP_t \equiv \left(\Delta V_t^{firm}\right)^{\phi_{lev}}. \tag{E.14}$$

To preserve balanced growth, we assume that government spending grows at a speed of $\gamma_{x,t-1}$ so that

$$G_t = G_{t-1}\gamma_{x,t-1}. \tag{E.15}$$

The government runs a balanced budget and uses lump-sum taxes to finance its spending and unemployment benefit transfers:

$$\tau_t = G_t + (1 - p_t)\, S_t \kappa_t. \tag{E.16}$$

To describe the matching process, we assume a Cobb-Douglas matching function:

$$M_t = \chi V_t^{\varepsilon} S_t^{1-\varepsilon}, \tag{E.17}$$

where ε stipulates the matching function elasticity while $M_t = p_t S_t = q_t V_t$ denotes matches between searching households and hiring firms.

To complete the model description, we again follow Chahrour et al. (2023) and assume an "agnostic" real wage, which postulates that real wage growth follows an MA(H) process. The MA process is augmented with an error-correction term so that wages are cointegrated with technology:

$$\Delta log(W_t) = \gamma(L)\varepsilon_t^W - \varphi_x \left(log(W_{t-1}) - log(X_{t-1}) \right). \tag{E.18}$$

E.2 Stationary Representation

We can solve the optimization problems and derive the stationary equilibrium equations. Denoting detrended variables according to $\tilde{\Delta}_t \equiv \frac{\Delta_t}{X_{t-1}}$ for $\Delta_t \in \left\{ Y_t, C_t, D_t, W_t, K_t, I_t, \varphi_t^N \right\}$ and $\tilde{U}_{C,t} \equiv \frac{U_{C,t}}{X_{t-1}^{-\sigma}}$, and $\tilde{U}_{F,t} \equiv \frac{U_{F,t}}{X_{t-1}^{1-\sigma}}$ we can write the model in terms of only stationary variables:

$$\tilde{Y}_t = \left(u_t \tilde{K}_t \right)^{\alpha} \left(\gamma_{x,t} N_t \right)^{1-\alpha} \tag{E.19}$$

$$F_t = N_t + (1 - p_t) S_t \tag{E.20}$$

$$N_t = (1 - \lambda) N_{t-1} + M_t \tag{E.21}$$

$$\tilde{K}_{t+1} = \gamma_{x,t}^{-1} \left[(1 - \delta(u_t)) \tilde{K}_t + \tilde{I}_t \right] \tag{E.22}$$

$$\tilde{Y}_t = \tilde{C}_t + \tilde{I}_t + \tilde{G}_t + \left(a_n + \nu \left(\frac{V_t}{V_{t-1}} \right) \right) \gamma_{x,t} V_t \tag{E.23}$$

$$\tilde{D}_t = \tilde{Y}_t - \tilde{W}_t N_t - u_t R_t \tilde{K}_t - \left(a_n + \nu \left(\frac{V_t}{V_{t-1}} \right) \right) \gamma_{x,t} V_t \tag{E.24}$$

$$1 = E_t \left\{ \Omega_{t,t+1} \left[1 - \delta(u_t) + u_{t+1} R_{t+1} \right] \right\} \tag{E.25}$$

$$\tilde{\varphi}_t^N = (1 - \alpha) \left(\frac{u_t \tilde{K}_t}{\gamma_{x,t} N_t} \right)^{\alpha} \gamma_{x,t} - \tilde{W}_t + (1 - \lambda) E_t \left\{ \Omega_{t,t+1} \gamma_{x,t} \tilde{\varphi}_{t+1}^N \right\} \tag{E.26}$$

$$\tilde{\varphi}_t^N = \frac{\gamma_{x,t}}{q_t} \left[a_n + \nu \left(\frac{V_t}{V_{t-1}} \right) + \nu' \left(\frac{V_t}{V_{t-1}} \right) \frac{V_t}{V_{t-1}} - E_t \left\{ \Omega_{t,t+1} \gamma_{x,t+1} \nu' \left(\frac{V_{t+1}}{V_t} \right) \left(\frac{V_{t+1}}{V_t} \right)^2 \right\} \right] \tag{E.27}$$

$$R_t = \alpha \left(\frac{u_t \tilde{K}_t}{\gamma_{x,t} N_t} \right)^{\alpha - 1} \tag{E.28}$$

$$-\frac{\tilde{U}_{F,t}}{\tilde{U}_{C,t}} = (1 - p_t) \tilde{\kappa}_t + p_t \left[\tilde{W}_t + (1 - \lambda) E_t \left\{ \Omega_{t,t+1} \gamma_{x,t} \left(\frac{1 - p_{t+1}}{p_{t+1}} \right) \left(-\frac{\tilde{U}_{F,t+1}}{\tilde{U}_{C,t+1}} - \tilde{\kappa}_{t+1} \right) \right\} \right] \tag{E.29}$$

$$\tilde{P}_t = \frac{\tilde{Y}_t - u_t R_t \tilde{K}_t - \left(a_n + \nu \left(\frac{V_t}{V_{t-1}} \right) \right) \gamma_{x,t} V_t}{N_t} \tag{E.30}$$

$$\tilde{W}_t = \omega_0 \tilde{P}_t^{\omega^F} \left(\tilde{W}_{t-1} / \gamma_{x,t-1} \right)^{1 - \omega^F} \tag{E.31}$$

$$\delta(u_t) = \delta_0 + \phi_1(u_t - 1) + \frac{\phi_2}{2}(u_t - 1)^2 \tag{E.32}$$

$$R_t = \phi_1 + \phi_2(u_t - 1) \tag{E.33}$$

where $\Omega_{t,t+1} \equiv \beta \frac{\tilde{u}_{c,t+1}}{\tilde{u}_{c,t}} \gamma_{x,t}^{-\sigma}$.

E.3 Parameter Calibration and Estimation

We calibrate a large set of parameters as listed in Table E.1. In particular, we calibrate the long-run growth rate, γ_x, to 0.5%, which is the average labor productivity growth over the sample. Consistent with Christiano et al. (2005) and Smets and Wouters (2007), we calibrate the steady-state depreciation rate, δ_0, to 0.025. We set the capital share, α, and the inverse of intertemporal elasticity of substitution, σ, respectively to 0.3 and 1.5 referring to the corresponding prior means selected in Smets and Wouters (2007). Similar to Petrongolo and Pissarides (2001) and Gavazza et al. (2018), we pick 0.5 as the value of the matching function elasticity, ϵ. We set the discount factor, β, to 0.9975, which implies that the annualized steady-state real interest rate, $r = 4(1/\beta\gamma^{-\sigma} - 1)$, equals 4%.[4]

Considering that the search model largely follows Chahrour et al. (2023), we calibrate the following parameters to the same values as in their paper. In particular, the disutility of participation parameter, ψ, is set to 1.088, and the steady state vacancy posting cost is calibrated to 0.29 to be consistent with standard long-run empirical labor market statistics.[5] The separation rate, λ, is set to 0.12 according to the estimates of Yashiv (2007). The replacement rate of unemployment benefits, κ, is calibrated to 0.2 to match the average replacement rate from OECD (1994). The leverage factor, ϕ_{lev}, is set to 1.5, which implies that the long-run debt-to-book value of public firms of 1/3. The wage correction parameter is fixed to 0.05.

We then estimate numerous parameters that lack guidance from (or agreement in) the literature. First, we estimate the labor supply parameter, θ, in the utility function, with labor supply elasticity formulated by $1/(\theta - 1)$. Second, we assume that capital

[4] Chahrour et al. (2023) calibrate β to 0.99 and γ_x to 1.004. They also report an estimate of σ to 2.058, which actually implies an annualized steady-state real interest rate of 7.37%.

[5] Chahrour et al. (2023) derive these values by imposing that the unemployment rate, $\bar{un}$ = 0.06, and the match probability for firms, $\bar{q}$ = 0.90, and our value for the ratio of vacancy posting costs to the marginal product of labor, Ψ^v = 0.17.

Table E.1: Calibrated Parameters

Parameter	Concept	Value	Source
γ_x	Productivity growth (average)	1.005	Data
σ	Inv. intertemporal elasticity	1.500	Smets and Wouters (2007)
α	Capital share	0.300	Smets and Wouters (2007)
δ_0	Depreciation rate (steady state)	0.025	Smets and Wouters (2007)
ε	Matching function elasticity	0.500	Gavazza et al. (2018)
β	Discount factor	0.9975	Moran and Queralto (2018)
λ	Separation rate	0.120	Chahrour et al. (2023)
ψ	Preference parameter	1.088	Chahrour et al. (2023)
κ	Replacement rate	0.200	Chahrour et al. (2023)
a_n	Vacancy posting cost (steady state)	0.290	Chahrour et al. (2023)
ϕ_{lev}	Leverage factor	1.500	Chahrour et al. (2023)
ϕ_x	Wage error-correction	0.050	Chahrour et al. (2023)

Notes: The table displays the parameter values used for calibration in the labor search and matching model.

depreciation depends on the utilization rate in a quadratic form and estimate the curvature parameter of the depreciation function, ϕ_2. A sizable ϕ_2 recommends a low degree of capital utilization variations. Third, we postulate that firms face a quadratic vacancy adjustment cost and estimate the curvature of the function denoted by ξ. Fourth, we consider a non-stationary technology with its growth rate following a simple AR(1) process driven by anticipated technology shocks. We estimate the persistence of the process, ρ_x, and the standard deviations of anticipated technology shocks, σ_x.[6] Finally, we follow Chahrour et al. (2023) and assume an "agnostic" real wage, which stipulates that real wage growth follows a moving average process with 40 lags. We estimate moving average parameters $\gamma_0, \gamma_1, \ldots \gamma_{40}$.

We infer the vector of model parameters, $\Theta \equiv \{\theta, \phi_2, \xi, \rho_x, \sigma_x, \gamma_0, \gamma_1, \ldots \gamma_{40}\}$, by minimizing the distance between model-implied responses following anticipated technology shocks, $\psi(\Theta)$, and their SVAR counterparts, ψ_{VAR}, for horizons of up to 50 periods. Formally,

$$\hat{\Theta} = \arg\min_{\Theta} (\psi_{VAR} - \psi(\Theta))' W (\psi_{VAR} - \psi(\Theta)), \tag{E.34}$$

where W is a diagonal matrix comprised of the inverse of the posterior variance of the

[6] In the benchmark, we postulate that anticipated technology shocks will be realized seven quarters after observing the shock. However, the results are robust when switching to other anticipation horizons.

SVAR impulse responses. Column "Benchmark" of Table E.2 reports parameter estimates. The preference parameter, θ, is estimated to be 3.101, which corresponds to an elasticity of labor supply around $1/(\theta - 1) = 0.48$. This is close to the estimates of the Frisch elasticity using micro data which cluster around 0.4 (Reichling and Whalen 2012). The estimated curvature parameter of the quadratic capital utilization function is 2.5, informing a moderate degree of utilization variation. The vacancy posting cost, ξ, is analogous to Chahrour et al. (2023) at 0.727. Technology growth is exceptionally persistent ($\rho_x = 0.981$) with small anticipated technology shocks ($\sigma_x = 0.018$), intimating that the half-life of the technology response starting from the maximum is around 41 quarters.[7] To conserve space, we refrain from reporting the numerical values of the moving average parameters associated with wage process and instead present their implications for wage responses in Figure E.1. In line with Chahrour et al. (2023), wage diminishes instantly following expansionary anticipated technology shocks but eventually elevates above its initial level when shocks are materialized.

Table E.2: Estimated Parameter Values

Parameter	Concept	Benchmark	BS	CCP
θ	Labor supply parameter	3.101	1.113	0.569
ϕ_2	Factor utilization	2.500	100000	0.241
ξ	Vac. posting cost	0.727	0.028	1.100
ρ_x	Technology growth (persistence)	0.981	0.935	0.939
σ_x	Technology growth (std. dev.)	0.018	0.030	0.055

Notes: The table displays the estimated parameter values by matching the impulse responses implied by the search and matching model with SVAR responses identified with different methods. Columns 3 to 5 correspond to the results when shocks are respectively identified with our benchmark procedure, Barsky and Sims (2011) method, and Chahrour et al. (2023) approach.

E.4 Impulse Responses

Figure E.2 collates SVAR impulse responses (in blue lines) with the ones created by the search and matching model (in black dashed lines). The theoretical model provides

[7]The presence of persistent technology growth implies that the real interest rate incorporates a persistent component driven by households' intertemporal consumption decisions. This finding aligns with the assumption made in the empirical literature that estimates the natural rate of interest, as proposed by Laubach and Williams (2003), and further explored by Wynne and Zhang (2018a) and Wynne and Zhang (2018b).

strikingly excellent accounts of the empirical responses to anticipated technology shocks. In particular, labor productivity responses resemble a sleeping J curve, which diminishes at short horizons but gets enhanced after the shocks start upgrading technology. Like empirical responses, macroeconomic variables respond in a hump-shaped pattern. The theoretical model manages to replicate the comovement among all macroeconomic indicators despite that the theoretical investment responses falling short of their empirical counterparts at short horizons. Finally, the model exactly matches the immediate overshooting and subsequent trajectories of stock prices.

Before finishing this section, we delve into how far we can go in matching the dynamics following the anticipated shocks identified with max-share approaches of Barsky and Sims (2011) and Chahrour et al. (2023). It deserves clarification that the target of this exercise is not to justify our SVAR identification. Instead, we aim to utilize the search and matching model to show that max-share approaches may deliver contrasting theoretical implications from our benchmark results in spite of their qualitatively similar effects. Columns "BS" and "CCP" record the parameter estimates when the targeted SVAR responses in equation (E.34) are established with Barsky and Sims (2011) and Chahrour et al. (2023) methods respectively. To match Barsky and Sims (2011) responses, the estimated labor supply parameter, θ, equals 1.113, which bears witness to a high labor supply elasticity of around 9. The capital depreciation parameter, ϕ_2, signifies no capital utilization variation as it is estimated to be a tremendously high number reaching its designated upper limit. To fit Chahrour et al. (2023) responses, the estimated θ turns into 0.569, suggesting an abnormally negative labor supply elasticity. The factor utilization parameter is smaller than the benchmark stipulating a larger factor utilization variation. In addition, both max-share approaches favor less persistent technology growth.

Figure E.3 shows that the empirical dynamics are largely matched with two exceptions. First, both max-share methods create more substantial short-run investment responses than prescribed by the theoretical model. Second, diverging from the theoretical responses, the Chahrour et al. (2023) anticipated technology shocks enhance labor productivity at short horizons. To sum up, the max-share approaches twist the theory distinctly from our method based on narrative information.

Figure E.1: Wage Responses

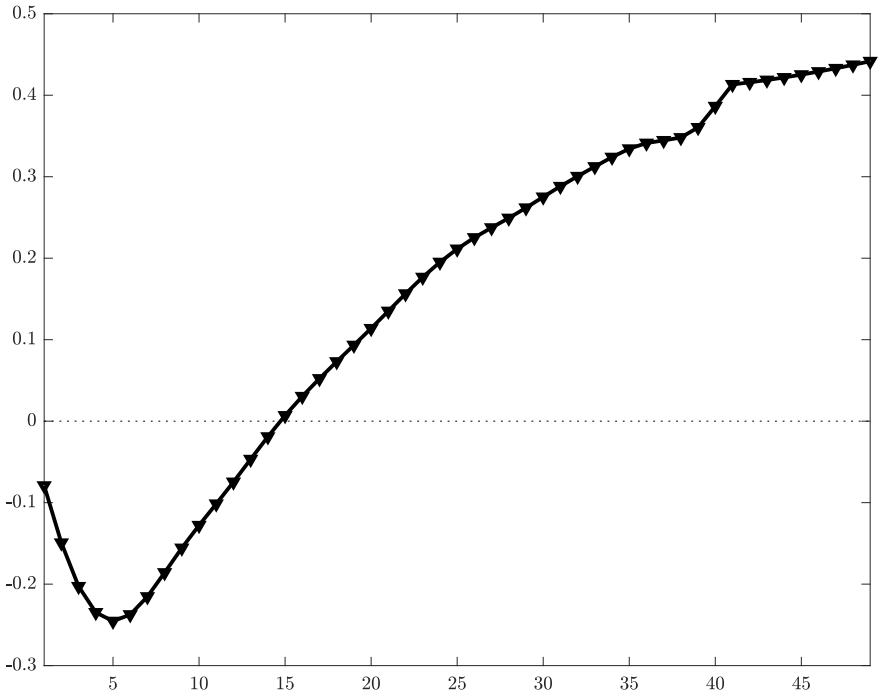

Notes: The Figure presents the estimated wage responses to anticipated technology shocks.

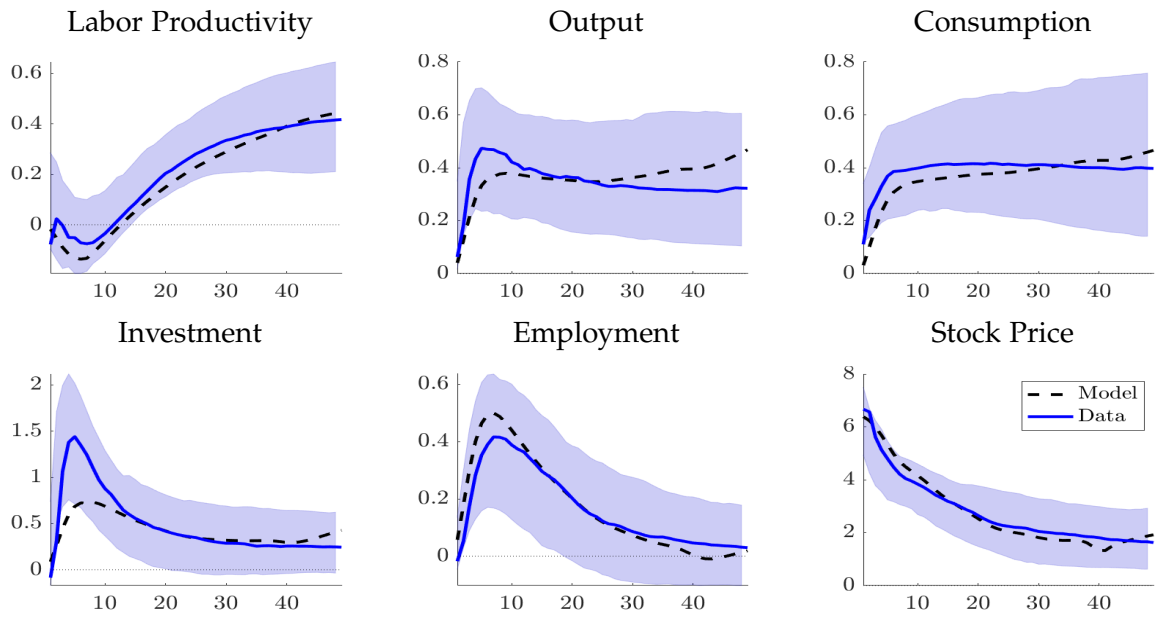

Figure E.2: Impulse Response Matching for Anticipated Technology Shocks

Notes: The blue solid lines and the shaded areas represent, respectively, the median and the 68% (pointwise) credible bands for impulse responses when technology shocks are identified with both IVs and narrative sign restrictions. The black dashed lines depict the effects of anticipated technology shocks implied by the labor search and matching model.

References

Akıncı, Ö. and R. Chahrour (2018). "Good news is bad news: Leverage cycles and sudden stops". In: *Journal of International Economics* 114, pp. 362–375 (cit. on p. 88).

Arias, J., J. F. Rubio-Ramirez, and D. F. Waggoner (2024). "Uniform priors for impulse responses". In: *Working Paper* (cit. on pp. 4, 11, 14, 21).

Arias, J. E., J. F. Rubio-Ramírez, and D. F. Waggoner (2018). "Inference based on structural vector autoregressions identified with sign and zero restrictions: Theory and applications". In: *Econometrica* 86.2, pp. 685–720 (cit. on p. 6).

— (2021). "Inference in Bayesian Proxy-SVARs". In: *Journal of Econometrics* 225, pp. 88–106 (cit. on pp. 4–7, 65).

Barsky, R. B. and E. R. Sims (2011). "News shocks and business cycles". In: *Journal of Monetary Economics* 58.3, pp. 273–289 (cit. on pp. 45, 55–59, 95, 96, 100).

Baumeister, C. and J. D. Hamilton (2015). "Sign restrictions, structural vector autoregressions, and useful prior information". In: *Econometrica* 83.5, pp. 1963–1999 (cit. on p. 7).

Ben Zeev, N. and E. Pappa (2017). "Chronicle of a war foretold: The macroeconomic effects of anticipated defence spending shocks". In: *The Economic Journal* 127.603, pp. 1568–1597 (cit. on pp. 46, 47).

Bu, C., J. Rogers, and W. Wu (2021). "A unified measure of Fed monetary policy shocks". In: *Journal of Monetary Economics* 118, pp. 331–349 (cit. on pp. 46, 47).

Budnik, K. and G. Rünstler (2023). "Identifying structural VARs from sparse narrative instruments: Dynamic effects of US macroprudential policies". In: *Journal of Applied Econometrics* 38.2, pp. 186–201 (cit. on pp. 45, 64).

Cascaldi-Garcia, D. and M. Vukotić (2022). "Patent-based news shocks". In: *Review of Economics and Statistics* 104.1, pp. 51–66 (cit. on pp. 55, 56).

Cesa-Bianchi, A. and A. Sokol (2022). "Financial shocks, credit spreads, and the international credit channel". In: *Journal of International Economics* 135, p. 103543 (cit. on pp. 46, 47).

Cesa-Bianchi, A., G. Thwaites, and A. Vicondoa (2020). "Monetary policy transmission in the United Kingdom: A high frequency identification approach". In: *European Economic Review* 123, p. 103375 (cit. on p. 30).

Chahrour, R., S. K. Chugh, and T. Potter (2023). "Anticipated productivity and the labor market". In: *Quantitative Economics* 14.3, pp. 897–934 (cit. on pp. 45, 55–59, 88, 90, 91, 93–96, 100).

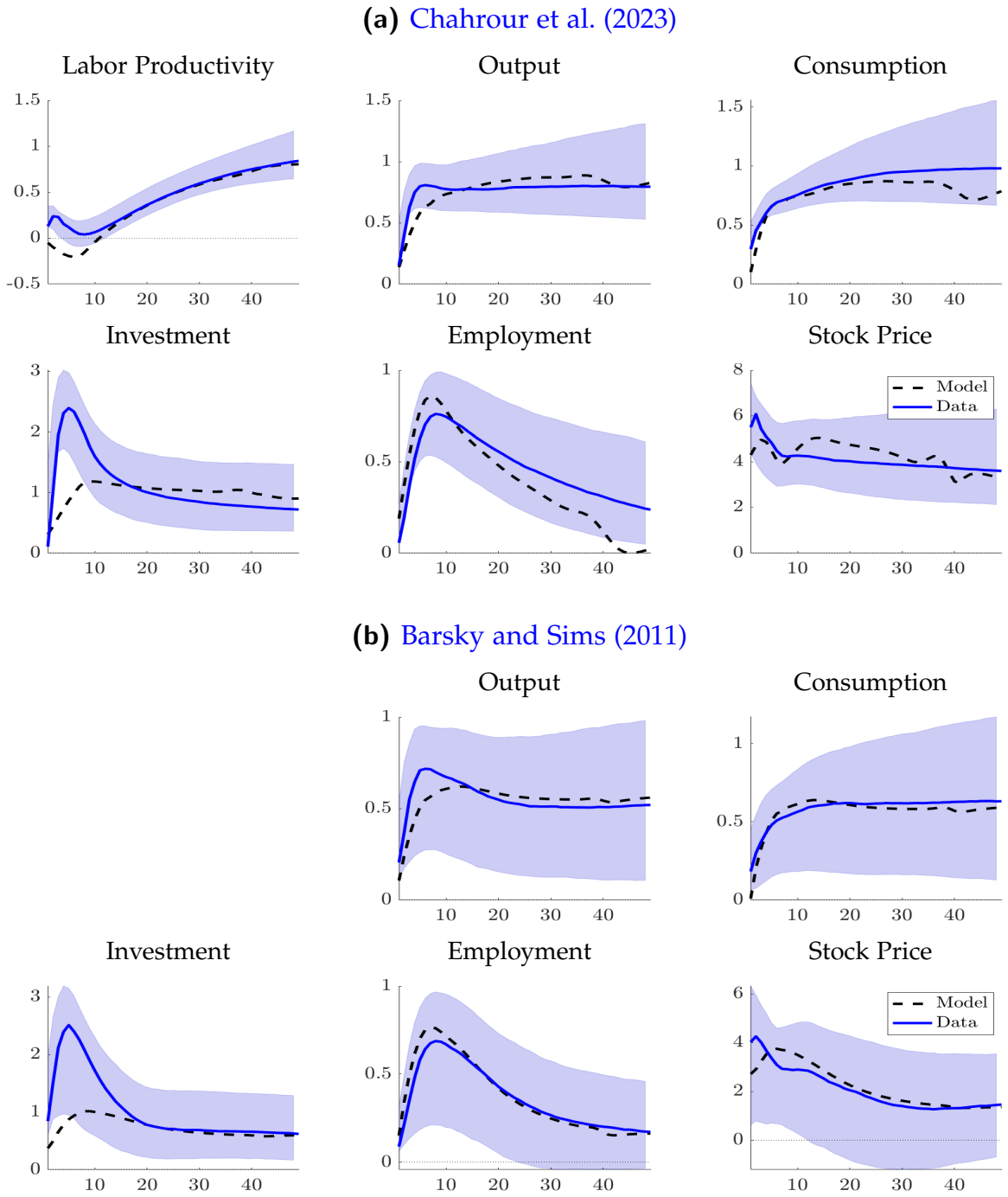

Figure E.3: Impulse Response Matching for Max-Share Anticipated Technology Shocks

Notes: The black dashed lines plot impulse responses implied by the labor search and matching model. The blue solid lines and shaded areas represent, respectively, the median and the 68% (point-wise) credible bands for impulse responses when anticipated technology shocks are identified with Chahrour et al. (2023) method (upper panel) and Barsky and Sims (2011) approach (lower panel). The Barsky and Sims (2011) labor productivity responses are not available as we use TFP instead of labor productivity as the technology proxy in the SVAR model.

Christiano, L. J., M. Eichenbaum, and C. L. Evans (2005). "Nominal rigidities and the dynamic effects of a shock to monetary policy". In: *Journal of Political Economy* 113.1, pp. 1–45 (cit. on p. 93).

Forni, M. and L. Gambetti (2014). "Sufficient information in structural VARs". In: *Journal of Monetary Economics* 66, pp. 124–136 (cit. on pp. 45, 53).

Gavazza, A., S. Mongey, and G. L. Violante (2018). "Aggregate recruiting intensity". In: *American Economic Review* 108.8, pp. 2088–2127 (cit. on pp. 93, 94).

Gertler, M. and P. Karadi (2015). "Monetary policy surprises, credit costs, and economic activity". In: *American Economic Journal: Macroeconomics* 7.1, pp. 44–76 (cit. on pp. 46, 47).

Giacomini, R. and T. Kitagawa (2021). "Robust Bayesian inference for set-identified models". In: *Econometrica* 89.4, pp. 1519–1556 (cit. on pp. 4, 7, 9, 10, 45, 70).

Giacomini, R., T. Kitagawa, and M. Read (2022a). "Narrative restrictions and proxies: Rejoinder". In: *Journal of Business & Economic Statistics* 40.4, pp. 1438–1441 (cit. on p. 80).

— (2022b). "Robust Bayesian inference in proxy SVARs". In: *Journal of Econometrics* 228, pp. 107–126 (cit. on pp. 7, 21, 70).

— (2023). "Identification and inference under narrative restrictions". In: *Reserve Bank of Australia Working Paper RDP 2023-07* (cit. on pp. 7, 8).

Görtz, C., J. D. Tsoukalas, and F. Zanetti (2022). "News shocks under financial frictions". In: *American Economic Journal: Macroeconomics* 14.4, pp. 210–43 (cit. on pp. 55, 56).

Greenwood, J., Z. Hercowitz, and G. W. Huffman (1988). "Investment, capacity utilization, and the real business cycle". In: *The American Economic Review*, pp. 402–417 (cit. on p. 88).

Inoue, A. and L. Kilian (2020). "The role of the prior in estimating VAR models with sign restrictions". Tech. rep. CEPR Discussion Papers (cit. on pp. 80, 83).

— (2022). "Joint Bayesian inference about impulse responses in VAR models". In: *Journal of Econometrics* 231.2, pp. 457–476 (cit. on pp. 14, 15, 74, 80, 83).

Jarociński, M. and P. Karadi (2020). "Deconstructing monetary policy surprises – the role of information shocks". In: *American Economic Journal: Macroeconomics* 12.2, pp. 1–43 (cit. on pp. 46, 47).

Känzig, D. R. (2021). "The macroeconomic effects of oil supply news: Evidence from OPEC announcements". In: *American Economic Review* 111.4, pp. 1092–1125 (cit. on pp. 46, 47).

Kim, K., T. Laubach, and M. Wei (2020). "Macroeconomic effects of large-scale asset purchases: New evidence". In: *FEDS Working Paper* (cit. on p. 30).

Klein, M. and L. Linnemann (2021). "Real exchange rate and international spillover effects of US technology shocks". In: *Journal of International Economics* 129, p. 103414 (cit. on pp. 30, 55, 56).

Kurmann, A. and C. Otrok (2013). "News shocks and the slope of the term structure of interest rates". In: *American Economic Review* 103.6, pp. 2612–32 (cit. on pp. 55, 56).

Lagerborg, A., E. Pappa, and M. O. Ravn (2023). "Sentimental business cycles". In: *The Review of Economic Studies* 90.3, pp. 1358–1393 (cit. on pp. 30, 46, 47).

Lakdawala, A. (2019). "Decomposing the effects of monetary policy using an external instruments SVAR". In: *Journal of Applied Econometrics* 34.6, pp. 934–950 (cit. on p. 30).

Lakdawala, A. and R. Sengupta (2021). "Measuring monetary policy shocks in emerging economies: Evidence from India". In: *Journal of Money, Credit and Banking* (cit. on p. 30).

Laubach, T. and J. C. Williams (2003). "Measuring the natural rate of interest". In: *Review of Economics and Statistics* 85.4, pp. 1063–1070 (cit. on p. 95).

Leeper, E. M., A. W. Richter, and T. B. Walker (2012). "Quantitative effects of fiscal foresight". In: *American Economic Journal: Economic Policy* 4.2, pp. 115–144 (cit. on pp. 46, 47).

Mertens, K. and M. O. Ravn (2014). "A reconciliation of SVAR and narrative estimates of tax multipliers". In: *Journal of Monetary Economics* 68, S1–S19 (cit. on pp. 46, 47).

— (2019). "The dynamic effects of personal and corporate income tax changes in the United States: Reply". In: *American Economic Review* 109.7, pp. 2679–2691 (cit. on p. 30).

Miranda-Agrippino, S. and H. Rey (2020). "US monetary policy and the global financial cycle". In: *The Review of Economic Studies* 87.6, pp. 2754–2776 (cit. on p. 30).

Moran, P. and A. Queralto (2018). "Innovation, productivity, and monetary policy". In: *Journal of Monetary Economics* 93, pp. 24–41 (cit. on p. 94).

Noh, E. (2024). "Revisiting the effects of conventional and unconventional monetary policies". In: *Journal of Applied Econometrics* 39, pp. 943–951 (cit. on p. 30).

OECD (1994). "The OECD jobs study: Evidence and explanations". In: (cit. on p. 93).

Olea, J. L. M., J. H. Stock, and M. W. Watson (2021). "Inference in structural vector autoregressions identified with an external instrument". In: *Journal of Econometrics* 225.1, pp. 74–87 (cit. on p. 30).

Petrongolo, B. and C. A. Pissarides (2001). "Looking into the black box: A survey of the matching function". In: *Journal of Economic Literature* 39.2, pp. 390–431 (cit. on p. 93).

Piffer, M. and M. Podstawski (2018). "Identifying uncertainty shocks using the price of gold". In: *The Economic Journal* 128.616, pp. 3266–3284 (cit. on pp. 45, 85).

Ramey, V. A. (2011). "Identifying government spending shocks: It's all in the timing". In: *The Quarterly Journal of Economics* 126.1, pp. 1–50 (cit. on pp. 46, 47).

Reichling, F. and C. Whalen (2012). "Review of estimates of the Frisch elasticity of labor supply". In: *CBO Working Paper 2012-13* (cit. on p. 95).

Rüth, S. K. (2020). "Shifts in monetary policy and exchange rate dynamics: Is Dornbusch's overshooting hypothesis intact, after all?" In: *Journal of International Economics* 126, p. 103344 (cit. on p. 30).

Smets, F. and R. Wouters (2007). "Shocks and frictions in US business cycles: A Bayesian DSGE approach". In: *American Economic Review* 97.3, pp. 586–606 (cit. on pp. 93, 94).

Stock, J. H. and M. W. Watson (2018). "Identification and estimation of dynamic causal effects in macroeconomics using external instruments". In: *The Economic Journal* 128.610, pp. 917–948 (cit. on p. 30).

Stock, J. H., J. H. Wright, and M. Yogo (2002). "A survey of weak instruments and weak identification in generalized method of moments". In: *Journal of Business & Economic Statistics* 20.4, pp. 518–529 (cit. on p. 30).

Stock, J. H. and M. Yogo (2005). "Testing for Weak Instruments in Linear IV Regression". In: *Identification and Inference for Econometric Models: Essays in Honor of Thomas Rothenberg* (cit. on p. 30).

Waggoner, D. F. and T. Zha (2003). "A Gibbs sampler for structural vector autoregressions". In: *Journal of Economic Dynamics and Control* 28.2, pp. 349–366 (cit. on pp. 5, 6).

Wynne, M. A. and R. Zhang (2018a). "Estimating the natural rate of interest in an open economy". In: *Empirical Economics* 55, pp. 1291–1318 (cit. on p. 95).

— (2018b). "Measuring the world natural rate of interest". In: *Economic Inquiry* 56.1, pp. 530–544 (cit. on p. 95).

Yashiv, E. (2007). "US labor market dynamics revisited". In: *The Scandinavian Journal of Economics* 109.4, pp. 779–806 (cit. on p. 93).